NASA CONTRACTOR REPORT

NASA CR-66756

EFFECTS OF ATMOSPHERE, WIND, AND AIRCRAFT MANEUVERS ON SONIC BOOM SIGNATURES

by

Rudolph C. Haefeli

Prepared by

AERONAUTICAL RESEARCH ASSOCIATES OF PRINCETON, INC.

Princeton, N.J.

for Langley Research Center

NATIONAL AERONAUTICS AND SPACE ADMINISTRATION APRIL 1969

NASA CR-66756

EFFECTS OF ATMOSPHERE, WIND, AND AIRCRAFT MANEUVERS ON SONIC BOOM SIGNATURES

by

Rudolph C. Haefeli

Prepared under Contract No. NAS1-8490 by

AERONAUTICAL RESEARCH ASSOCIATES OF PRINCETON, INC.

50 Washington Road, Princeton, New Jersey 08540

for

NATIONAL AERONAUTICS AND SPACE ADMINISTRATION

April, 1969

CONTENTS

EFFECTS OF ATMOSPHERE, WIND, AND AIRCRAFT MANEUVERS ON SONIC BOOM SIGNATURES

Rudolph C. Haefeli
Aeronautical Research Associates of Princeton, Inc.

SUMMARY

Sonic boom propagation in a horizontally stratified atmosphere is computed for a broad scope of atmosphere and flight conditions, using both a fighter-type (F-104) and an SST-type (SCAT 15-F) aircraft. Atmospheric conditions include various temperature inversions, lapse rates, and wind profiles. Flight conditions include variations in aircraft altitude and Mach number, together with maneuvers of steady flight, longitudinal acceleration, pullup, pushover, and circular turns.

A computer program is used which was developed using geometric acoustic theory, accounting for nonlinear effects by means of an appropriate age variable. The program therefore yields the entire sonic boom signature, with its proper distortion (aging) in either uniform or nonuniform atmospheres with winds, and accounting for any specified aircraft maneuver. This program gives output in both tabular and graphical formats, including plots of the resulting sonic boom pressure signature with shock waves properly located.

Results of the calculations are presented and discussed. Comparisons with data from other sources are shown. Important effects near ray focusing and for maneuvers are described, including large overpressures and major changes in the shape of the pressure signatures for specified flight conditions.

INTRODUCTION

The development of a new analysis technique for computing sonic boom pressure signatures was reported in reference 1. This analysis offers a unique capability to calculate the sonic boom propagation through variable, horizontally stratified atmospheres with winds from any direction and for general aircraft maneuvers. The maneuver parameters affect the strength and aging (distortion) of the signature, and are completely included in the ray-tube area equations. There is no restriction, then, as to the type of maneuver; it may be specified for any steady or accelerating flight

path, including banked turns out-of-plane. The analysis of the propagation of the sonic boom is based on linear geometric acoustic theory, employing an age variable to define essential nonlinear effects on the shape of the pressure signature. Effects of atmospheric turbulence are not included in this analysis, nor are the special nonlinear effects near ray focusing (caustics) where in the present theory the pressure becomes infinite. The analysis provides equations for the sonic boom which have been incorporated in a versatile computer program written in ASA FORTRAN IV (ref. 1).

This analysis and computer program provide means for calculating the sonic boom signatures for more general variables than with previous programs, without asymptotic or uniform atmosphere assumptions, and for arbitrary maneuvers. As examples of previous work, reference 2 has presented methods for calculating the ground locations of sonic booms for a specified atmosphere from maneuvering aircraft, but does not give the sonic boom signatures. Reference 3 has presented a digital program for obtaining sonic boom shock-overpressures and restricted to maneuvers in a vertical plane. Overpressure results from this and other previous analyses have been conflicting, even for level uniform flight with and without winds, leading to confusion and lack of confidence in predictions of sonic boom overpressures. The present study, therefore, was undertaken to establish a sound basis for sonic boom predictions using the developments of reference 1, and to provide a broad scope of results for understanding various effects on overpressures and signature shapes (wave forms).

This study provides calculations and interpretations for sonic boom propagation through various stratified atmospheres and winds from maneuvering aircraft. The atmospheres include the 1962 U.S. standard, three variations of temperature, and three wind profiles. The maneuvers include level flight at various altitudes and Mach numbers, accelerating flight, pullups, pushovers, and circular turns. Two aircraft were used in this study. The fighter aircraft class was represented by the F-104 and the supersonic transport class (SST) was represented by the SCAT 15-F, a hypothetical aircraft defined and used in analytical studies at NASA, Langley Research Center.

This report describes the computational study and its results in detail. Modifications to the computer program are mentioned which enabled rapid computer processes using the IBM 1130, Model 2B computer. The input data are presented, including aircraft characteristics, atmosphere and wind data, maneuver corrections, and the selected altitude and Mach number variations. Results are then presented in tabular and graphical form for both aircraft. Comparisons are made with previously available data, in particular that of reference 4. Important changes in over-

pressure and pressure signature shapes caused by atmospheric refraction leading to ray focusing and maneuvers are described.

SYMBOLS

a	speed of sound, $(\gamma_e RT)^{1/2}$
A	ray-tube area cut by horizontal plane
C_D	drag coefficient
C_L	lift coefficient
$C_T - C_D$	net axial force coefficient
D	drag
g	gravitational acceleration
h	altitude of aircraft above sea level
h_g	altitude of ground above sea level
HAS	high altitude shear, wind profile
HATI	high altitude temperature inversion
K_A	atmospheric correction factor applied to UNW results
K_R	reflection factor
L	lift; for F-function, distance along aircraft axis; for signature, length parameter
L_a	aircraft reference length
L_l	signature length between leading and trailing shocks
LAS	low altitude shear, wind profile
LATI	low altitude temperature inversion
M	Mach number of aircraft, V/a
MAS	medium altitude shear, wind profile

n_L, n_T	normal and axial load factors
p	pressure
Δp	pressure increment; maximum overpressure
p_{ref}	pressure at reference Mach number, SNW
p_{std}	pressure at M = 1.25, SNW
s	distance
S_{ref}	reference wing area for force coefficients
SLR	summer lapse rate, temperature profile
SNW	1962 U.S. standard atmosphere; no wind
t	time along ray
t_a	time along aircraft trajectory
T	absolute temperature; thrust
UNW	uniform atmosphere, no wind
V	aircraft velocity relative to atmosphere, Ma
W	weight of aircraft
x,y,z	fixed coordinate system, east, north, and above ground, respectively
x_c	lateral distance to cutoff (horizontal ray)
γ	aircraft climb angle
γ_e	ratio of specific heats
Δ	perturbation from undisturbed value
η	wind heading angle (whence wind blows)
μ	Mach angle, $\sin^{-1}$ (1/M)
τ	age
ϕ	azimuth angle of wave normal from vertical plane

ϕ_a	aircraft bank angle
ϕ_r	azimuth angle of wave normal relative to aircraft
ψ	heading angle of aircraft

GENERAL DESCRIPTION AND PROGRAM INPUTS

The main objective of the current study was to obtain an understanding of sonic boom overpressures and pressure signatures resulting from representative light-weight and heavy-weight aircraft types with a variety of maneuvers, wind profiles and atmospheres. The plan for achieving this goal included establishing a schedule of variations of parameters summarized in table I. The set and run numbers given on this table were used to identify the specific variations shown in other columns of this table and the corresponding computational results. The symbols and abbreviations used in this table are defined in the following paragraphs and in the list of SYMBOLS.

Two aircraft used in this study were the F-104 and SCAT 15-F with the following characteristics:

		F-104	SCAT 15-F
Weight W	lbs	15 600	450 000
	Mg	7.06	204
Length L_A	ft	50	250
	m	15.3	76.2
Wing area S_{ref}	ft^2	173.2	5000
	m^2	16.1	465
Wing loading W/S_{ref}	lb/ft^2	90	90
	kg/m^2	439	439

Each aircraft has the same wing loading and, therefore, the same lift coefficient for the same flight condition. This commonality may be helpful when comparing signatures of the two aircraft at the same flight condition, as any differences must then be attributed to other parameters.

The F-functions (ref. 5) for these aircraft, which represent the pressure signature near (several spans from) the air-

craft are required inputs to the sonic boom computer program. The form for the F-functions, calculated at NASA, Langley Research Center, was given as

$$F = F_f \left(F_A + F_B\right)$$

where

$$F_A = F_{A1} \sqrt{2L}$$

$$F_B = F_{B1} \left(\frac{\beta}{2} C_L S_{ref}\right) / (2L)^{3/2}$$

and

$$\beta = \sqrt{M^2 - 1}$$

$$F_f = M^2 / \sqrt{2\beta}$$

Reference 6 describes a numerical procedure for calculating the F-functions. The contributions from the aircraft volume distribution and from the lift distribution, F_{A1} and F_{B1}, respectively, were given at specified aircraft stations L_a. Tables of F_{A1} and F_{B1} were input to the program and taken to vary linearly between the specified stations.

The input parameters F_{A1} and F_{B1} are implicit functions of Mach number. They were only available, however, for $M = 1.4$ (both aircraft) and $M = 2.7$ (SCAT 15-F), and only for the azimuth directly under the aircraft ($\phi_r = 0$, fig. 1). For the present study, then, these parameters were varied with Mach number only when the SCAT 15-F F-function derived at $M = 1.4$ was replaced by the one derived at $M = 2.7$. The lift term F_B, however, is explicitly dependent on Mach number through the factors $\beta = \sqrt{M^2 - 1}$ and $C_L = \frac{2(W/S)}{(aM)^2}$. For the present study, then, the F-function does vary with Mach number. Also, the term F_B is proportional to the lift coefficient (load factor), so that the F-function changes when the maneuver load factor n_L is changed, and also varies with aircraft altitude and weight. The F-functions for $M = 1.4$ were used for all calculations in this study, except for SCAT 15-F runs at $M = 3$ for which the $M = 2.7$ data were also used. The consequences of the change in F-function for SCAT 15-F solutions at $M = 3$ are shown later to be small, lending substance to the belief that in general F_{A1} and F_{B1} are weakly dependent on Mach number so that they may be used over a suitable range of Mach numbers. Also, it is felt that they vary

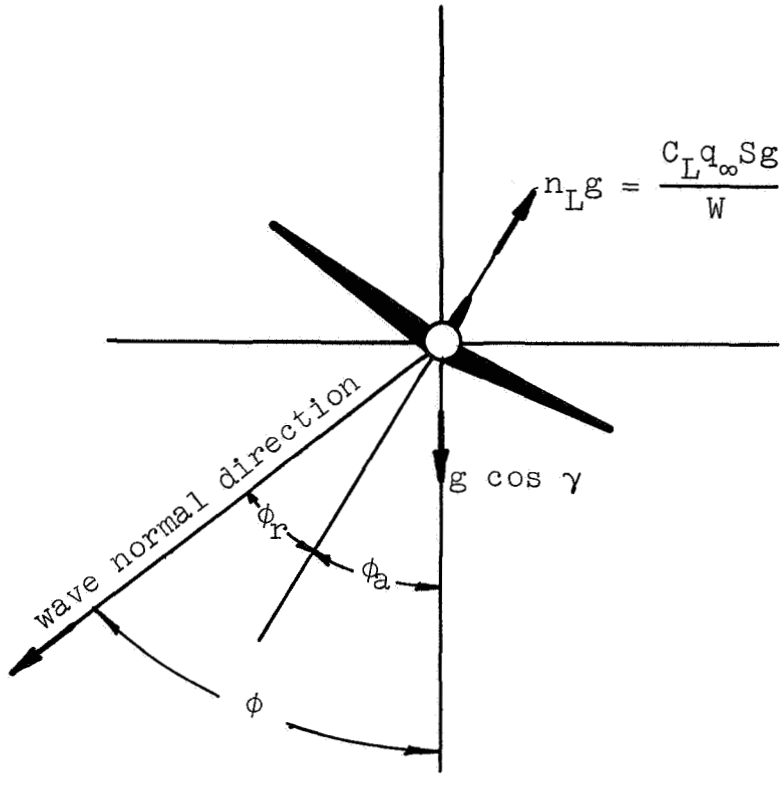

Figure 1. View looking forward along flight axis showing acceleration components, bank angle, and azimuth angle.

slowly with ϕ_r near $\phi_r = 0$, so again may be used throughout a range of azimuth angles without serious discrepancy. In this study the F-functions, computed and input for $\phi_r = 0$ only, were therefore used at all azimuth angles, but recognizing that there may be in reality significant changes, particularly at the larger angles (above 30 deg, say).

Figure 2 shows the two F-functions for flight at $M = 1.25$ and $h = 40\,000$ ft (12.2 km). A linear variation is assumed between data points. They are given at increments of $0.025\ L_a$ and $0.020\ L_a$ for the F-104 and SCAT 15-F, respectively, from the station at the nose of the aircraft to a station in the wake. These curves, shown for L/L_a up to 2, were extended farther aft to approximately $8\ L_a$ in the input table for the sonic boom program. The extended part of the F-function was taken to be essentially zero. This added length, although representing near-zero values, was needed for some calculations to determine the location of the trailing shock in the pressure signature.

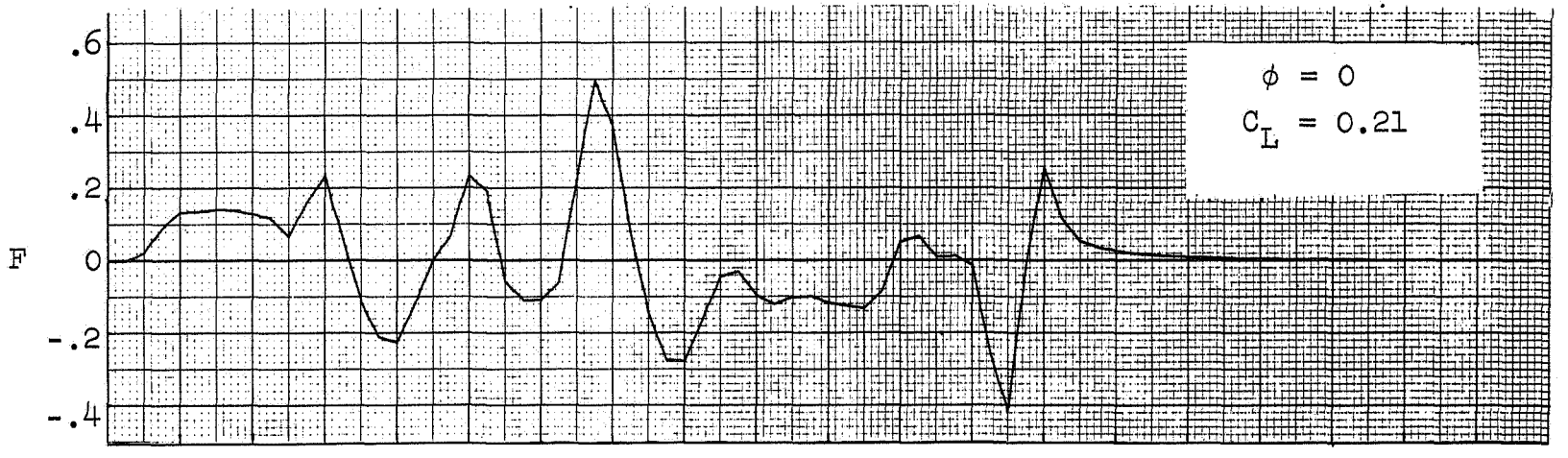

a) F-104

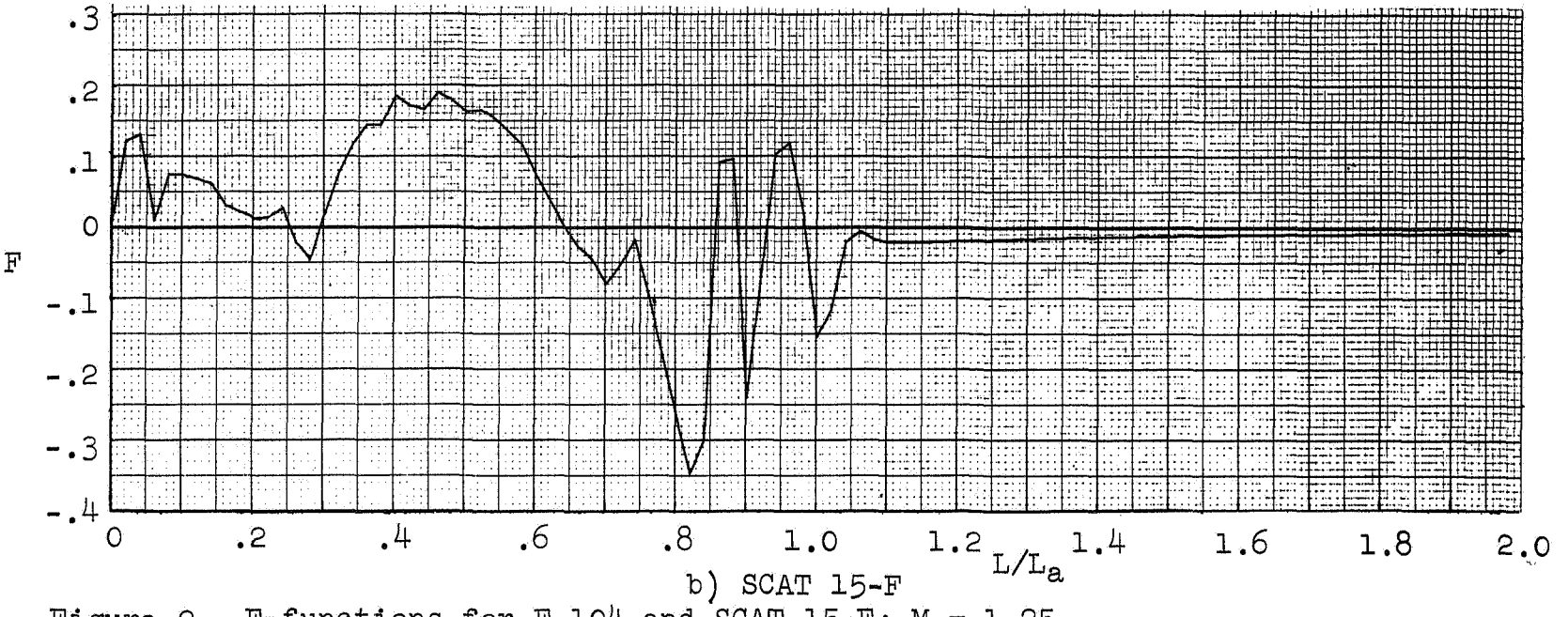

b) SCAT 15-F

Figure 2. F-functions for F-104 and SCAT 15-F; M = 1.25

The aircraft maneuvers designated in table I for this study included horizontal steady and accelerating flight, pullups, pushovers and circular turns. Figures 3, 4, and 5 define nomenclature pertinent to the aircraft maneuvers, ray paths, and azimuth angles (from ref. 1). Flight path and heading angle variations used in the computations are shown for reference in figures 6 and 7.

Atmospheric characteristics selected for this study are shown in figure 8 in terms of the temperature variations with altitude. Pressure variations for an equilibrium atmosphere were computed and used with each of these temperature profiles. The high altitude temperature inversion (HATI) is characteristic of a frontal inversion (Atm D-3 of ref. 4). The low altitude temperature inversion (LATI) is characteristic of smog (Atm B-4 of ref. 4). The summer lapse rate (SLR) atmosphere is characteristic of a hot ground temperature (Atm A-3 of ref. 4). The 1962 U.S. standard (SNW, standard no wind) is from reference 7. Uniform atmospheres were also used herein for some calculations for comparisons, since other reports have made wide use of the simplifications to propagation calculations thereby introduced. The uniform atmospheres (UNW, uniform no wind) are defined to have constant temperature and density everywhere as determined using the 1962 U.S. standard atmosphere at the altitude of the aircraft.

Wind profiles selected for this study are presented in figure 9. The high altitude shear (HAS) profile is the wind profile which is exceeded less than 1% of the time in the northeastern United States. It represents a high-speed jet-stream at an altitude of 35 000 ft (10.7 km). The medium altitude shear (MAS) profile represents a jet-stream at 20 000 ft (6.1 km) with constant wind speeds above 22 000 ft (6.7 km) and below 17 000 ft (5.2 km). The low altitude shear (LAS) profile represents a jet-stream at 3000 ft (0.9 km). These winds were used with the 1962 U.S. standard atmosphere (SNW) temperature and density.

The abbreviations introduced here for the atmospheric conditions are used in the remainder of the report for simplicity. In summary, they are identified in figures 8 and 9 using the following nomenclature:

UNW :	Uniform atmosphere, no wind
SNW :	1962 U.S. standard atmosphere, no wind
LAS :	Low altitude shear, wind profile
MAS :	Medium altitude shear, wind profile
HAS :	High altitude shear, wind profile
LATI :	Low altitude temperature inversion

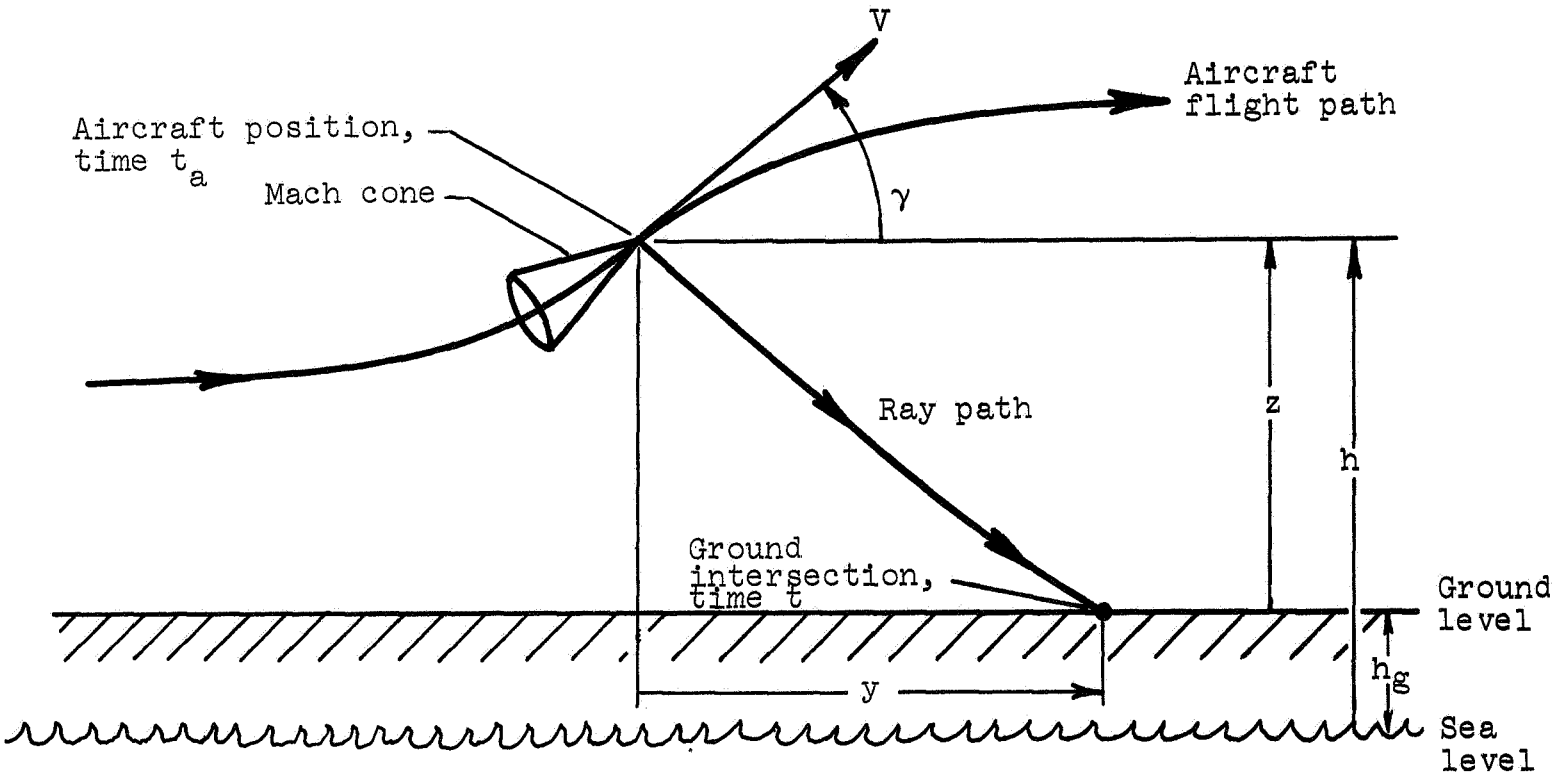

Figure 3. Schematic of flight path and ray path

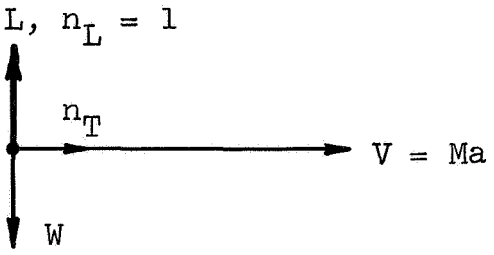

a) Horizontal acceleration

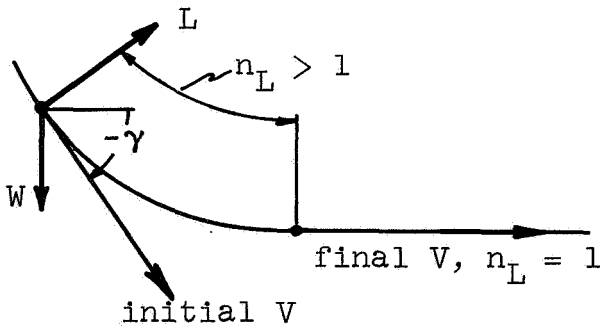

b) Dive - pullup

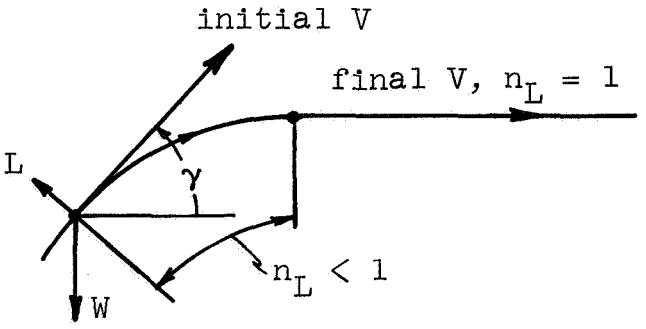

c) Climb - pushover

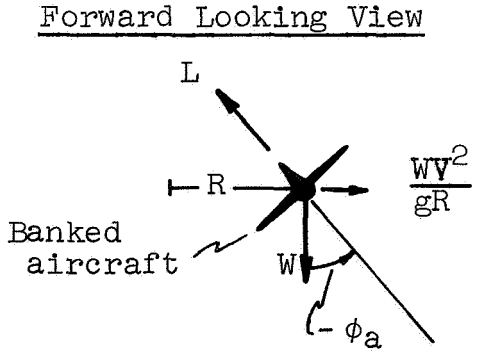

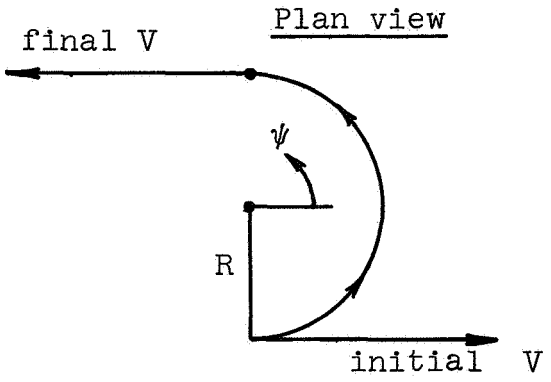

d) Circular turn

Figure 4. Sketch of velocity, force and acceleration vectors for maneuvers

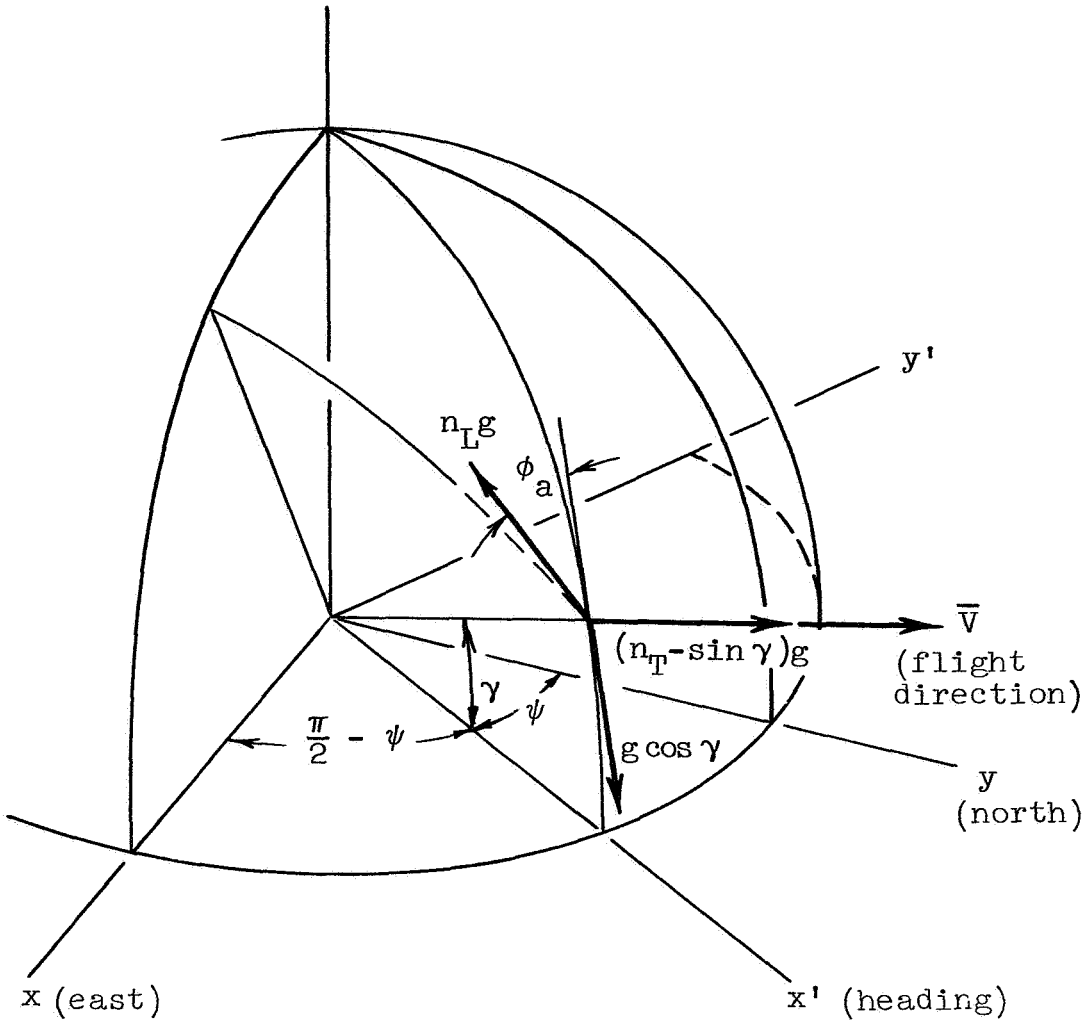

Figure 5. Acceleration diagram for maneuvering aircraft.

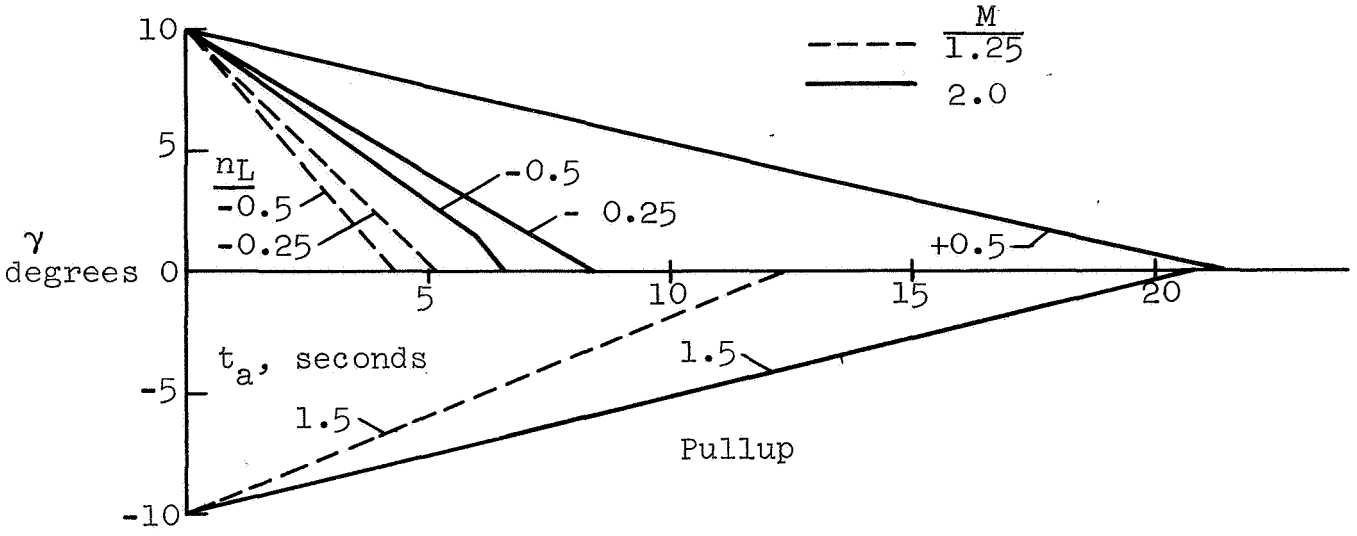

Figure 6. Flight path angle variations for pullup and pushover maneuvers

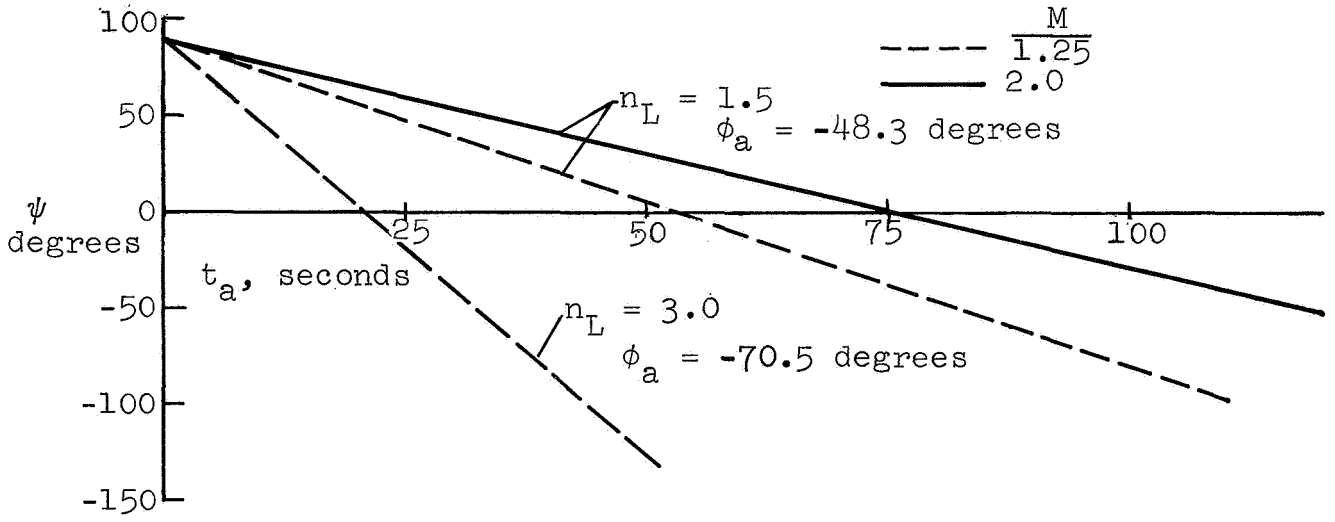

Figure 7. Heading angle variations for turn maneuvers

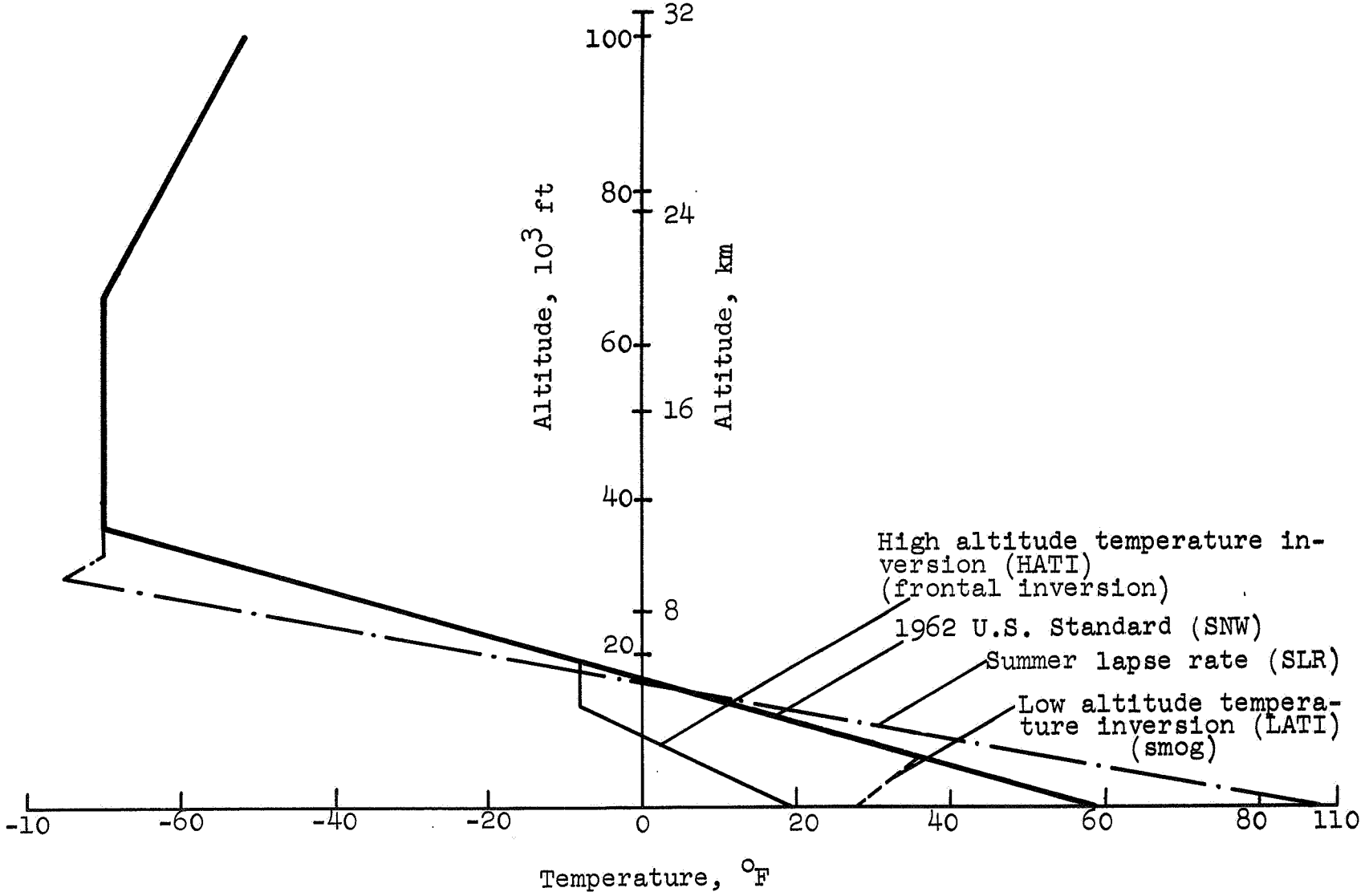

Figure 8. Temperature profiles

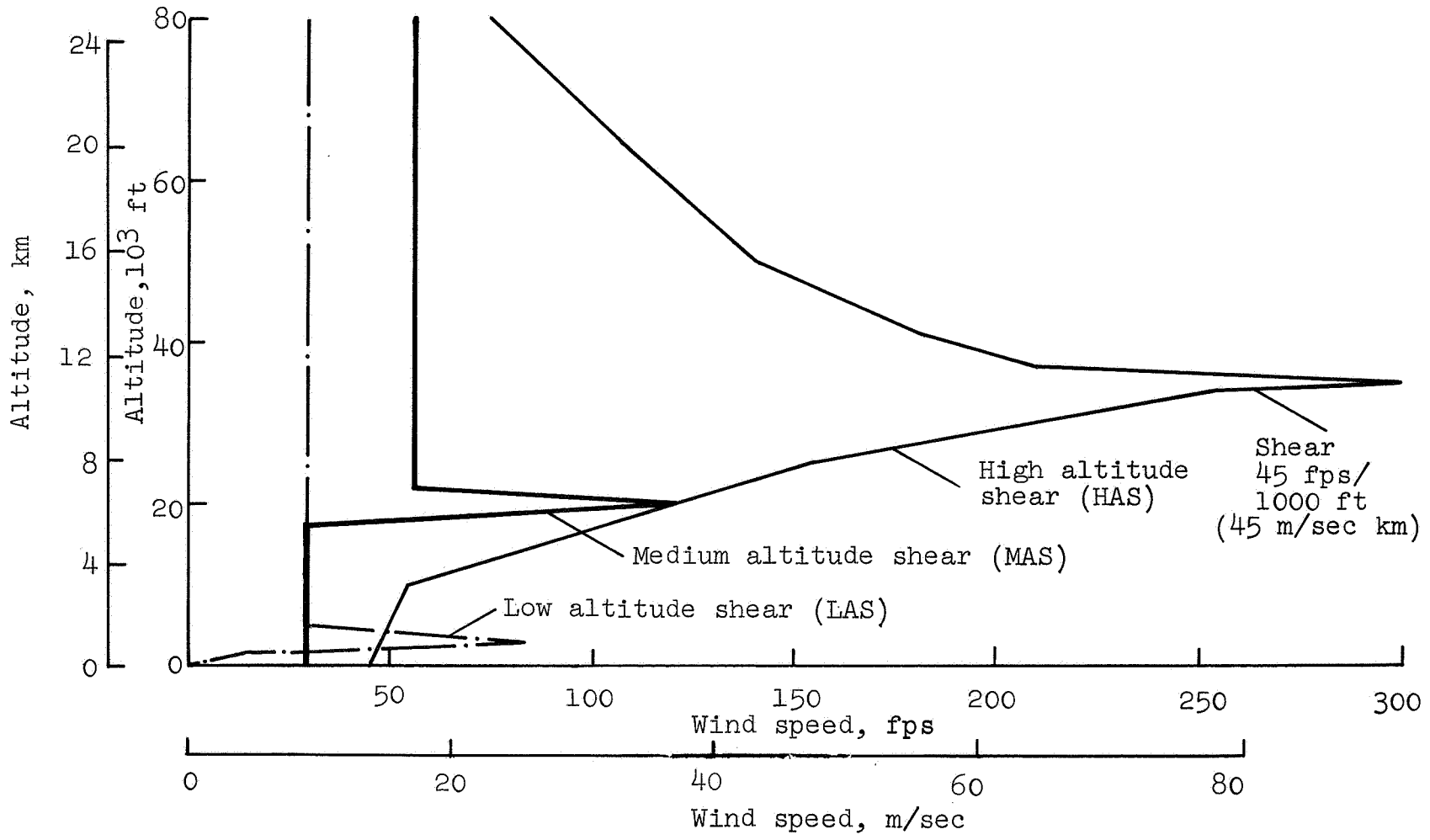

Figure 9. Wind Profiles

HATI : High altitude temperature inversion

SLR : Summer lapse rate, temperature profile

Another input for the present calculations was an arbitrary choice of ground reflection factor $K_R = 1.9$. Theoretically the K_R value should be 2 for a sensor at the ground where the incident signal (shock-waves) is reflected. The reduced value of 1.9 used here may be considered a temporary compromise with considerations of possible surface conditions on the alleviation of the peak pressures of sonic boom shock waves. Some data were computed at altitudes other than sea level, and for these data the reflection factor $K_R = 1.9$ was maintained. It should be noted, however, that the pressures should be calculated with $K_R = 1$ if data are desired with no ground reflection. This also applies if the shock waves happen to be normal to the ground (i.e., if ray paths are horizontal at the ground).

COMPUTER PROGRAM MODIFICATIONS

The development of the sonic boom analysis and computer program is reported in reference 1. The computer program was modified for the current study to expedite the calculations on an IBM-1130, Model 2B computer as follows:

1. The calculation time using the IBM-1130 was reduced by a factor of 1/3 by incorporating various changes to the computational flow diagram logic. For example, disk files were created for storing input data such as atmosphere specifications, wind profiles, F-functions and maneuvers. These data are read into the computer only once, and thereafter are called by file name, thus saving repetitive read-in requirements. Also, simplifications were made to integration subroutines and requirements were eliminated for calling interpolation routines repetitively.

2. A subroutine was added to obtain the shock locations automatically. This includes a new algorithm which examines an integral of the pressure function (σ-curve of ref. 1) and determines where shocks are located. The computer program then investigates the appropriate branches of the distorted pressure signal to find the values of pressures at each shock location. These pressure values and the corresponding pressure jumps are included in the output listing.

3. A capability was added to obtain automatic plotting of the pressure signatures at the same time they are listed by the printer. Plotting scales are adjusted automatically to keep the curve within a specified size (thereby providing a standardized format).

4. This sonic boom computer program is too large to be formulated for an IBM-1130, Model 2B without splitting it into logical computational units connected by programmed links. Five links are used in the present IBM-1130 program connecting input, maneuver, ray tracing-area-age, shock location, print-plot, and ground intersection modules. The computer flow was revised from that of the original program (ref. 1) so that each link computes and stores all data for a given run before proceeding to the next link. Thus, for example, the complete maneuver is calculated and stored at the beginning of the program. This process of linking avoids time-consuming transfers back and forth between links and saves about 1/4 of the machine time that might otherwise be required. It also enables the computer to call a second set of aircraft characteristics and determine its pressure signature and shock locations without redoing input, maneuver and ray-area-age calculations.

The overall machine time using this computer program on an IBM-1130, Model 2B tied in with a digital incremental plotter varies between 1 and 3 minutes per signature. This time depends on the maneuver time duration, the number of rays called for, and the complexity of the F-function.

RESULTS

This section presents data derived for the various maneuver and atmospheric conditions selected for this study. Each subsection presents tables and graphs for a particular type of maneuver, starting with level uniform flight and progressing through level accelerating flight, pullups, pushovers, turns and porpoising maneuvers. Overpressures and complete signatures are shown pertaining to each of these flight conditions, together with certain significant comparisons to previous calculated results, to flight test measurements, and to reference conditions.

A summary tabulation of results for all runs is presented in table II for the use of the reader who may wish to make further analyses of results. This table shows overpressures, signature lengths, and ray ground intersection data for selected maneuver times t_a and azimuth angles ϕ. Table I provides the run number for a specified calculation condition; with this run number, table II provides the resulting overpressure and ray-path data. Figures 6 and 7 may be required to obtain maneuver condition information using the aircraft maneuver time t_a given in table II. The results are shown in other chart and graph formats to be presented in the following discussion of results, so that the general reader need not interpret table II.

Level Uniform Flight

Pressure signatures and overpressures.- Pressure signatures for the F-104 and SCAT 15-F are shown in figure 10 for an aircraft at $M = 1.25$, $h = 40\ 000$ ft (12.2 km) and for a standard no-wind (SNW) atmosphere. These signatures are computed at sea level on the ground track of the aircraft ($\phi = 0$). The particular flight and atmosphere conditions selected here are often used as reference values in this report, and therefore these signatures (fig. 10) are termed nominal. The ordinate Δp is the pressure variation from its ambient value, whereas the abscissa may be considered a distance phase which is proportional to a time phase (ref. 1, eq. (41)), so that the signature also represents pressure fluctuations with time such as would be measured by a stationary microphone with a nonturbulent atmosphere. The zero value of L/L_a corresponds to the phase which originated at the nose of the aircraft (or its equivalent body of revolution). The signature length, defined as L_1, is the distance between the leading and trailing shocks. The station L or length L_1 is obtained from L/L_a and L_1/L_a by multiplying by the aircraft length L_a. The SCAT 15-F is five (5) times as long as the F-104. Its nominal signature length L_1 is therefore 306 ft, compared to 133 ft for the F-104. The different characteristics of the signatures for the two aircraft result from their considerable difference in configuration which is input through their F-functions (fig. 2). They have not become fully developed N-waves for this reference condition.

The sonic boom overpressure is taken as the maximum value of pressure on the compression side of the signature. Thus, in figure 10 the overpressure for the F-104 is equal to the jump of the leading shock, whereas that for the SCAT 15-F is the peak value at the third shock. The overpressures are given in table III at various Mach numbers for level uniform flight at 40 000 ft (12.2 km) altitude. These values are used as reference values in subsequent data presentations.

Pressure signatures for several Mach numbers are shown in figures 11 and 12 for level flight at 40 000 ft (12.2 km) altitude. Signatures are shown for each aircraft using both the uniform atmosphere (UNW) and a real atmosphere (SLR). (The signatures for the standard atmosphere (SNW) would be essentially the same as for the SLR atmosphere). The results using UNW are considerably lower than for SNW, and should be multiplied by an atmospheric correction factor K_A to obtain realistic pressure values. In the presentation of these and subsequent pressure signatures, the scales were determined by the format for the digital incremental plotter, and therefore are not always consistent; they are properly identified, however.

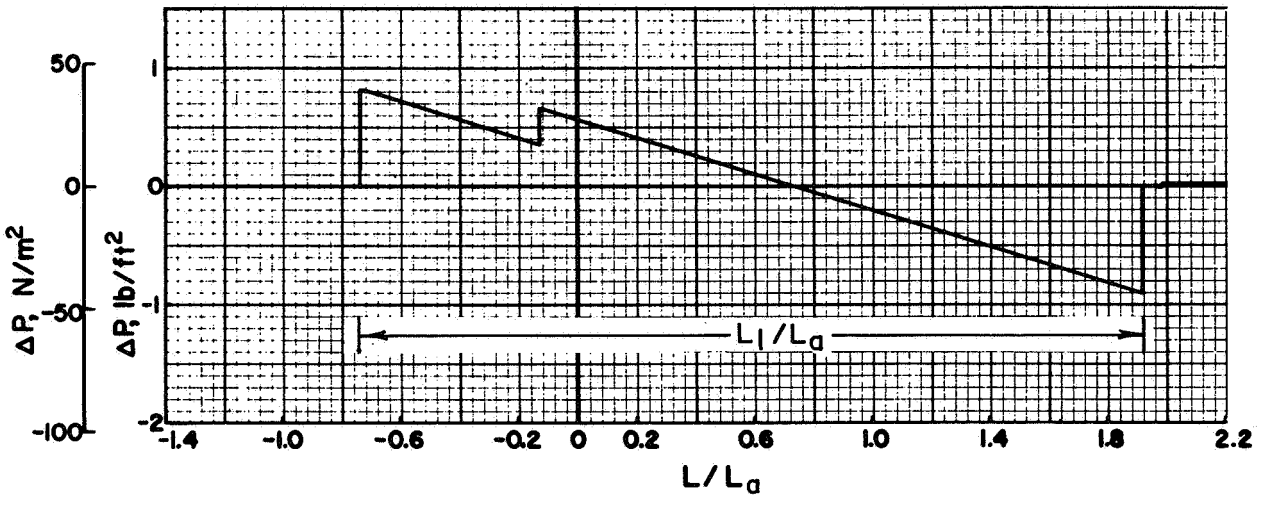

a) F-104

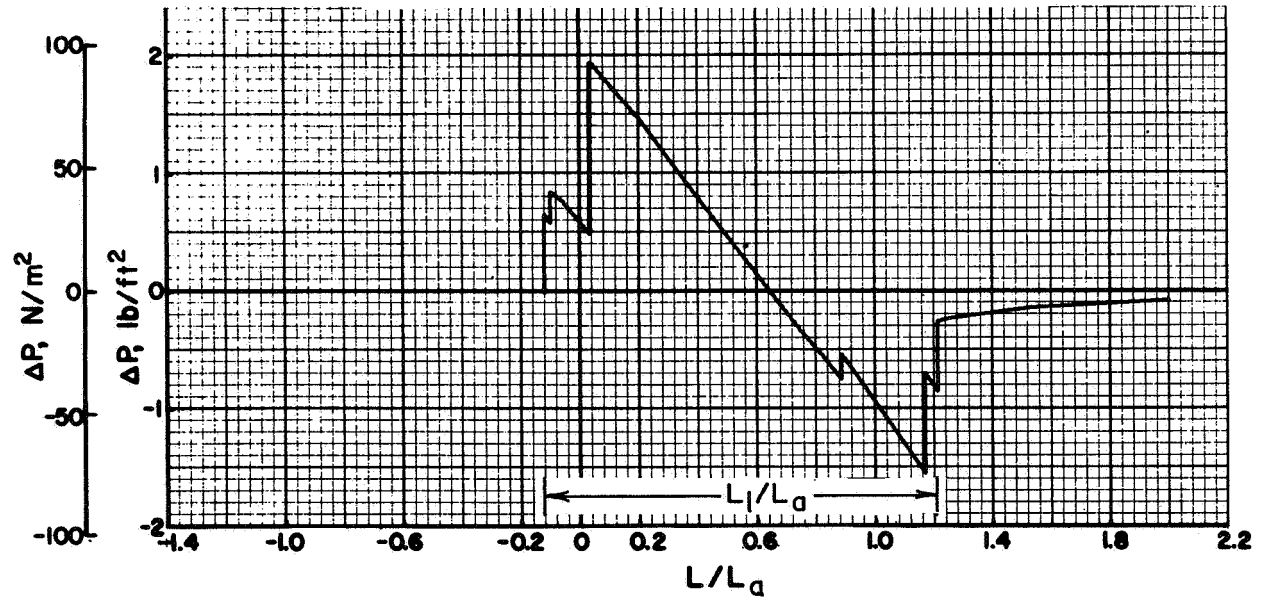

b) SCAT 15-F

Figure 10. Nominal pressure signatures for F-104 and SCAT 15-F; M = 1.25, h = 40 000 ft (12.2 km), SNW

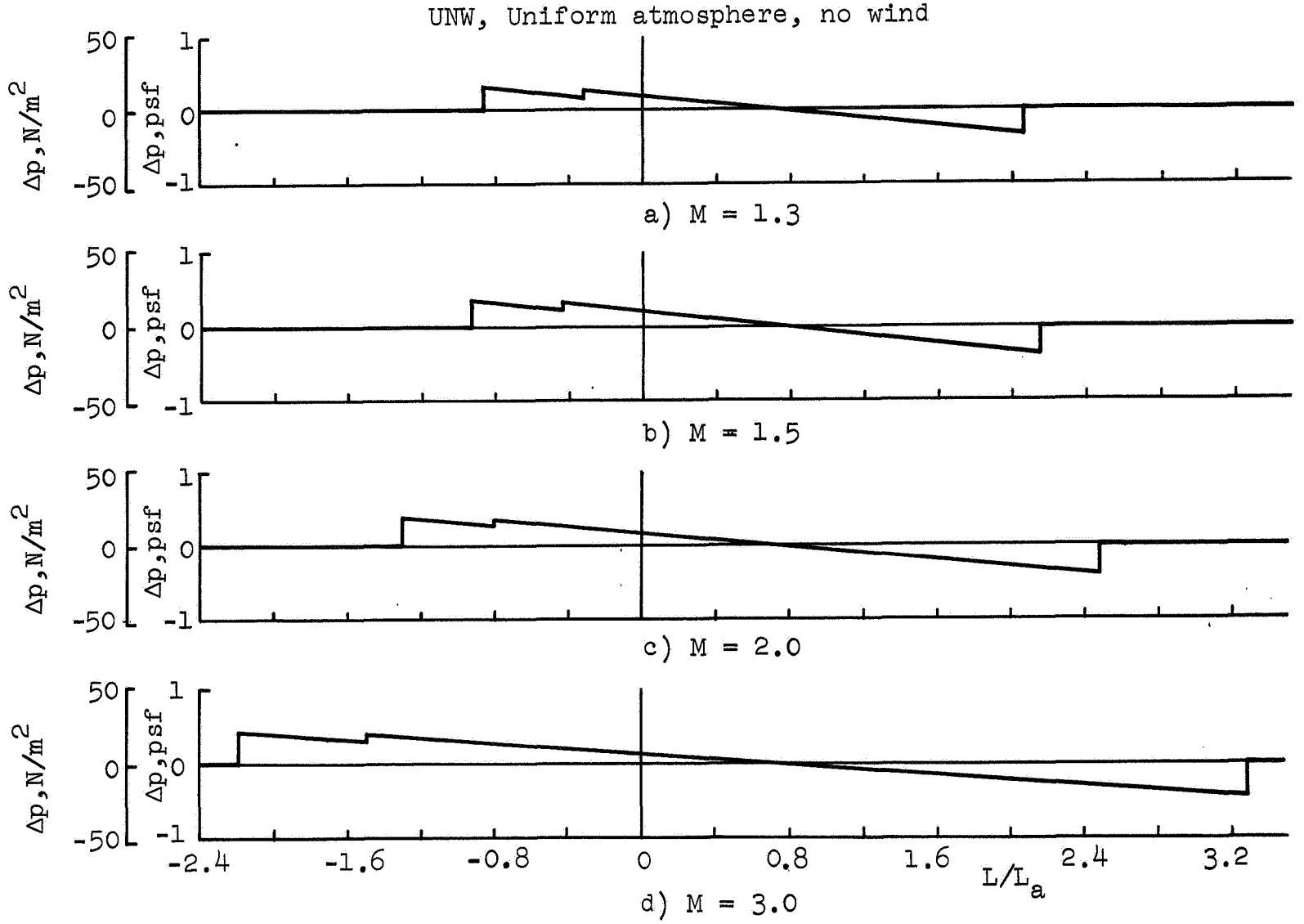

Figure 11. Mach number effects on signature at sea level; F104, h = 40 000 ft (12.2 km)

SLR, Summer lapse rate

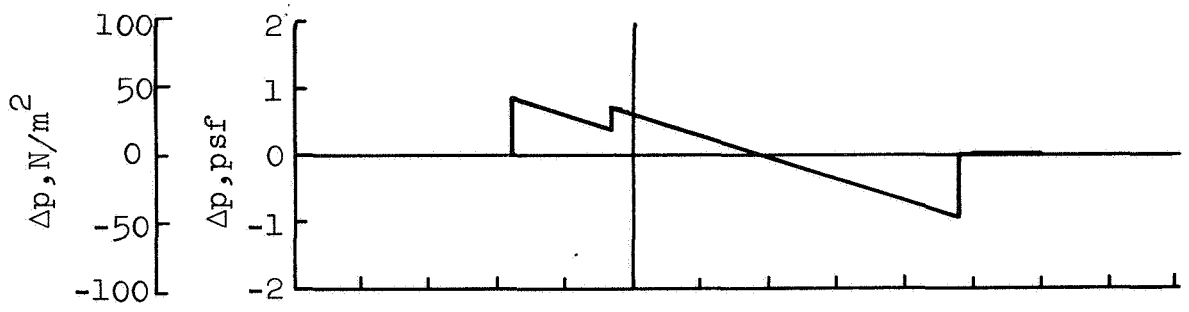

e) M = 1.3

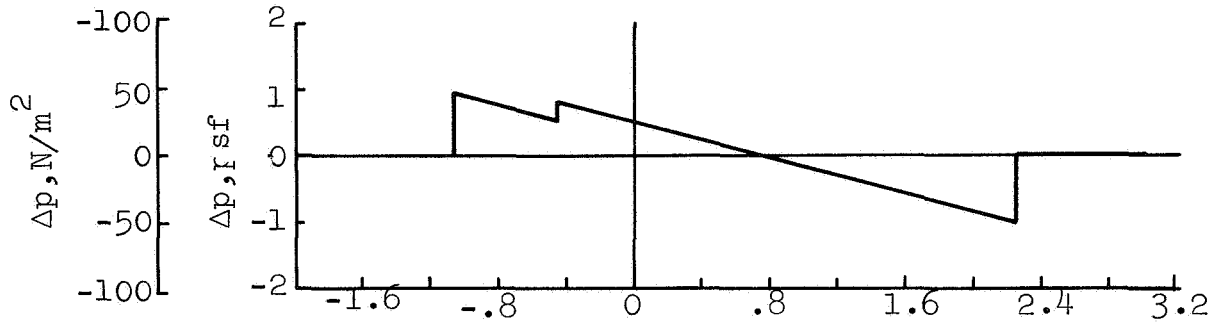

f) M = 2.0

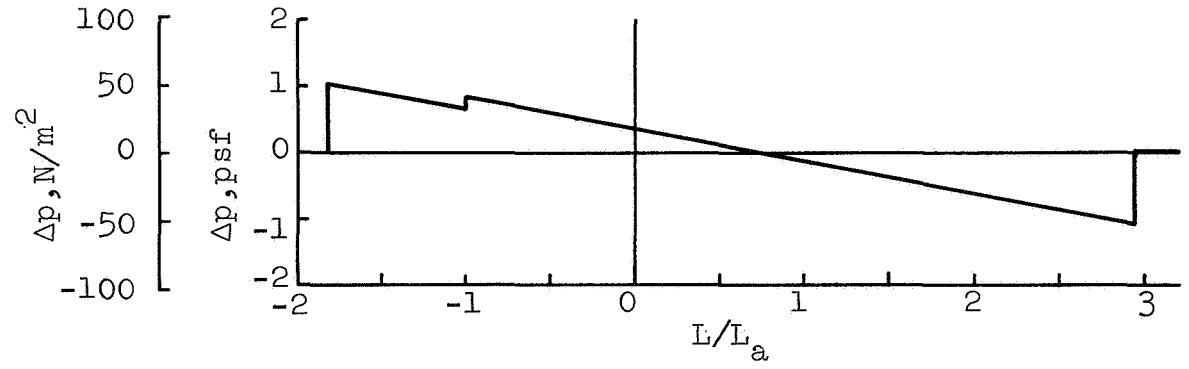

g) M = 3.0

Figure 11. Concluded

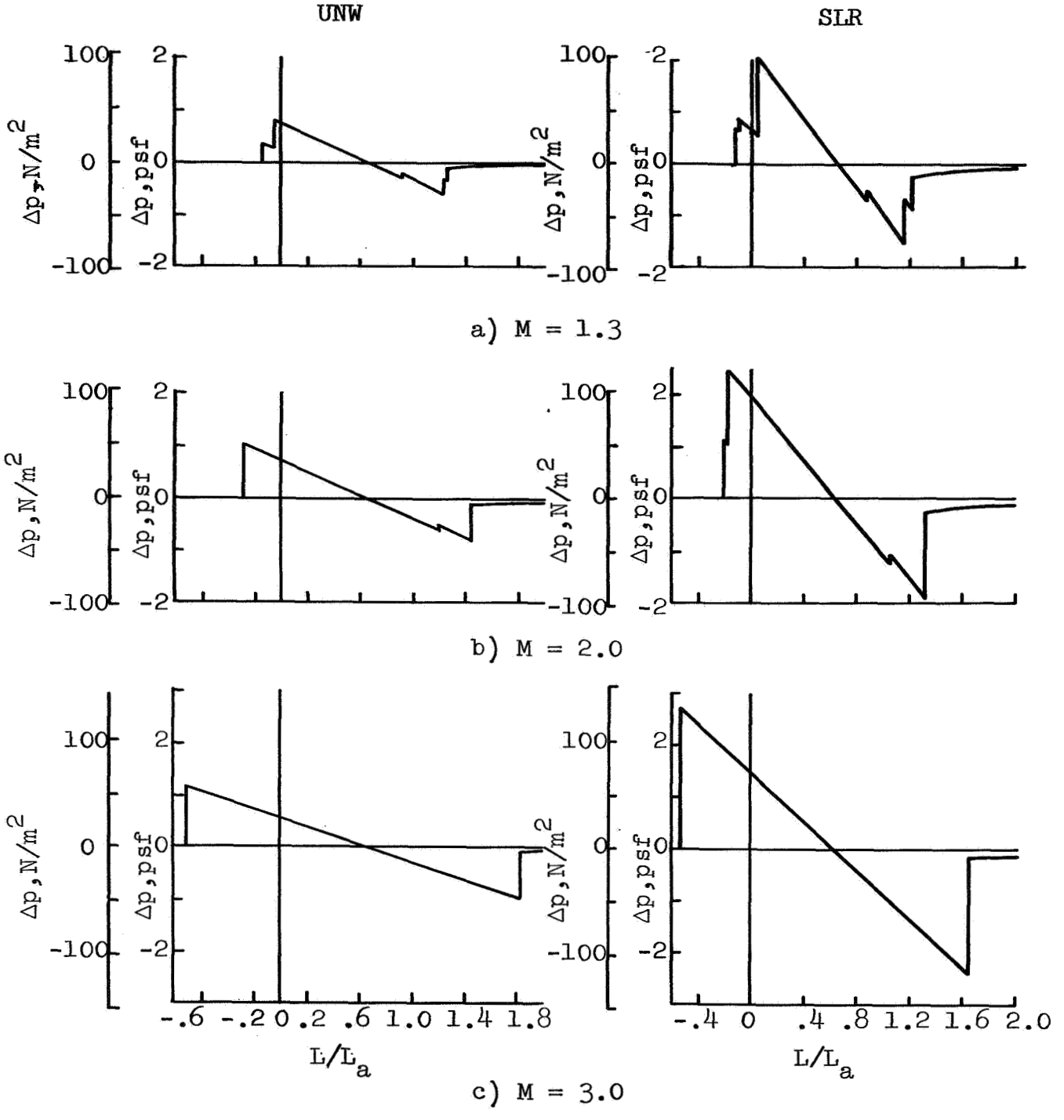

Figure 12. Mach number effects on signature at sea level; SCAT 15-F, h = 40 000 ft (12.2 km)

The Mach number dependence of overpressure is plotted in figures 13 and 14 for various atmosphere and wind conditions; here the overpressure is shown relative to its nominal value at $M = 1.25$, SNW (table III). The wind data normally refer to a headwind, unless stated otherwise. The HAS headwind is shown here to yield very large overpressures near $M = 1.3$ as a result of ray focusing caused by the large wind decrement between the aircraft altitude and the ground. The ray-tube area calculations show that this focusing occurs just above ground level for $M = 1.3$, $h = 40\ 000$ ft (12.2 km). The overpressure deviations in other atmospheres (compared to SNW) are small, except, of course, for the uniform atmosphere (UNW).

Using factors K_A which were derived (ref. 4) to correct UNW solutions to SNW values, the curve labeled UNW x K_A in figure 13 results. It is a good match to the correct SNW values for this set of input data.

In figure 14 are indicated the data calculated at Mach 3 (dashed curve faired into the original curve at Mach 2) using both the $M = 1.4$ and the $M = 2.7$ F-functions of the SCAT 15-F. The $M = 2.7$ F-function yields only slightly larger overpressures. Also, the signatures appear quite similar. Thus, there is some confidence that an F-function computed at a particular Mach number in this range can be accepted as a good approximation at other Mach numbers in this range.

Further comparisons of the influence of atmospheric conditions are indicated in the bar charts of figure 15. As mentioned before, the HAS headwind is critical for this flight condition. The value of the data point shown at an overpressure ratio of 2.0 is not especially unique; it is a value for a flight condition (M,h) where the headwind results in a grazing flight path at a caustic near the ground.[1] The overpressure is sensitive to flight condition here, so that small changes in M or h cause large changes in the overpressure results. The type of wind profile used in this study, where wind speed is lower at ground level than at aircraft altitude, causes larger overpressures in a headwind than with no wind (when the Mach number is small). Tailwinds, on the other hand, result in lower overpressures. The $M = 2$ data shown here are relative to the $M = 1.25$, SNW condition to point out the Mach number effect. Further effects of wind speed and direction are discussed later.

---

[1]At grazing the wave front is perpendicular to the ground so that no reflection occurs and K_r should be taken as unity. For present calculations, $K_r = 1.9$.

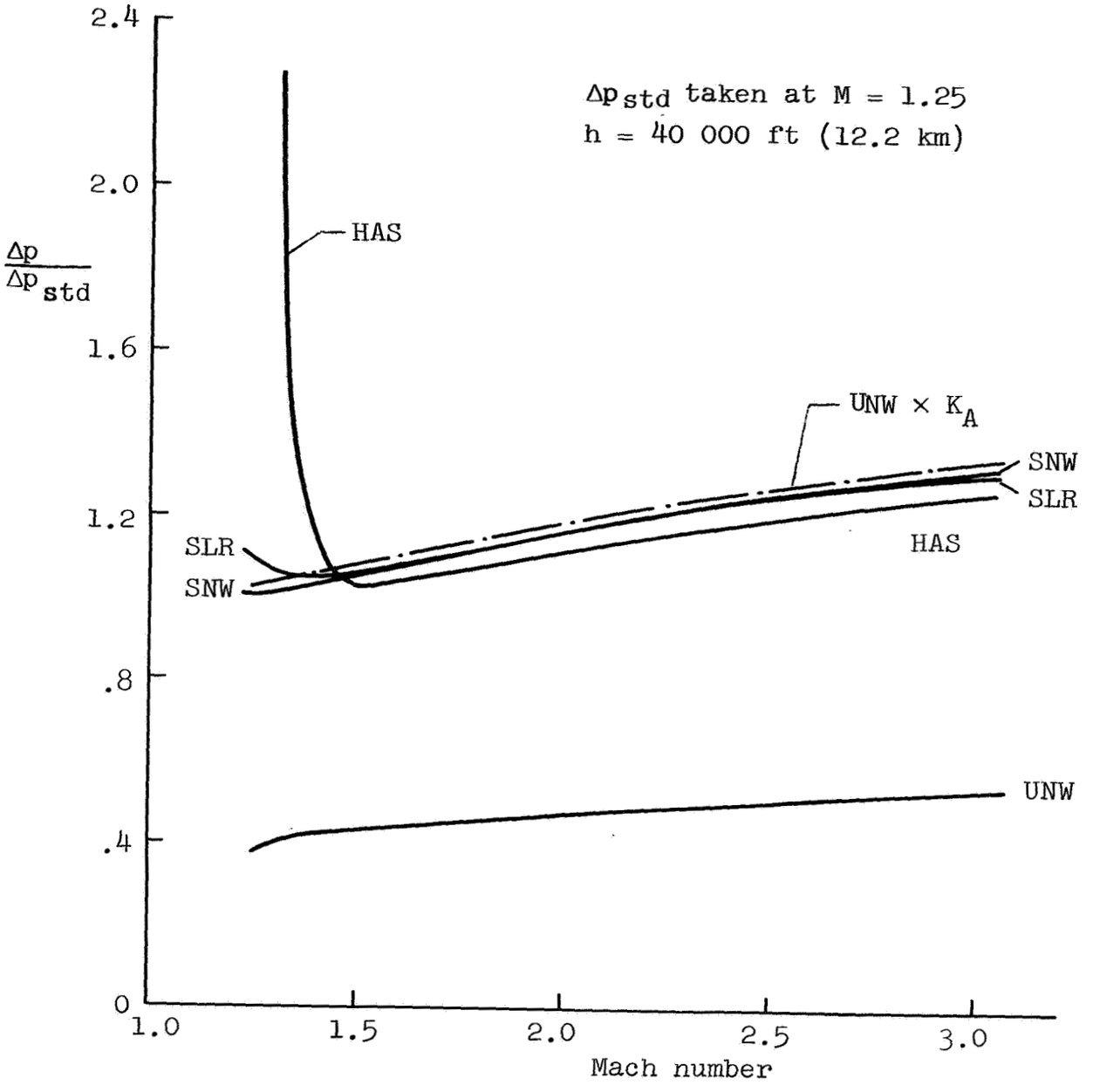

Figure 13. Mach number effects on overpressure ratios; F-104

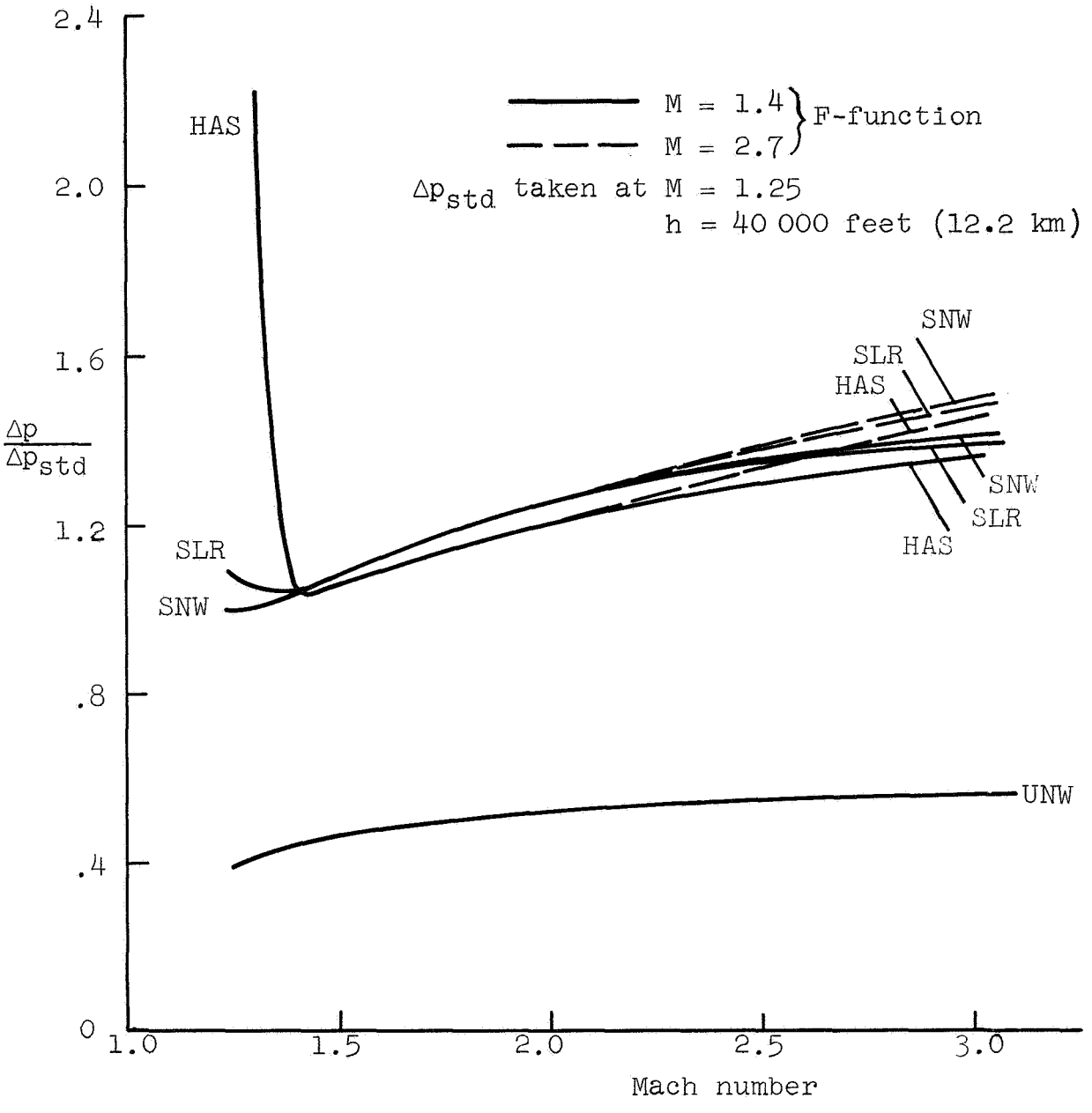

Figure 14. Mach number effects on overpressure ratios; SCAT 15-F

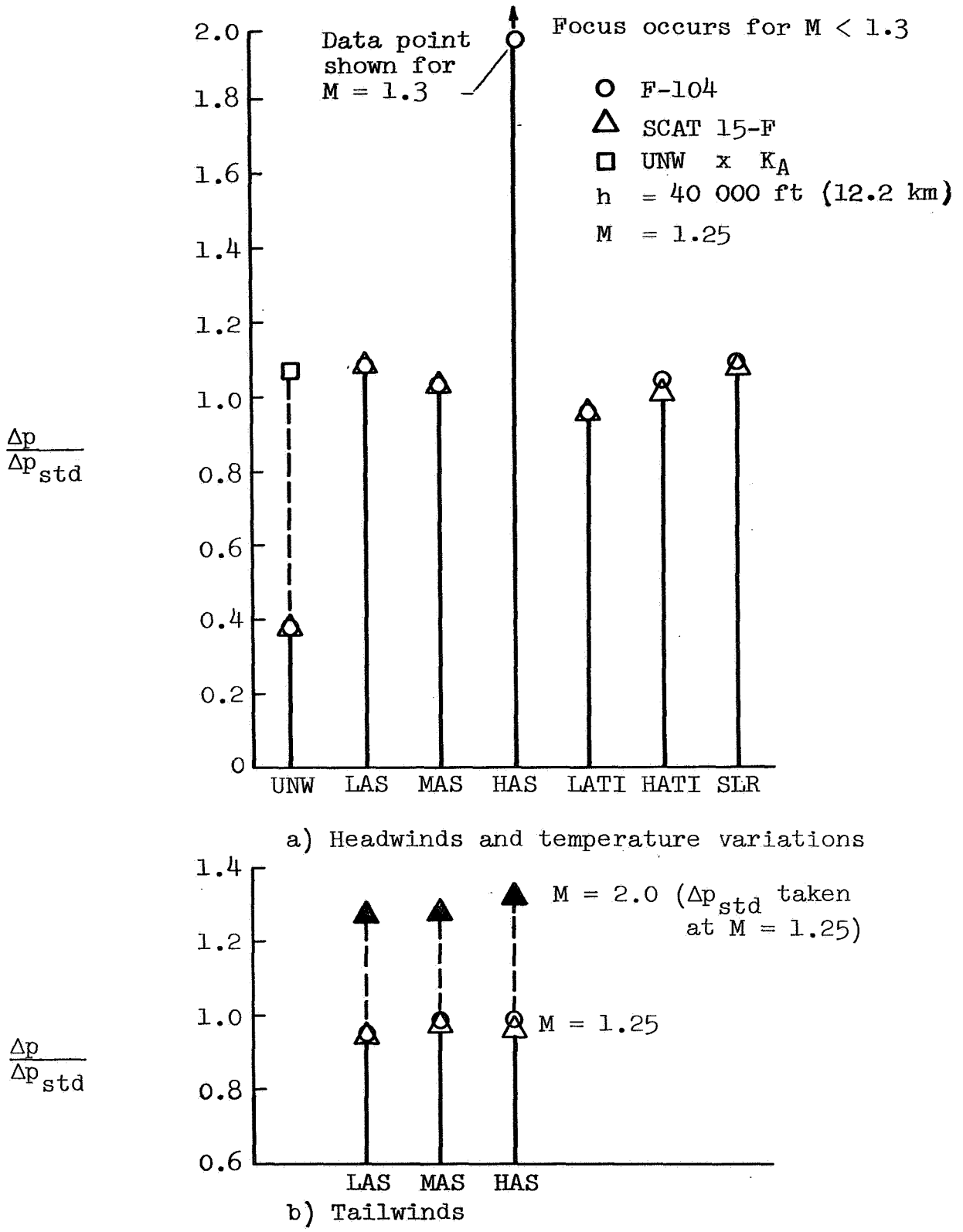

Figure 15. Winds and temperature effects on overpressure

Signature distortion during propagation.- Near the aircraft the acoustic signal has essentially the form of the F-function. As the acoustic signal propagates away from the aircraft (along a ray path (fig. 3)), it is distorted because of a weak nonlinear effect caused by differences in propagation speed. These differences are dependent on the local signal strength (pressure level above or below ambient) which is a function of phase. The distortion is a cumulative effect which results in formation and merging of shock waves. The amount of distortion is governed by an age variable τ defined in reference 1 (eq. 46). The age variable is an integral which is, in part, proportional to the distance traversed and inversely proportional to the half-power of atmospheric density times the ray-tube area; that is,

$$\tau \propto \int dz/\sqrt{\rho A}$$

Thus the age of the signal increases with distance, but at a slower rate if the rays are propagating downward into a region of larger density. If ray focusing is approached ($A \rightarrow 0$), the age variable tends to increase; in other words, the pressure signature tends to be more distorted. An analogous statement is that the phase shift of the signal becomes greater as the age increases. The distortion of the signature (phase shift) also tends to increase with Mach number (ref. 1, eqs. (45), (46), and (49)).

The results of calculations of the pressure signature as it propagates downward from the aircraft are shown in figures 16 and 17 for flight at 40 000 ft (12.2 km) and in figure 18 for flight at 25 000 ft (7.6 km). The altitudes (h_g) for displaying the signatures were selected to illustrate the rapid formation and merging of shock waves near the aircraft. For example, in figure 18a the signature only 500 ft (150 m) below the aircraft has developed six shock waves. During the next 500 ft (150 m) (fig. 18b) two pairs of shocks have merged, leaving four shocks. The two trailing shocks here later merge, so that the signature at ground level (fig. 18c) contains three shocks. So that comparisons with ground signatures are consistent, the midfield solutions are shown here with $K_R = 1.9$.

The major effects of aging (distortion) occur within 5000 ft (1.5 km). The rapid increase in the age variable near the flight altitude is shown in figure 19 along with the ray-tube area for aircraft altitudes of 40 000 and 80 000 ft (12.2 and 24.4 km). Results for uniform atmospheres (UNW) are shown for comparison with those for the standard atmosphere (SNW). In the uniform atmosphere, the ray-tube area increases linearly as the ray-path altitude decreases to sea level ($z = 0$). The age variable continually increases with $(\sqrt{z_o} - \sqrt{z})$. In the standard atmosphere the area deviates from linearity with z because of the density increasing

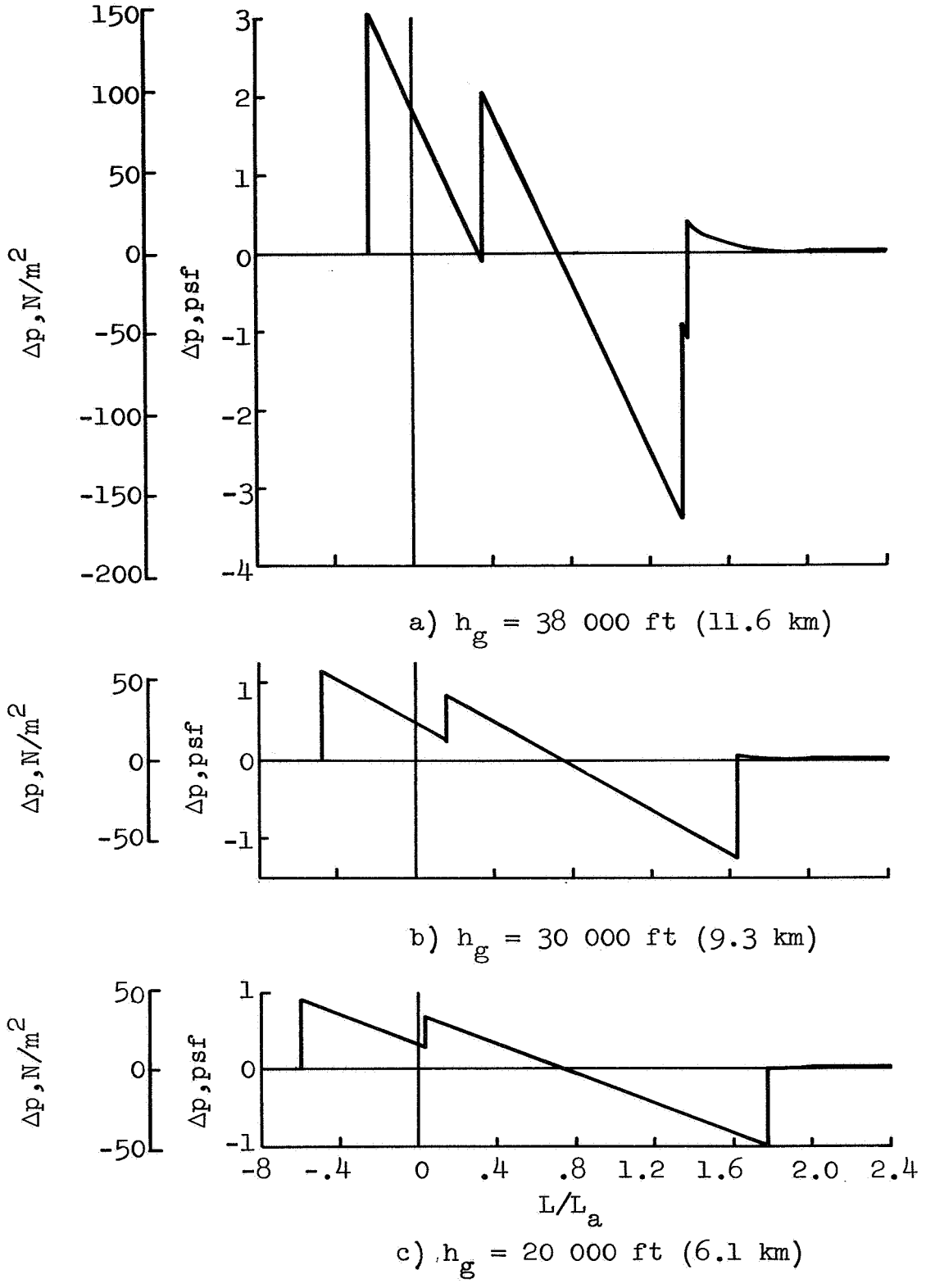

Figure 16. Signature during descent from aircraft at 40 000 ft (12.2 km); F-104, M = 1.25

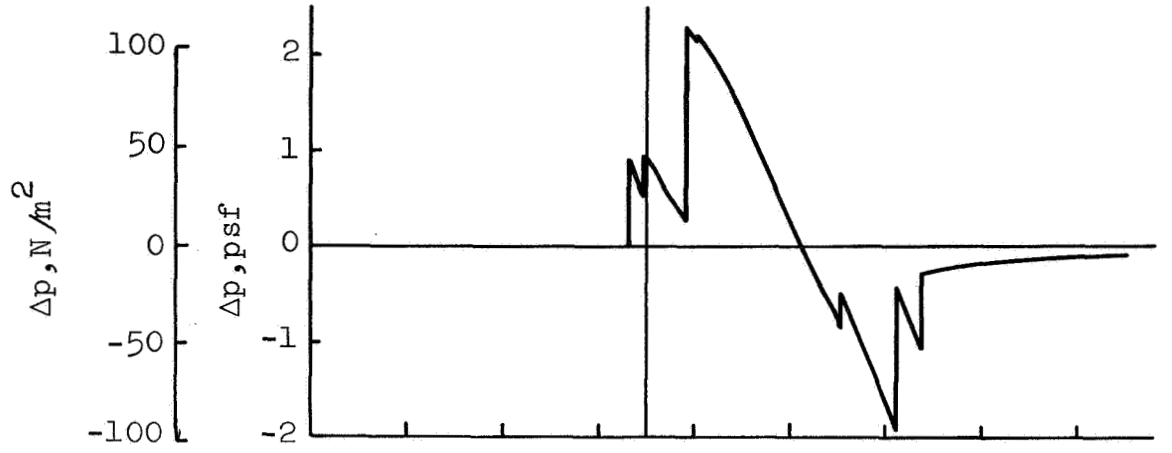

a) h_g = 30 000 ft (9.3 km)

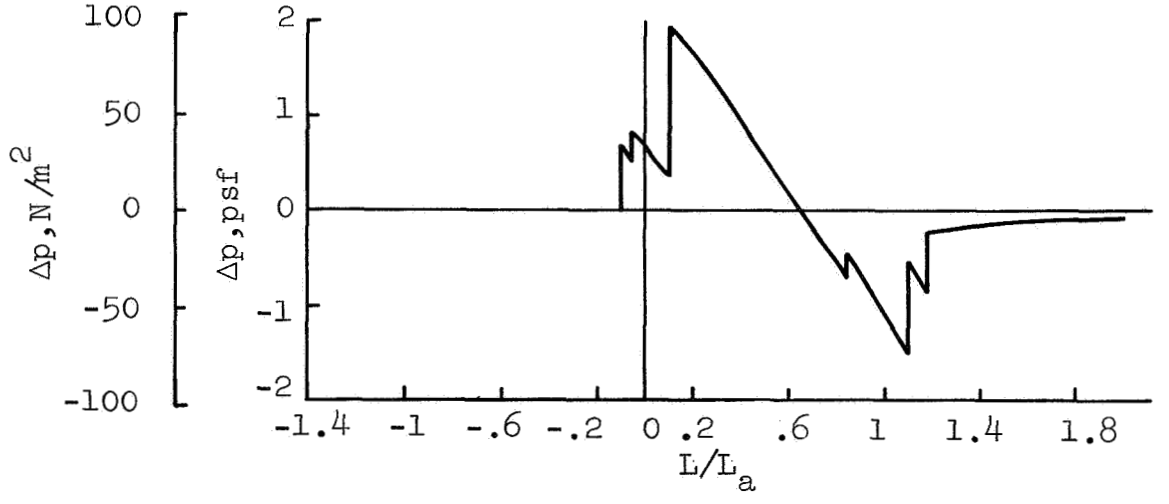

b) h_g = 20 000 ft (6.1 km)

Figure 17. Signature during descent from aircraft at 40 000 ft (12.2 km); SCAT 15-F, M = 1.25

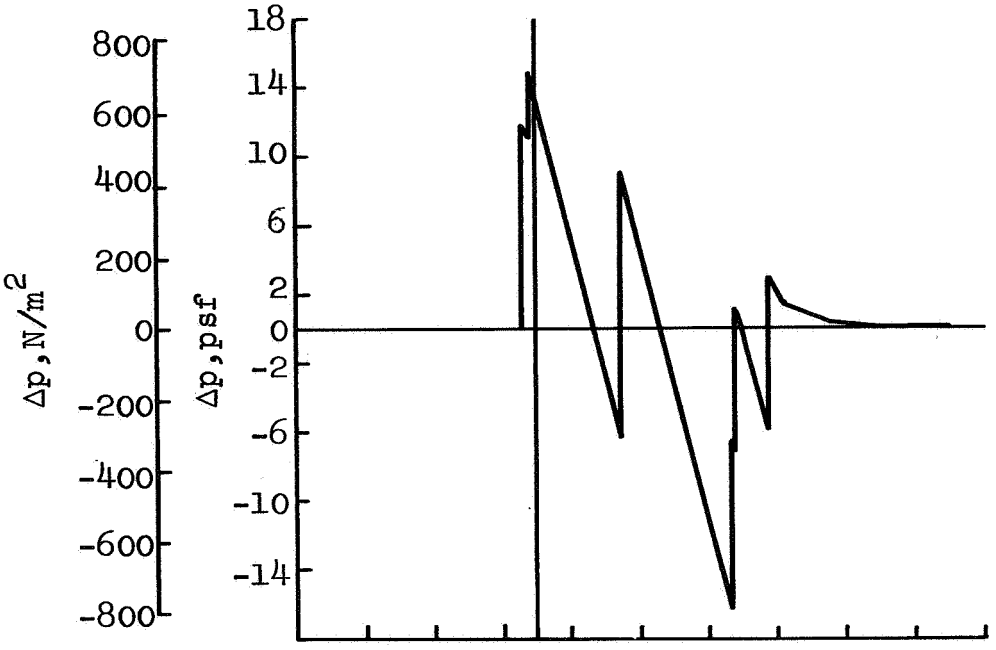

a) h_g = 24 500 ft (7.5 km)

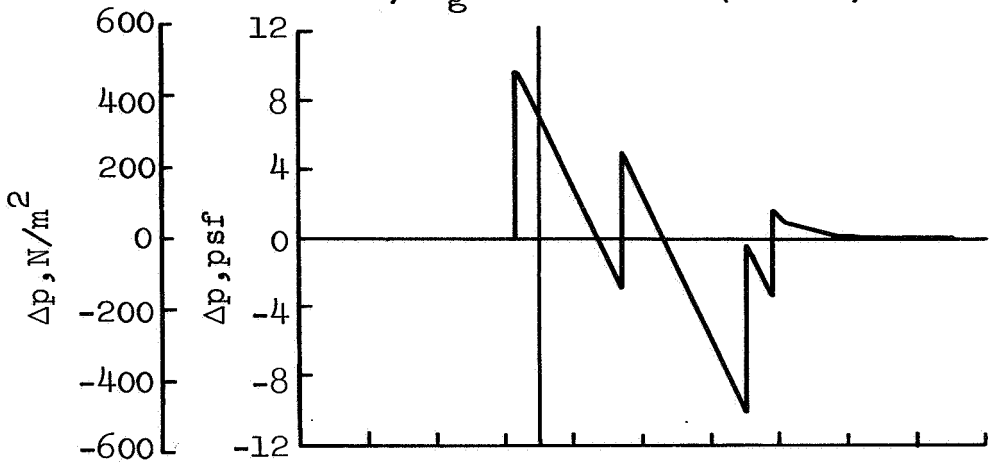

b) h_g = 24 000 ft (7.3 km)

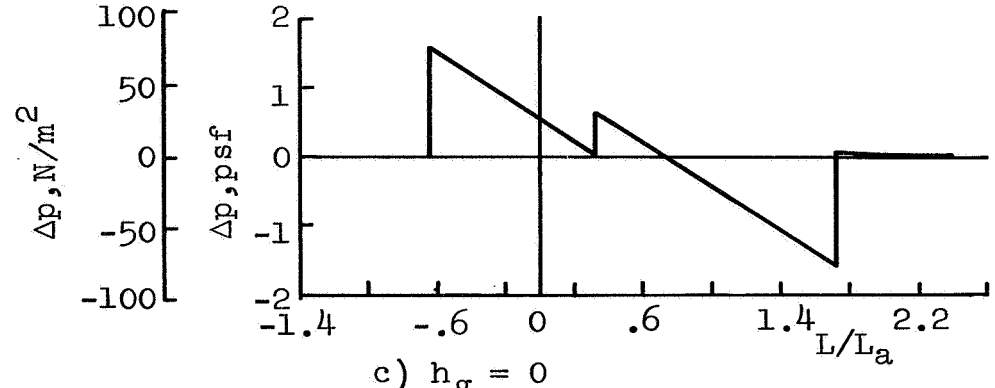

c) h_g = 0

Figure 18. Signature during descent from aircraft at 25 000 ft (7.6 km); F-104, M = 1.25, LAS

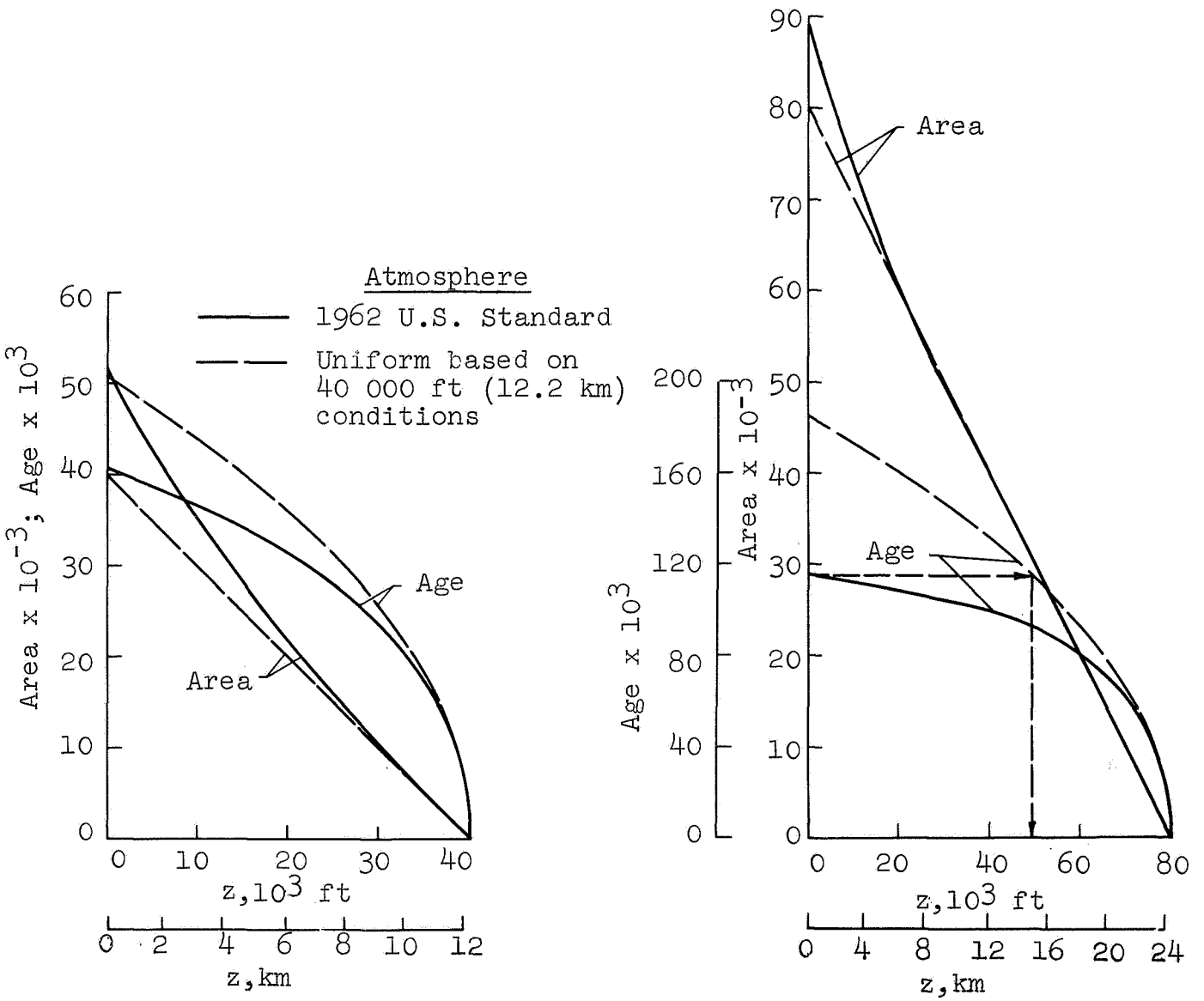

a) h = 40 000 ft (12.2 km) b) h = 80 000 ft (24.4 km)

Figure 19. Variation of ray-tube area and age variable with altitude

at lower altitudes. The age variable increases but tends towards an asymptotic limit. For propagation from high altitudes (fig. 19b) the age variable approximately one scale-height[2] below the aircraft (z = 50 000 ft) (15.2 km) is close to the asymptotic value of the age variable (~ z = 0) for the standard atmosphere. This is an illustration that the asymptotic age in a real atmosphere has a finite limit (ref. 1). The signature distortion, then, need not develop to the extent of the classic N-wave. In the uniform atmosphere, on the other hand, the age variable is not limited, and the asymptotic solution always yields an N-wave.

The overpressure ratios for both aircraft are presented in figures 20a and 21a as a function of the altitude of the signature for nominal flight conditions (M = 1.25, h = 40 000 ft (12.2 km)). As mentioned before, the rays focus before reaching the ground for the high altitude wind shear (HAS) environment as a headwind. Thus, high overpressures are realized near the ground for aircraft flying near 40 000 ft (12.2 km) at Mach numbers near 1.3 for this wind.

The variations of signature length ratio L_1 for the above flight conditions are shown in figure 22a. The ray-path travel time t from the aircraft to the stated altitude h_g is given in figure 23a, and the ground distance y traversed in this time by the ray path is given in figure 24a. The ray path is independent of the aircraft type.

Effects of Aircraft Altitude.- Overpressure, signature length and ray-path results are shown in figures 20b through 24b as functions of aircraft altitude. These data are for M = 1.25 except where noted otherwise.

In figures 20b and 21b, solid curves present the variation of the overpressure ratio for three atmospheres, UNW, SNW, and HAS. Data points are shown for SLR. In addition, a dashed curve shows the overpressure ratio obtained by multiplying the UNW values by the altitude-dependent atmospheric correction factor K_A of reference 4 (UNW times K_A). In figure 20b, this curve agrees well with the SNW curve, indicating that these K_A factors applied to UNW results yield good approximations to the realistic atmosphere (SNW) results for this F-104 flight condition. In figure 21b, the corresponding comparison for the SCAT 15-F is not as good, the actual overpressures (SNW) being as much as 10% lower than the approximation (UNW times K_A).

The changing curvatures in these curves, including the dip

---

2) Density scale height is the altitude increment in which the density changes by a factor e = 2.718....; it is about 21 000 ft (6.4 km) in the standard atmosphere.

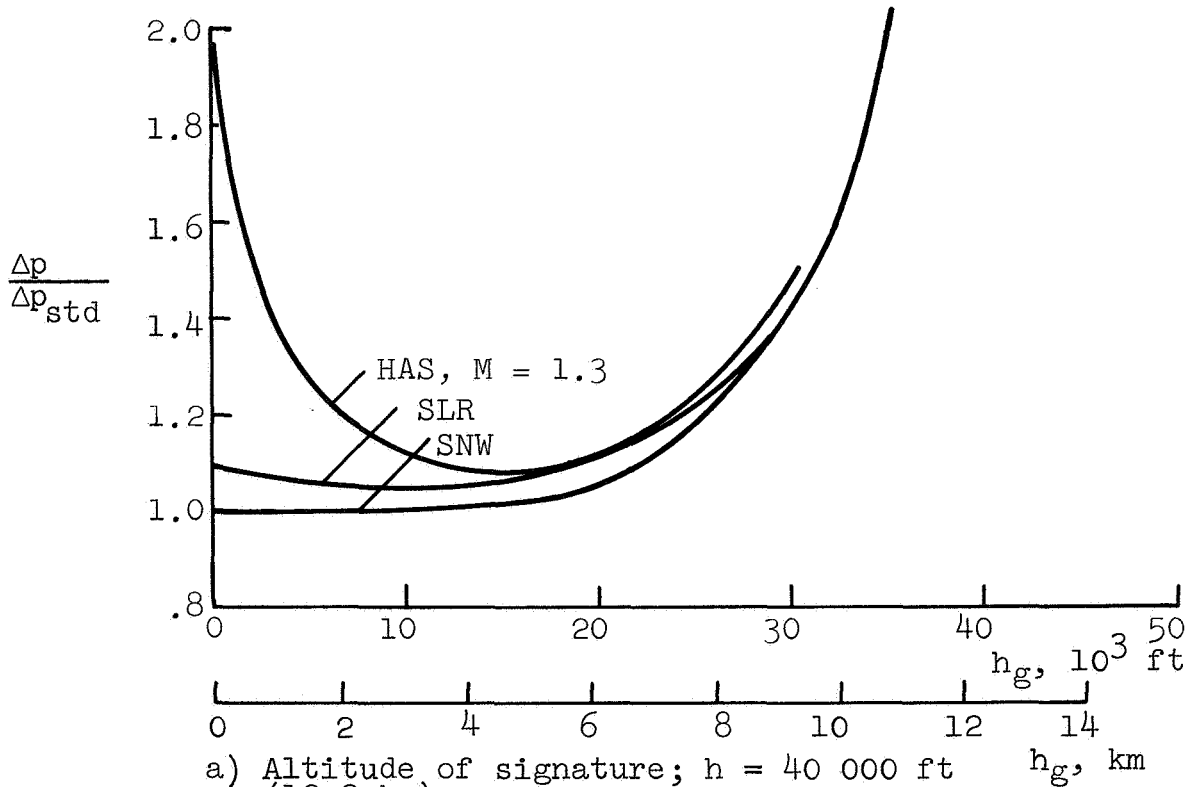

a) Altitude of signature; h = 40 000 ft (12.2 km)

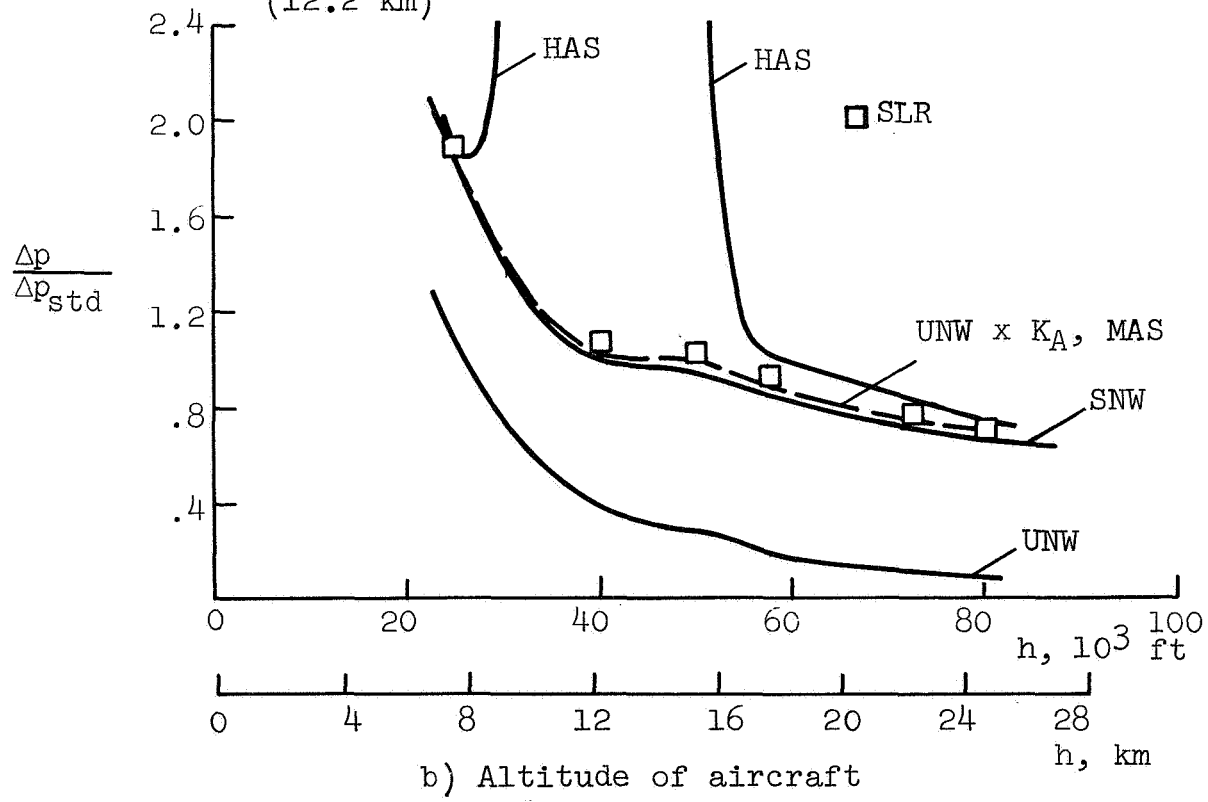

b) Altitude of aircraft

Figure 20. Effects of altitudes of signature and aircraft on overpressure ratios; F-104

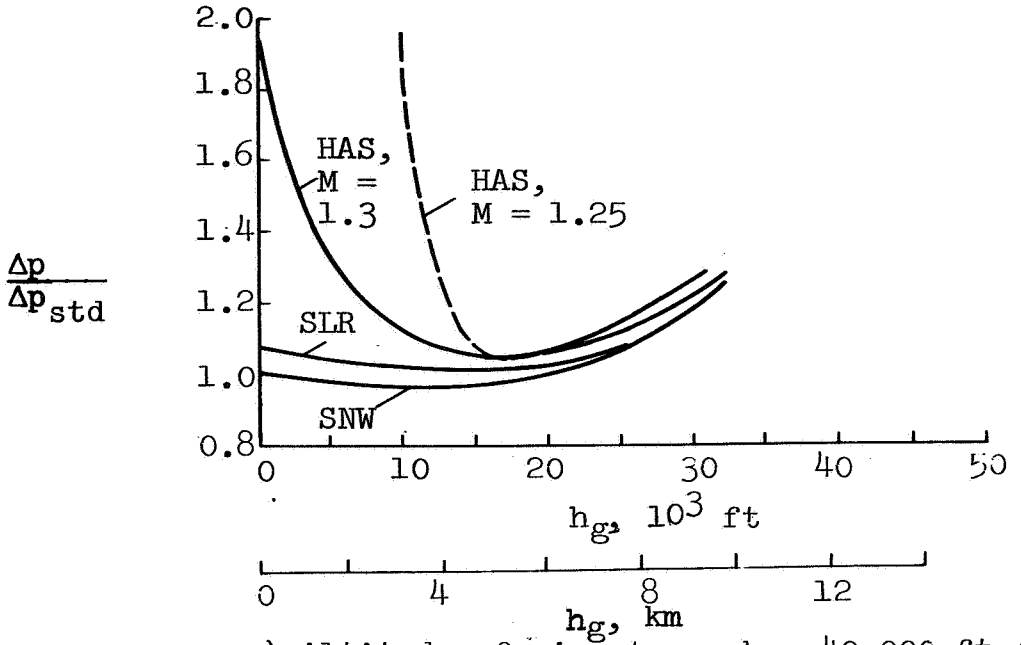

$\frac{\Delta p}{\Delta p_{std}}$

a) Altitude of signature, h = 40 000 ft (12.2 km)

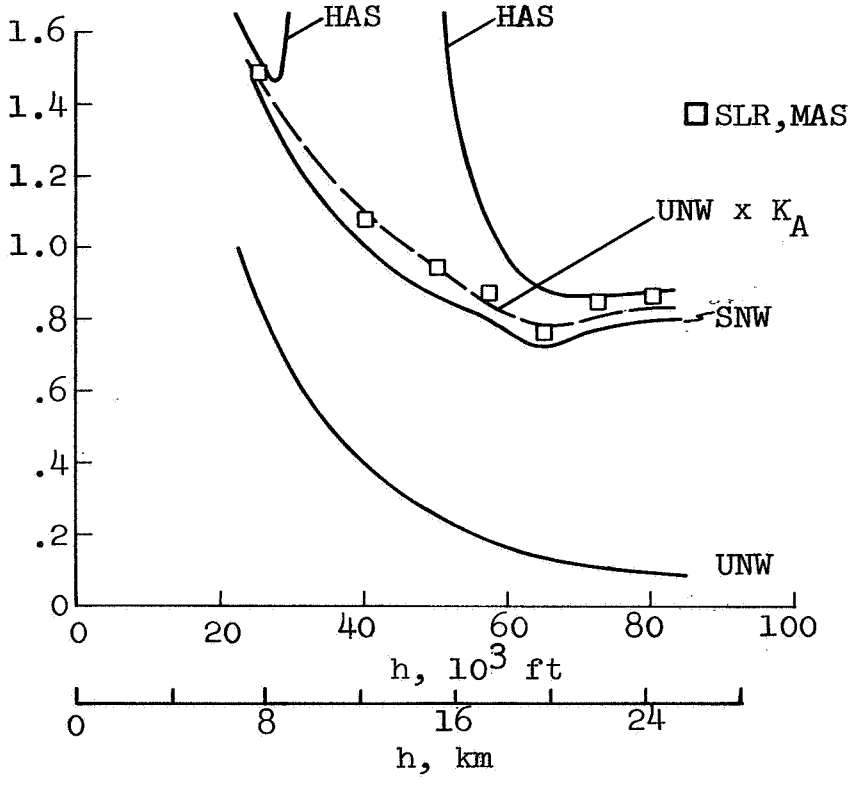

$\frac{\Delta p}{\Delta p_{std}}$

b) Altitude of aircraft, $h_g = 0$

Figure 21. Effects of altitudes of signature and aircraft on overpressure ratios; SCAT 15-F

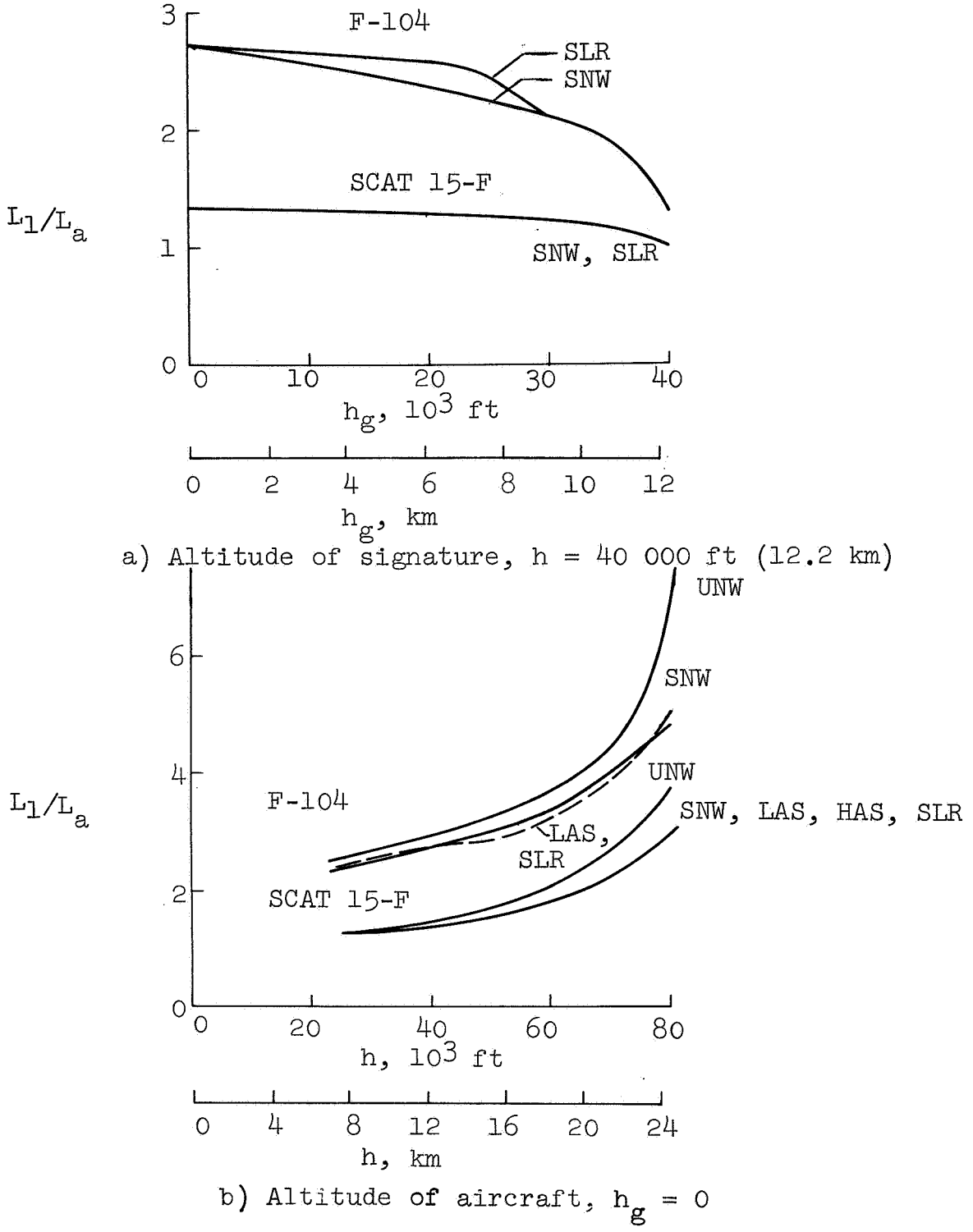

Figure 22. Effects of altitudes of signature and aircraft on signature length

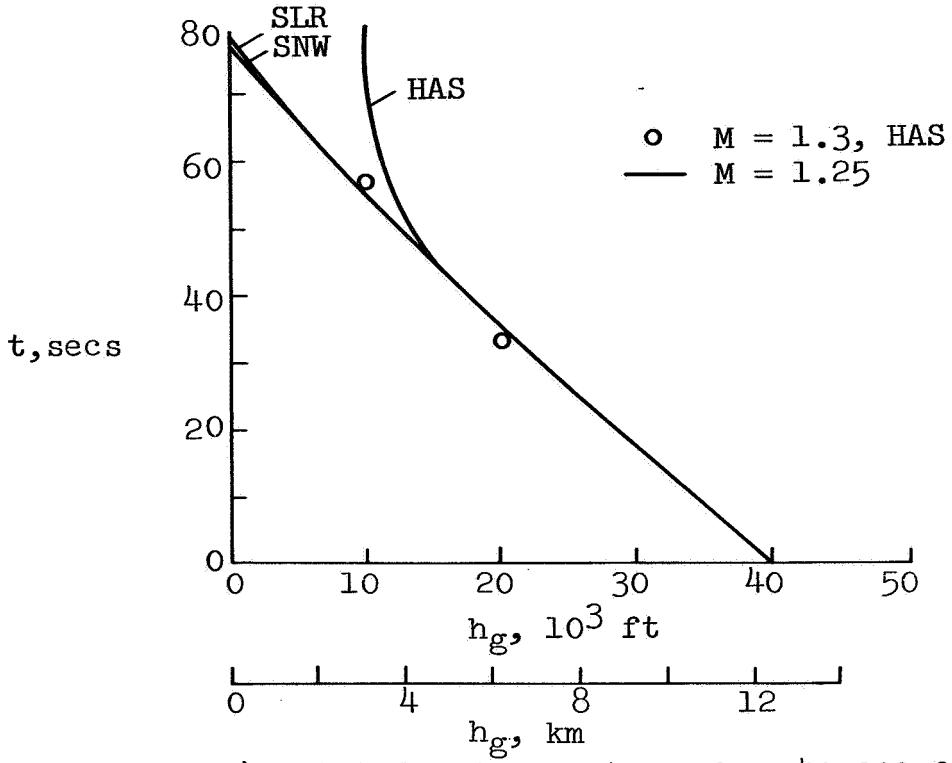

a) Altitude of signature, h = 40 000 ft (12.2 km)

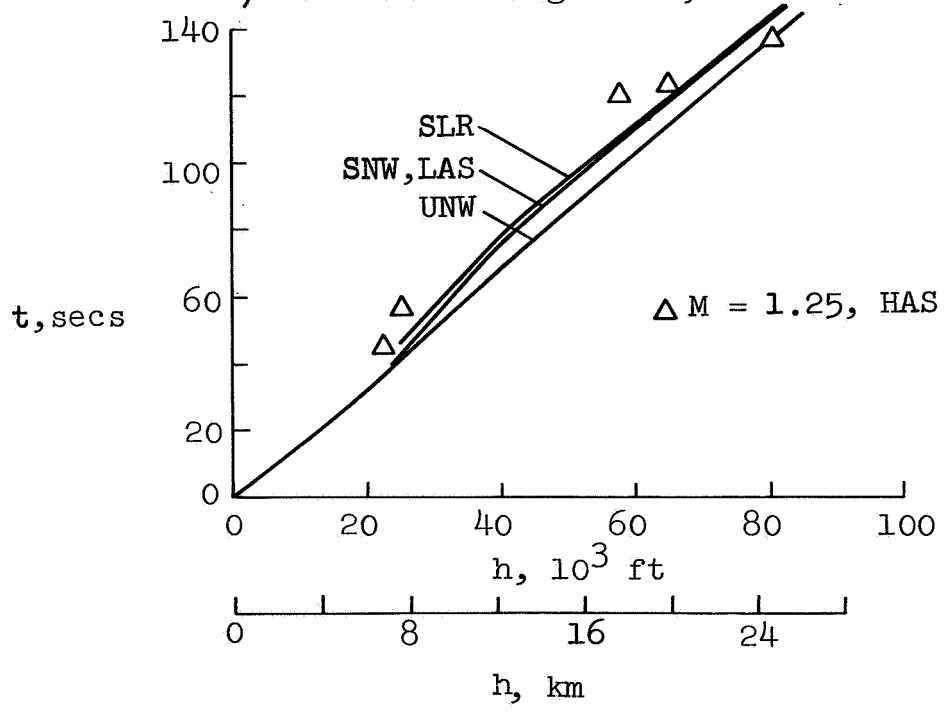

b) Altitude of aircraft, $h_g = 0$

Figure 23. Effects of altitudes of signature and aircraft on ray travel time

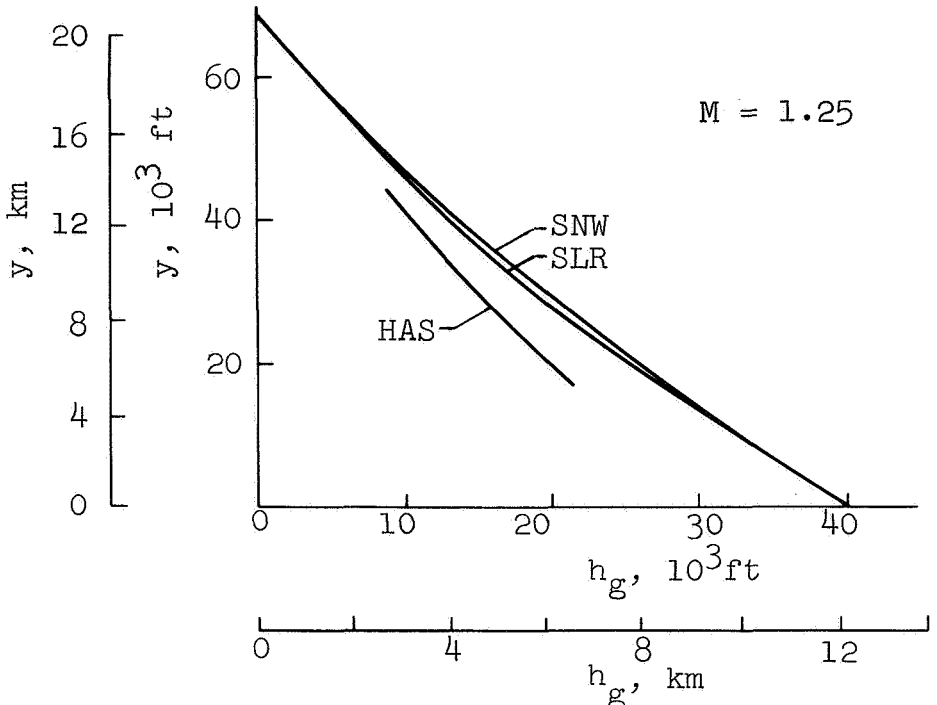

a) Altitude of signature, h = 40 000 ft (12.2 km)

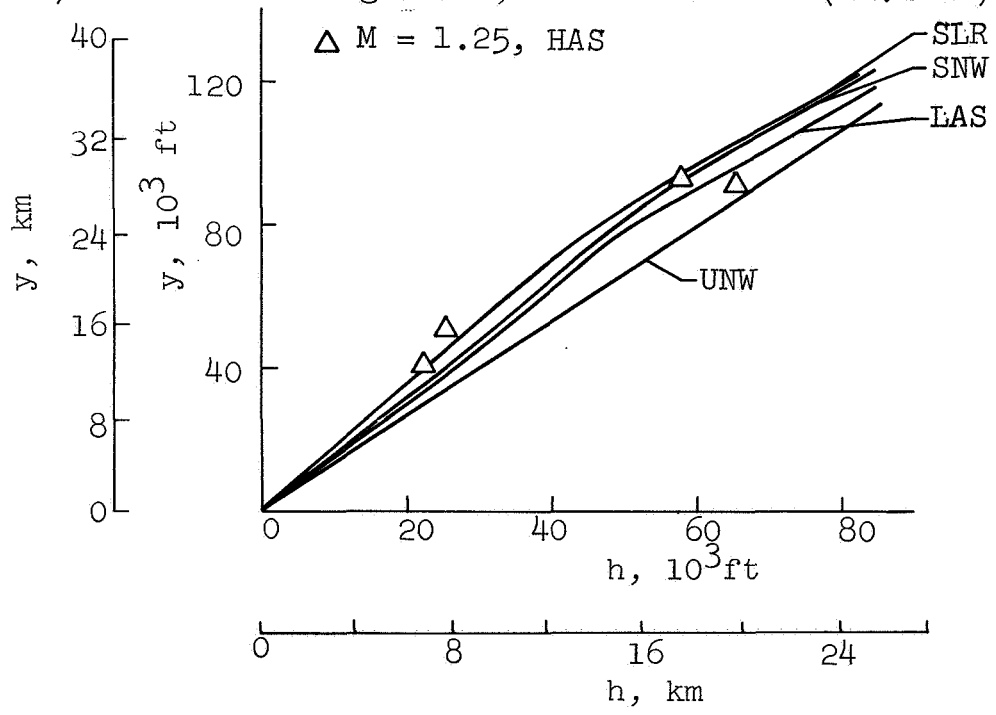

b) Altitude of aircraft, $h_g = 0$

Figure 24. Effects of altitudes of signature and aircraft on ray ground distance

in the SCAT 15-F curves at 65 000 ft (19.8 km), arise from the manner of development and merging of the shock waves in the complete signature. These would not become evident if only the strength of the leading shock (an N-wave approximation) had been calculated. These results show that one should calculate overpressures without the uniform atmosphere or N-wave assumptions for specific aircraft flight considerations.

For the high altitude wind shear (HAS), large overpressures occur for aircraft altitudes between 30 000 and 50 000 ft (9.2 and 15.2 km). In this altitude range the aircraft are flying into a high speed wind and the rays converge significantly as they propagate towards the ground where the wind speed is much smaller. The two branches of the HAS curves occur because of the effect of the jet stream on the ray paths. For the aircraft altitudes just above the jet stream, the ray paths become horizontal before reaching the ground.

In figure 22b, the signature length L_1 is shown to be larger for UNW than for the realistic atmospheres (SNW and others) throughout the range of aircraft altitudes. This difference is larger for the higher altitudes as can be expected because of the larger difference in age between UNW and SNW atmospheres, as shown in figure 19.

The pressure signatures at sea level for several aircraft altitudes are presented in figures 25 and 26. The older age of the high altitude signatures is evident by their longer length and smaller strength, together with the merging of the shock waves.

Effects of Mach number.- Variations of pressure signature and overpressure ratios with Mach number have already been introduced in figures 11, 12, 13, and 14, and in table III. The signatures of figures 11 and 12 illustrate the greater distortion exhibited by those of the larger Mach numbers. This is a result of the phase shift increasing with Mach number, mentioned previously. Summary curves showing the Mach number effects on signature length, ray travel time, and ray-path ground distance are given in figures 27, 28, and 29, respectively. As indicated in figure 27, and supported by further data in table II, signature lengths obtained using UNW are significantly longer than signature lengths calculated using a realistic atmosphere (e.g., SLR or SNW) over the entire range of Mach numbers (and altitudes, see above). This difference is larger at the higher Mach numbers because the signature aging (distortion) increases with Mach number.

Temperature effects.- Some effects of varying the temperature environment were shown in figure 15. Additional data are presented in table IV and figure 30 for various Mach numbers. Results which are presented in reference 4 are compared with

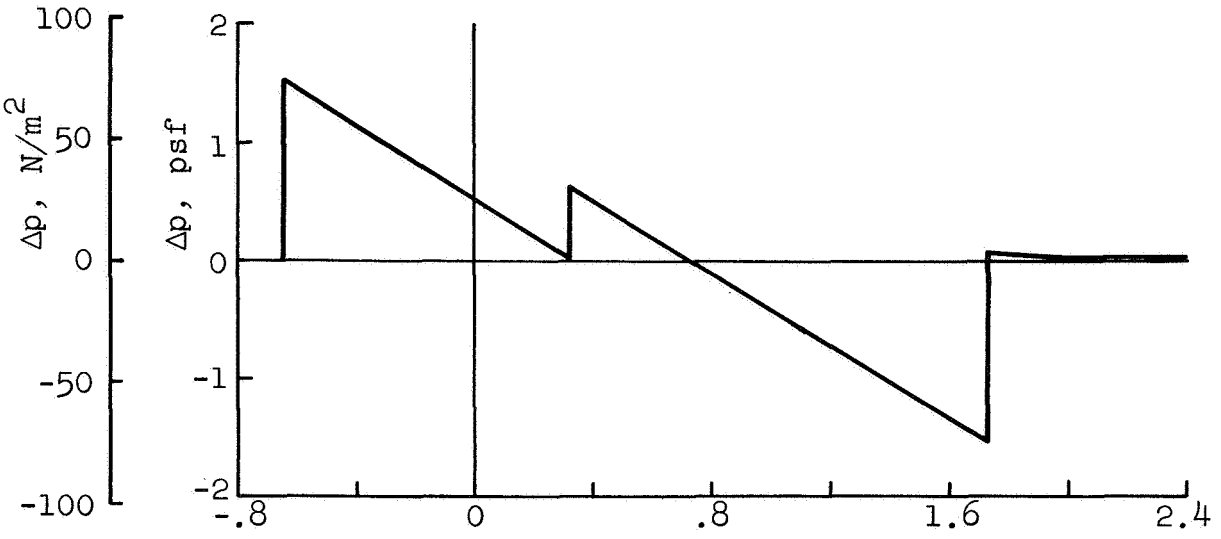

a) h = 25 000 ft (7.6 km)

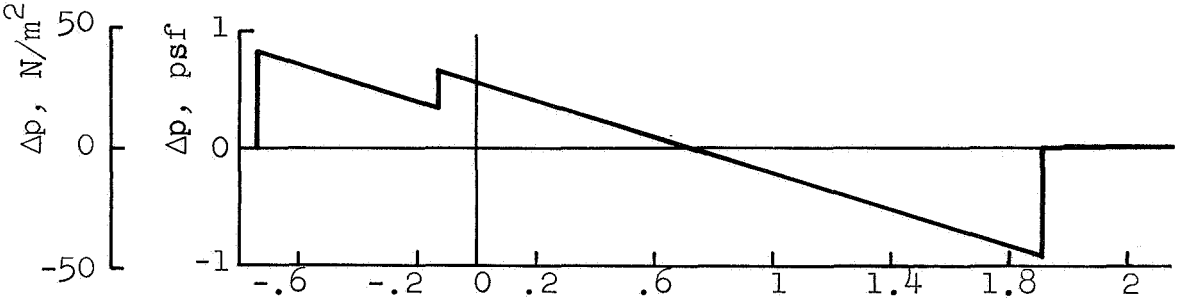

b) h = 40 000 ft (12.2 km)

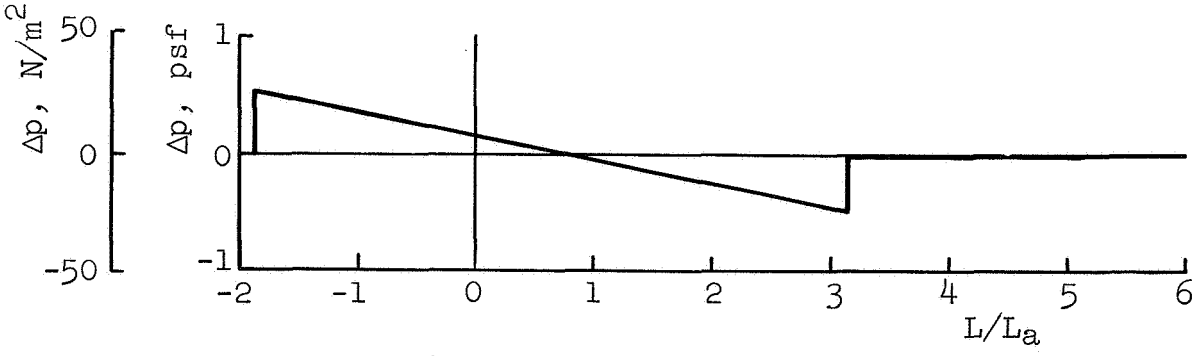

c) h = 80 000 ft (24.4 km)

Figure 25. Signature at sea level for several aircraft altitudes; F-104, M = 1.25

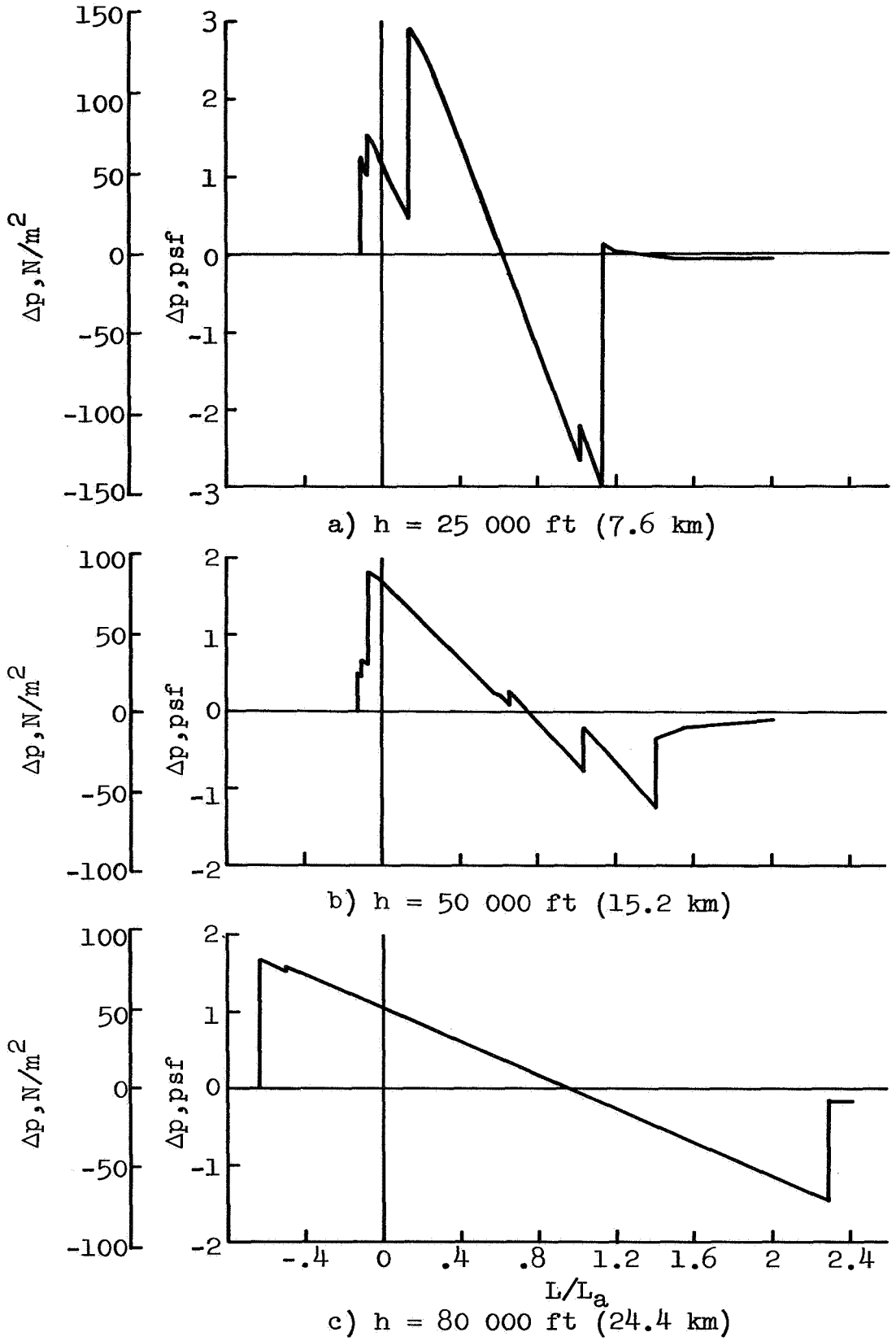

Figure 26. Signature at sea level for several aircraft altitudes; SCAT 15-F, M = 1.25, SLR

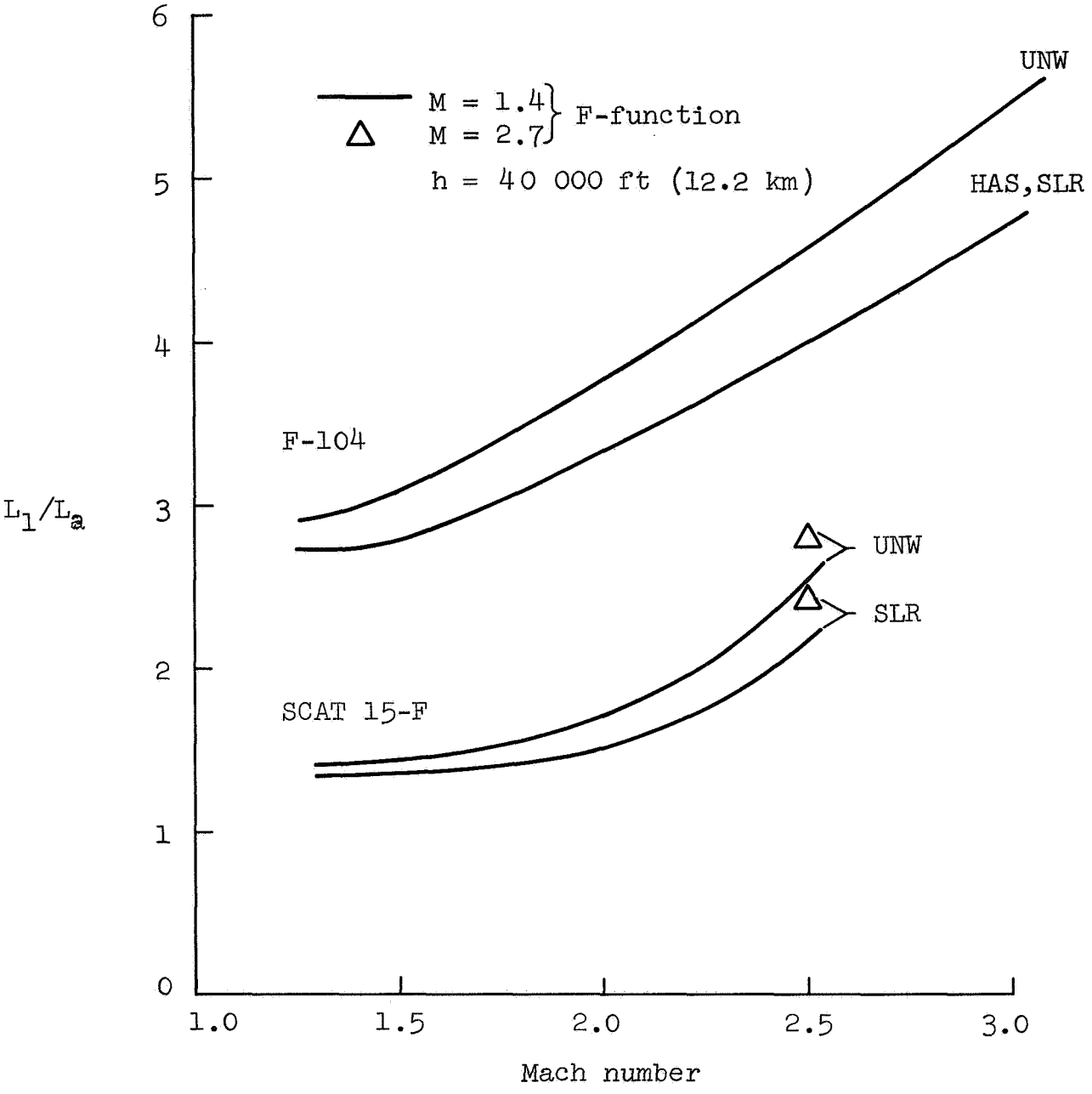

Figure 27. Mach number effects on signature length

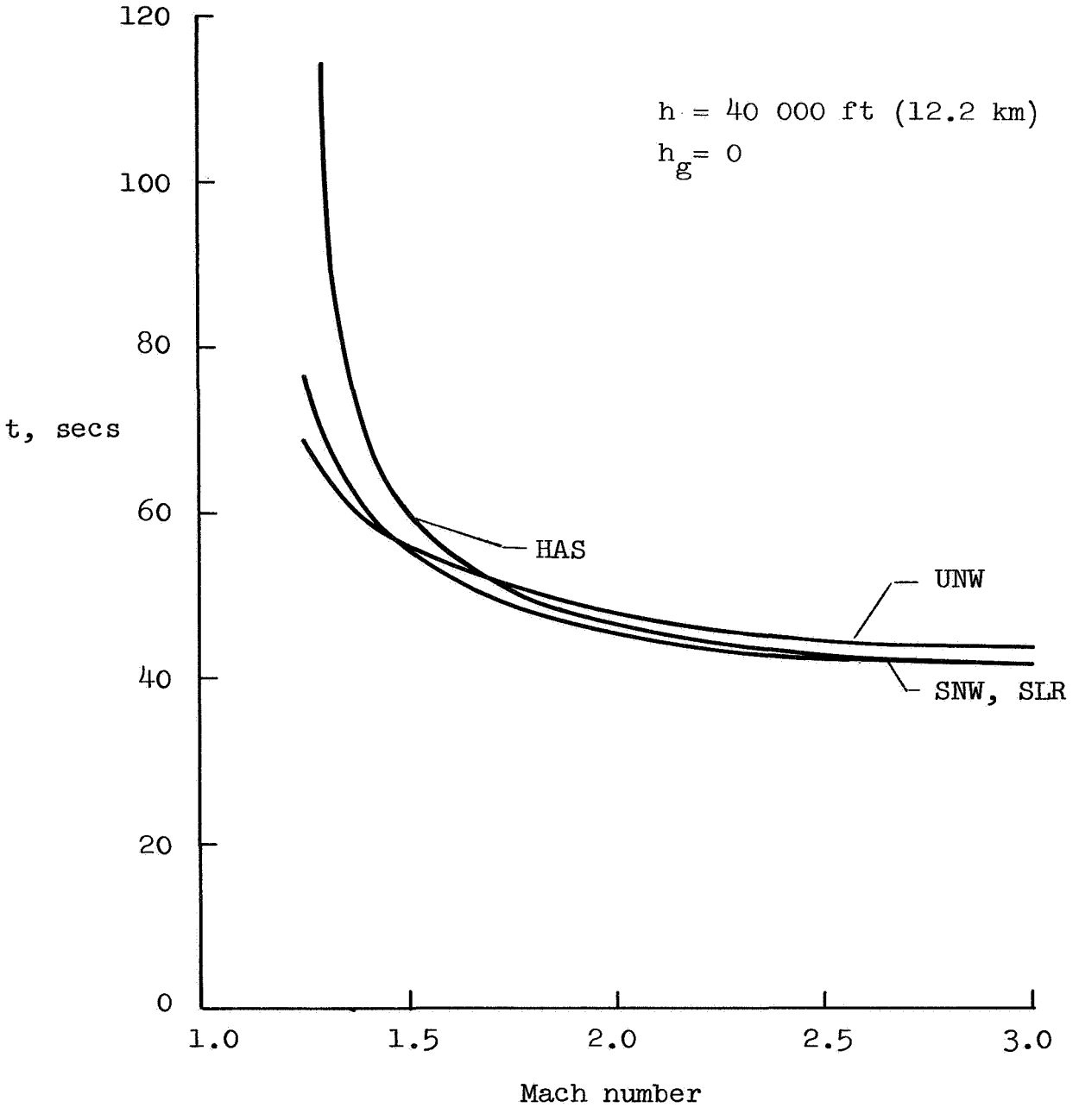

Figure 28. Mach number effects on ray travel time

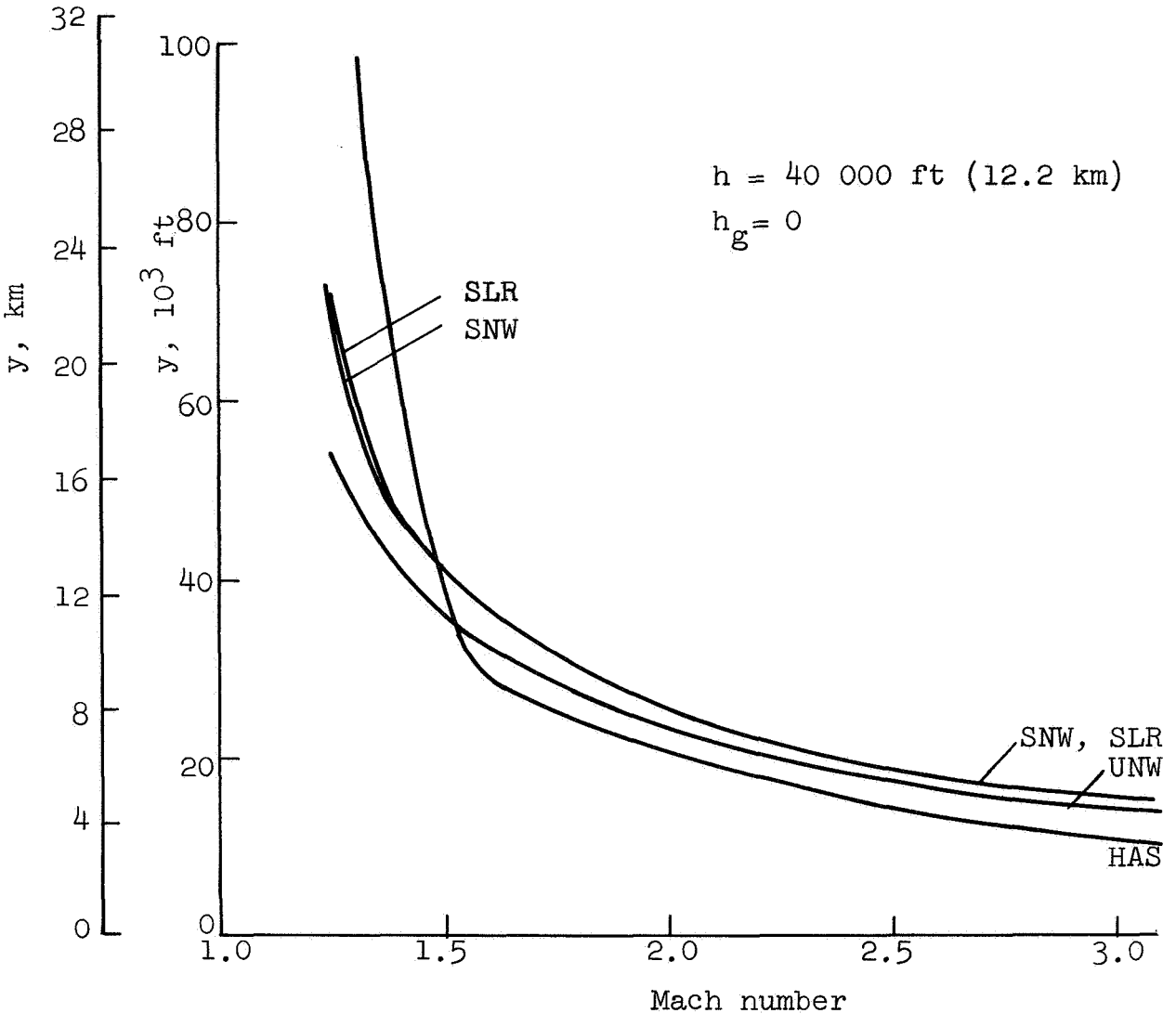

Figure 29. Mach number effects on ray ground distance

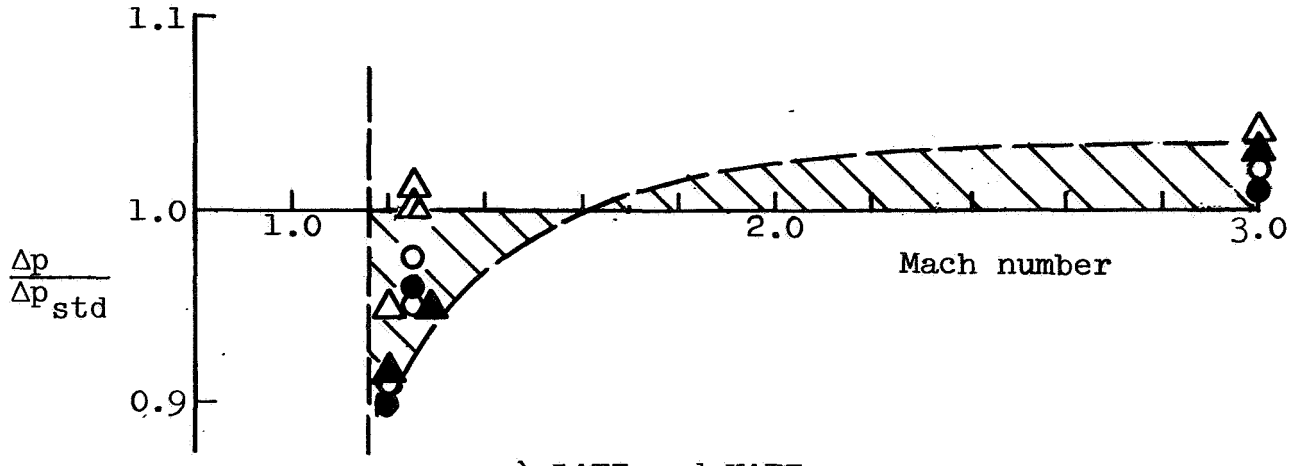

a) LATI and HATI

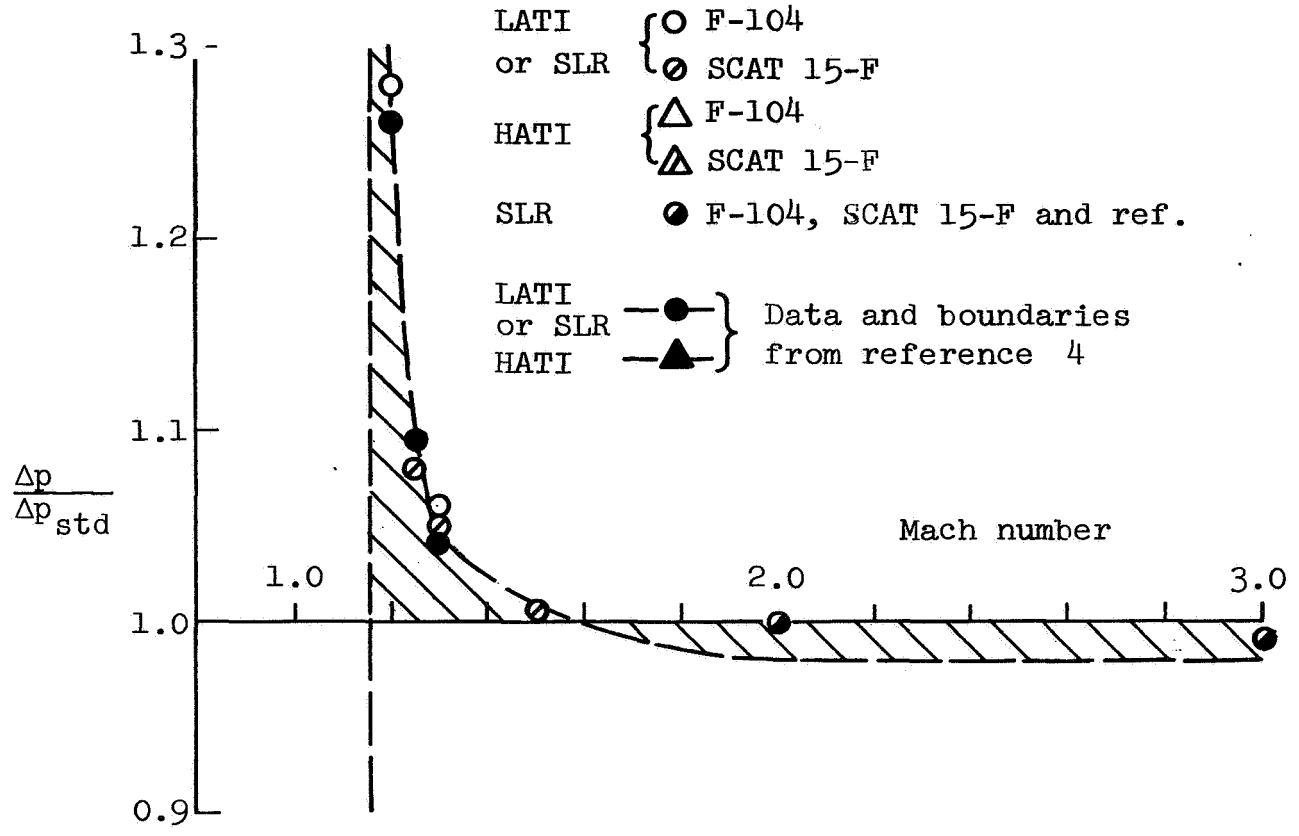

b) SLR

Figure 30. Temperature effects on overpressure

present data. In figure 30, overpressure boundaries taken from reference 4 are also shown. The open symbols are present results; the closed symbols are from reference 4. Both the F-104 and the SCAT 15-F show essentially the same overpressure ratios. The data of reference 4 are in agreement with present data except for HATI where they are 2 to 5% smaller. The general agreement is excellent, particularly for the LATI and SLR atmospheres where the pressure ratios from reference 4 are close even near the cutoff Mach number of 1.16.

Wind effects.- Some effects of winds have been introduced in the previous discussions. A summary of overpressure ratios for the several wind environments is shown in table V and in figure 31. The overpressure ratios for both aircraft are essentially the same. Data from reference 4 again are shown for comparison. The wind profiles in reference 4 are essentially the same as those used here, except for variations in the MAS and LAS profiles. The overpressure results of reference 4 are within 2% of the present results, except for the HAS near cutoff ($M = 1.3$). Here the present results show about twice the overpressure of reference 4. It should be noted, however, that the flight altitudes of the referenced data are not stated, and these results may apply at an aircraft altitude other than 40 000 ft (12.2 km).

The medium altitude wind-shear profile (MAS) was used to investigate in detail the effects of wind direction on pressure signatures. The SCAT 15-F was used, flying at $M = 1.5$ at an altitude of 40 000 ft (12.2 km). Data were obtained for wind directions of 0, 45, 90, 135 and 180 degrees. By varying the initial value of the ray azimuth angle between $\pm$ 30 degrees, lateral effects on both sides of the ground track were also determined. The overpressures are given in table VI and figure 32. The headwind overpressure is largest, except near windward cutoff. For $\phi = 0$, it is 5% more than the tailwind overpressure. For $\eta = 45$ and 90 degrees cutoff occurs for $\phi \approx -30$ degrees (windward rays); here the overpressure is 10 to 15% less than near the ground track ($\phi = 0$).

Ray-path and signature parameters are shown in figure 33 as functions of wind heading angle η for $\phi = 0$. The overpressure ratio varies from 1.07 for a headwind to 0.98 for a tailwind. The ray-path travel time t changes by 6 seconds and the ray-path ground distance y changes by 900 ft (0.27 km). The signature length L_1 is essentially unchanged for this wind and flight condition. Representative signatures are shown in figure 34.

Variations off the ground track.- In a standard atmosphere, the overpressure decreases with distance from the ground track, as illustrated by the empirical curve of figure 35 (from ref. 4). Present data for nominal conditions at $M = 1.25$ and 2.0 are

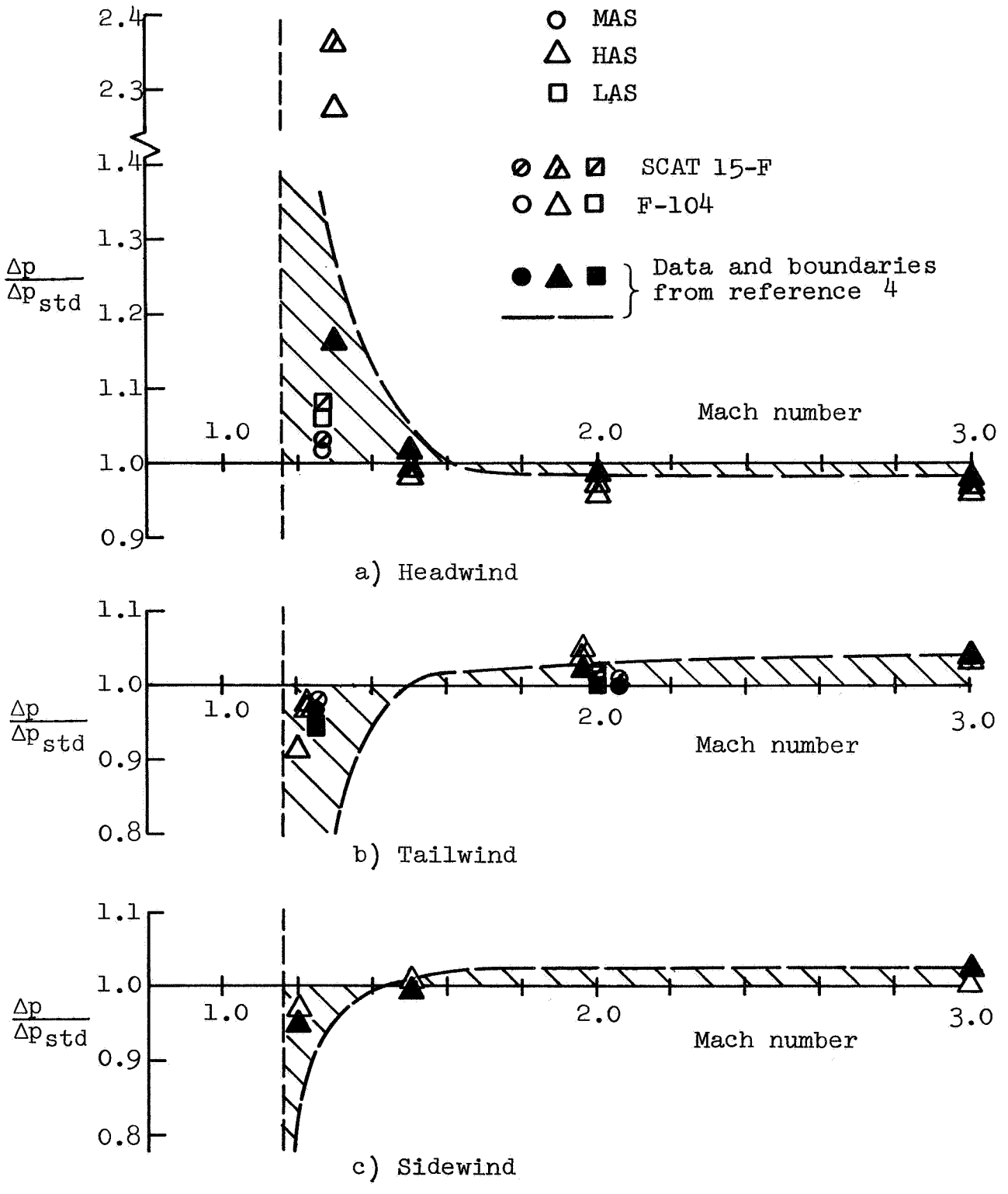

Figure 31. Wind effects on overpressure

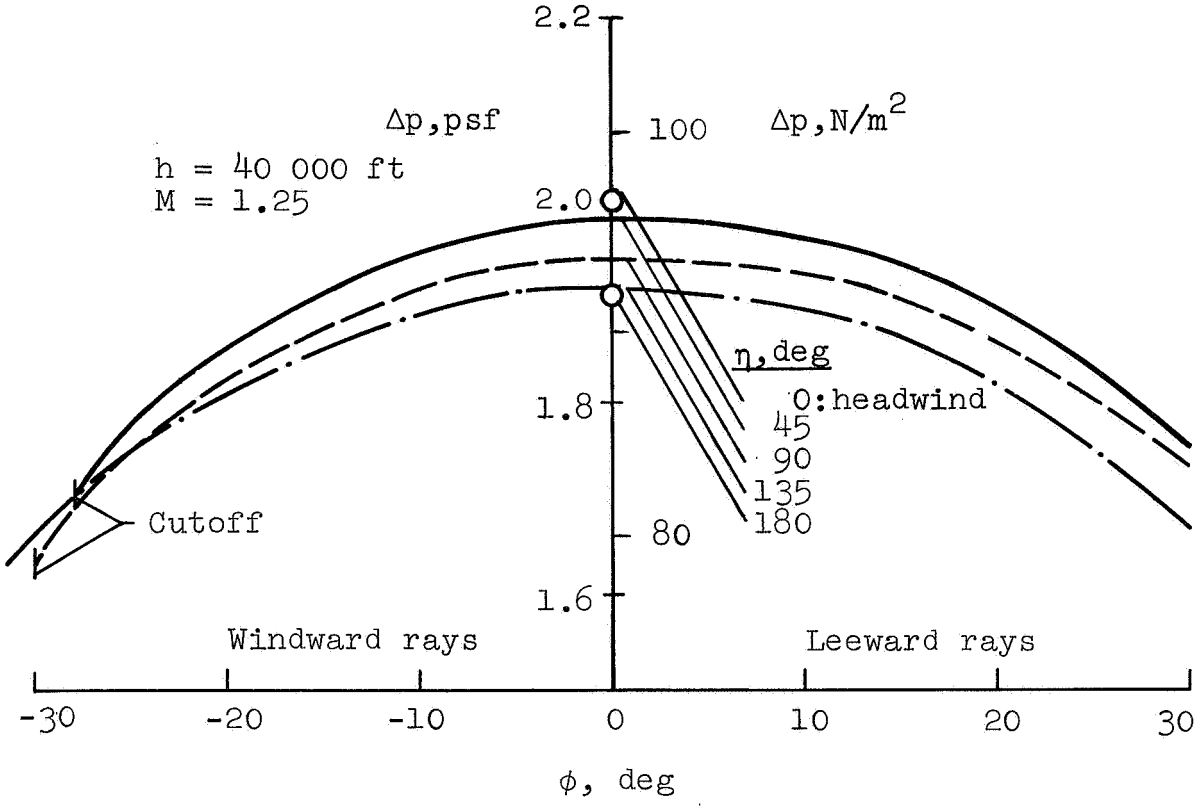

Figure 32. Wind direction effects on overpressure; SCAT 15-F in MAS wind profile

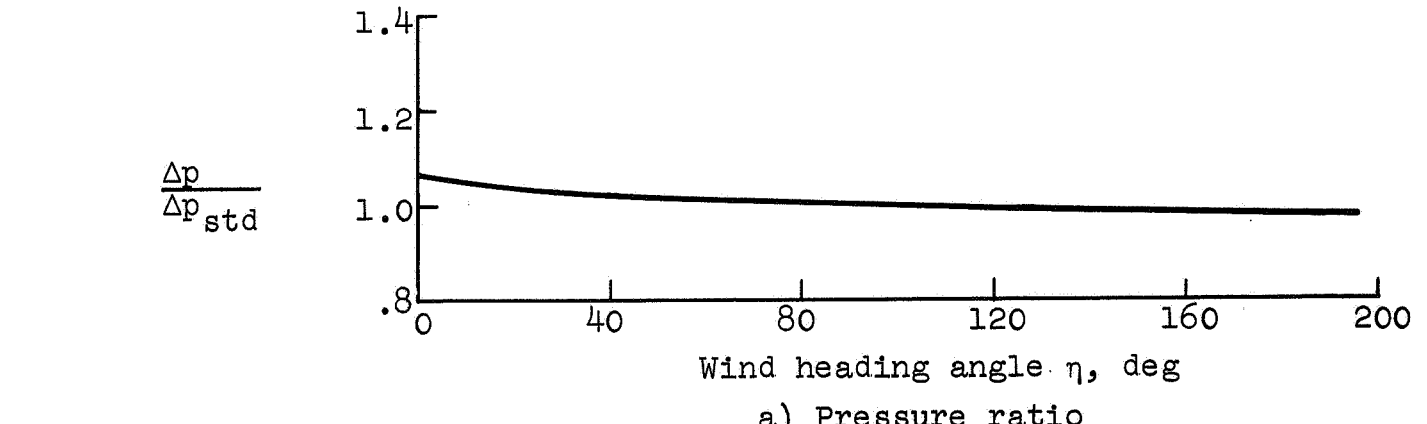

a) Pressure ratio

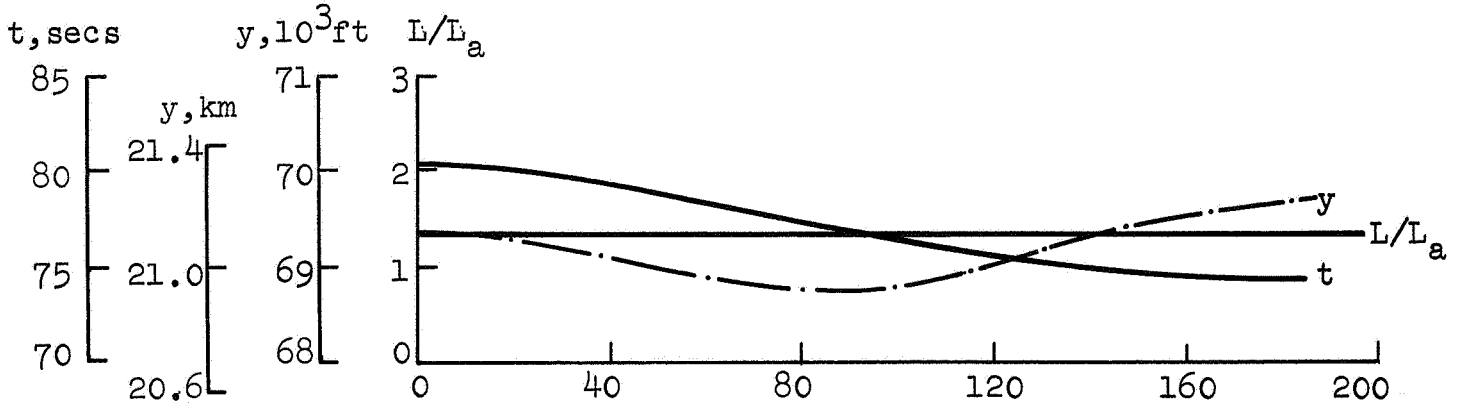

b) Time t, distance y, and length L/L_a

Figure 33. Wind direction effects

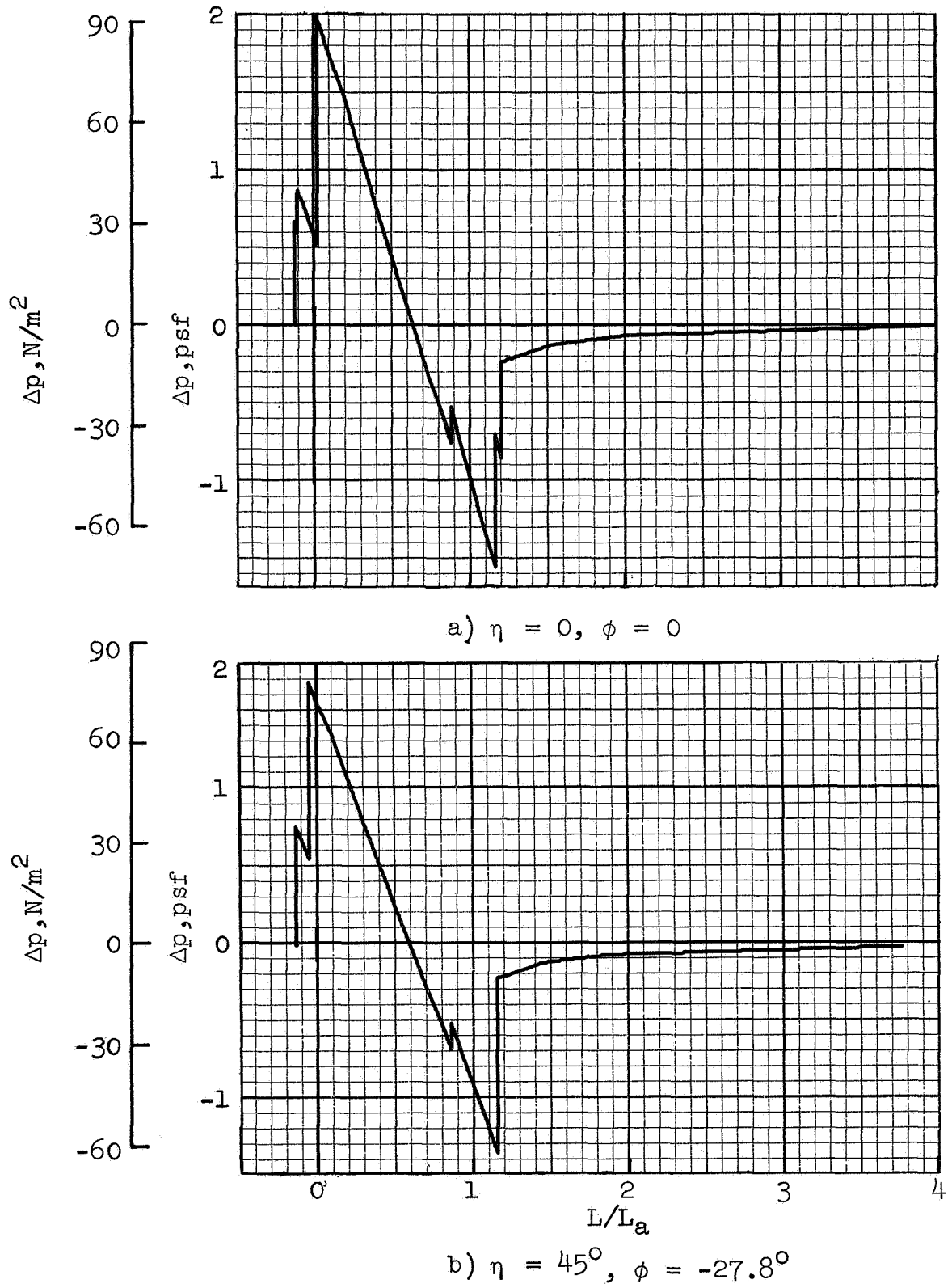

Figure 34. Wind direction effects on pressure signature; SCAT 15-F, MAS wind profile

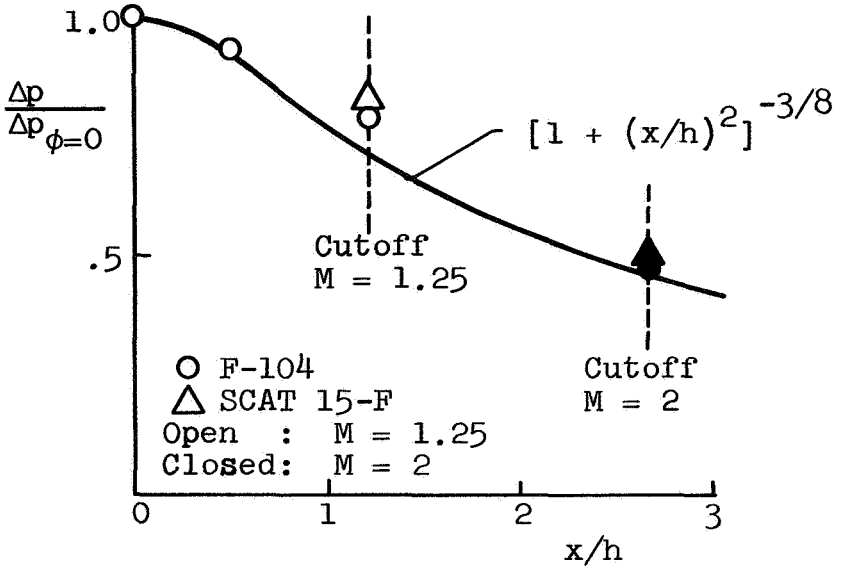

Figure 35. Lateral distance effects on overpressure ratio; h = 40 000 ft (12.2 km), SNW

also shown here. The lateral distance parameter x/h varies with azimuth angle ϕ as shown in figure 36 for two flight conditions. The cutoff values x_c/h and ϕ_c are defined to be the values for which the ray parameterized by $\phi = \phi_c$ becomes horizontal ($\theta = 0$) at the ground (ref. 1). The cutoff azimuth angle ϕ_c is, of course, the same for all aircraft, since the ray path is taken to be independent of the F-function.

Depending on flight and atmospheric conditions, cutoff may occur near a region of ray focusing, in which case larger overpressures will occur there. The lower two curves of figure 37 for level uniform flight show the normal falloff of the overpressure with azimuth angle for the SNW atmosphere and the increasing pressure near cutoff for the SLR atmosphere. The four upper curves apply for maneuvering aircraft to be discussed later; they are shown here for comparison and to emphasize that there are circumstances for which much larger overpressures can be obtained laterally off the ground track than immediately below the aircraft on the ground track. The ray paths off the ground track are longer, so that the tendency to focus the rays has a longer time to develop prior to intersecting the ground.

Changes in signature between the ground track and the lateral cutoff are shown in figures 38 and 39 for the F-104 and SCAT 15-F, respectively. These curves are for uniform flight in the standard atmosphere (SNW) with $h = 40\ 000$ ft (12.2 km). It is noteworthy that the signatures are generally shorter near cutoff than on the flight track (e.g., fig. (38b)), sometimes resulting primarily from the trailing shock moving to the left in phase L/L_a (e.g., fig. (39b)). The data of table II (set number 7) show, on the other hand, that the signatures are longer near cutoff for the uniform atmosphere (UNW) calculations.

Level Accelerating Flight

Parametric results.- Discussions of characteristics of sonic boom propagation for aircraft in maneuvering flight, together with flight test data, have been presented in references 4, 8, 9 and 10. As shown there, an important aspect of accelerating flight, particularly near Mach 1, is the tendency for ray focusing. In level supersonic flight, rays leaving the aircraft at some reference time and azimuth angle have a larger initial inclination angle (downward relative to horizontal) than the corresponding rays which were initiated earlier at lower speeds, and therefore neighboring rays may intersect. At small supersonic speeds and normal flight altitudes, this ray focusing leads to higher overpressures, commonly termed superbooms.

Another important aspect of maneuvering flight is the

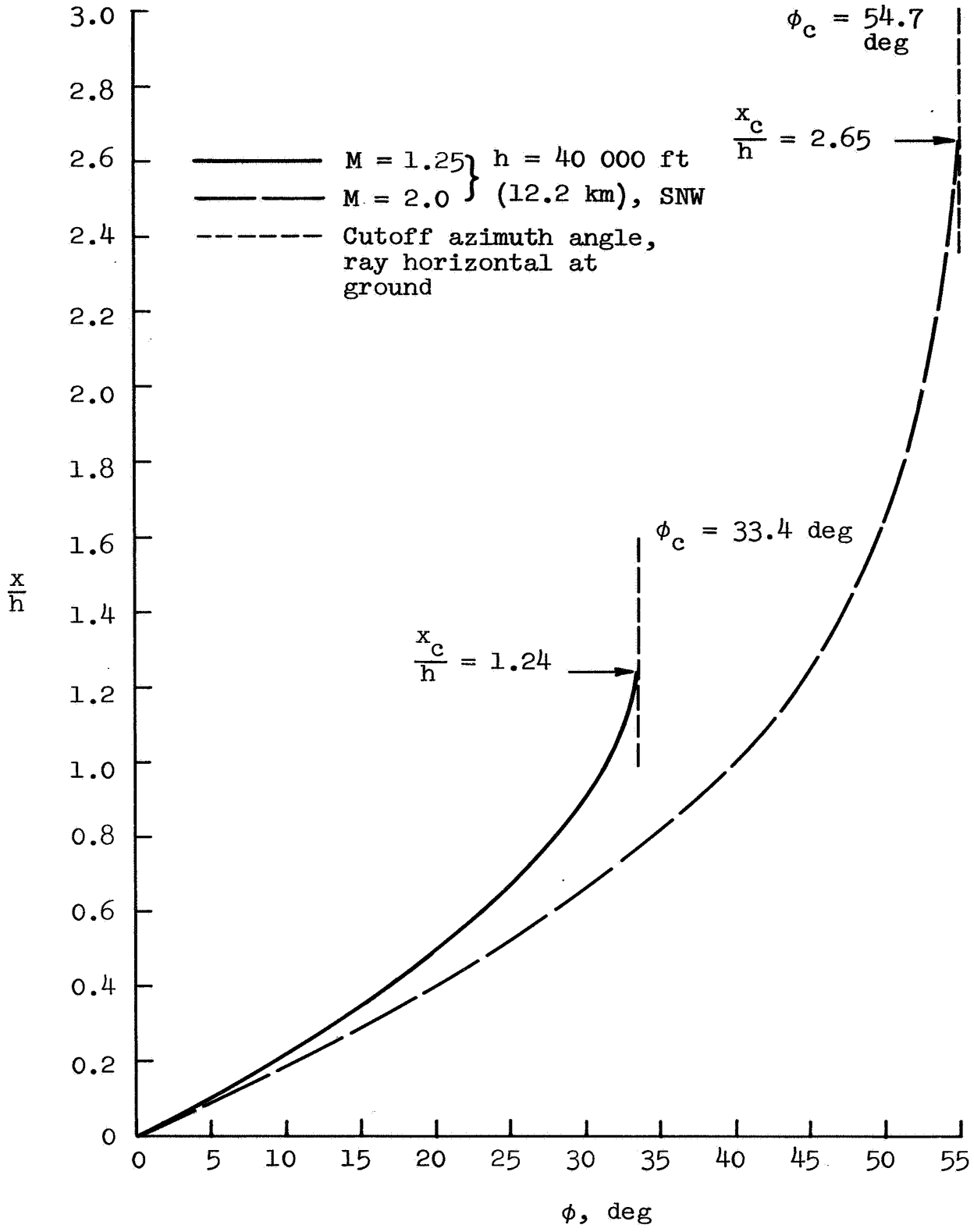

Figure 36. Lateral distance variations with azimuth angle

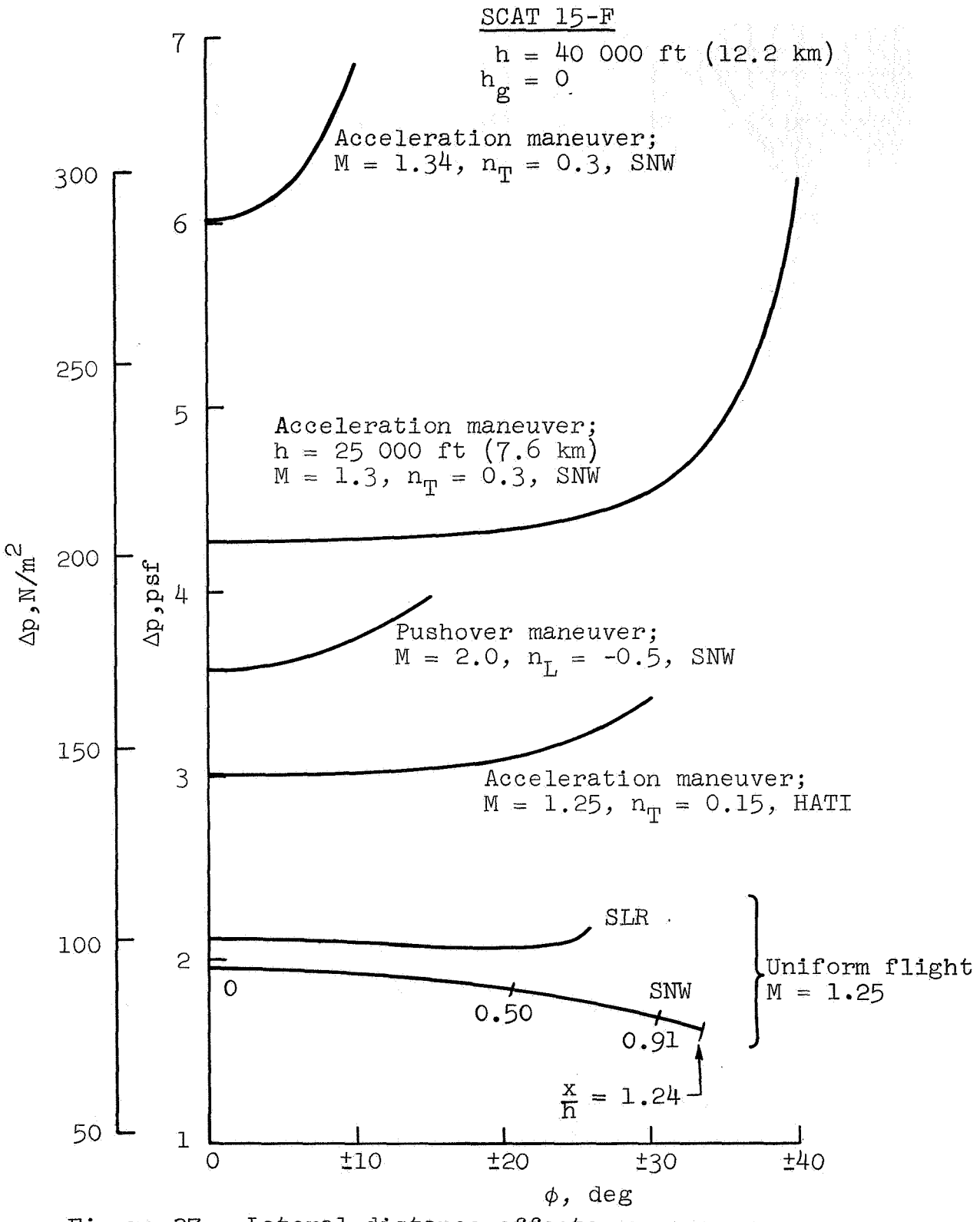

Figure 37. Lateral distance effects on overpressure

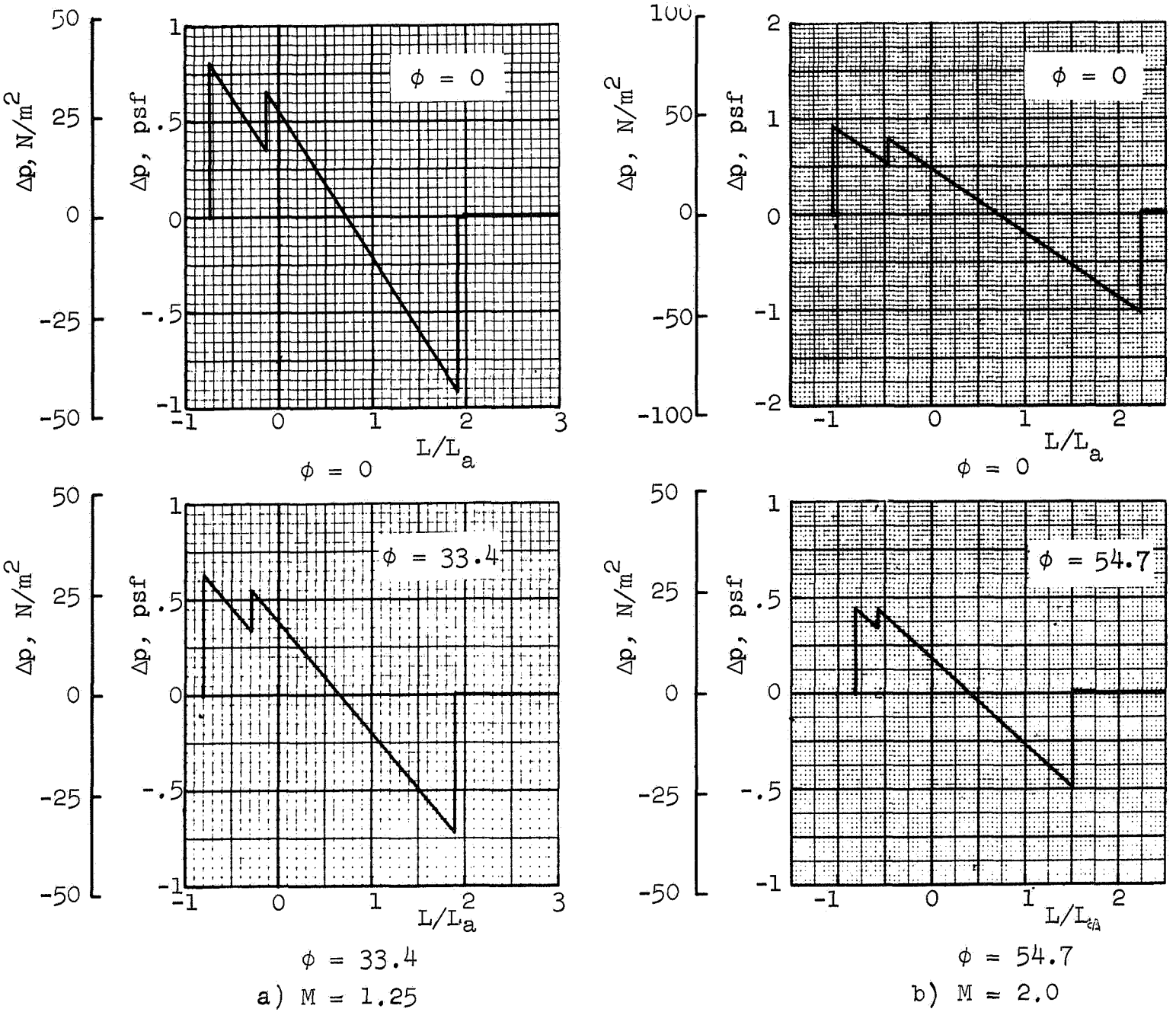

Figure 38. Signatures under ground track and at cutoff; F-104

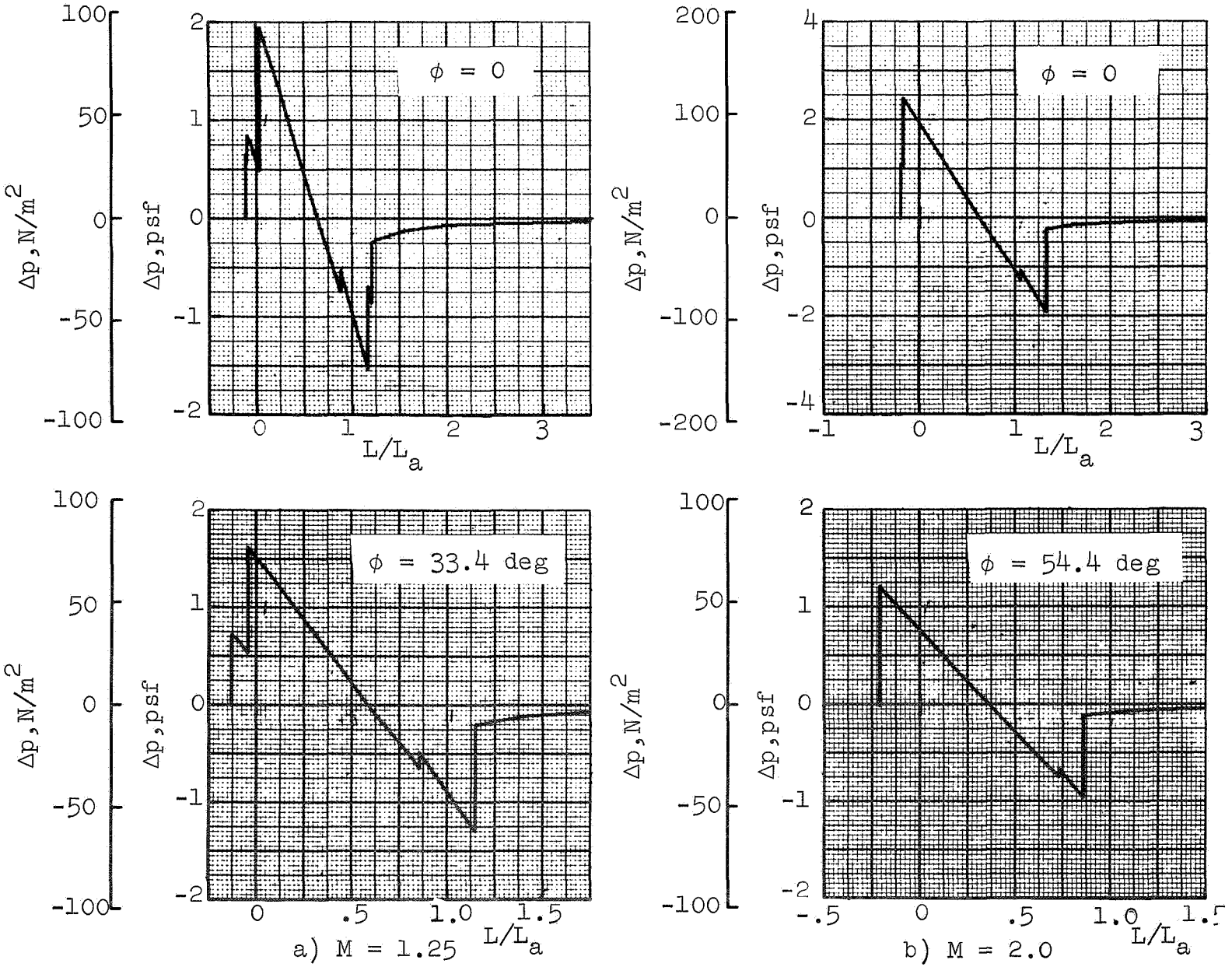

Figure 39. Signature under ground track and at cutoff; SCAT 15-F

occurrence of multibooms (e.g., refs. 2,8,10) wherein at certain ground locations two or more sonic booms may occur successively. Although not studied here, the present digital program (ref. 1) can be used to yield such ground locations and the pressure signatures for each sonic boom there (unless a focus or caustic has occurred). Of course, the pressure signatures which occur as parts of the multiboom set are exactly the same (for a specified flight and atmospheric condition) as those that occur singly and that are to be presented in the following sections of the report.

Overpressures calculated for uniformly accelerating flight are presented in figure 40 for axial load factors $n_T = 0.15$ and 0.30. Data for nonaccelerating flight ($n_T = 0$) are also shown for comparison. The effects of acceleration, as expected, are large at the smaller Mach numbers where ray focusing is predominant. For an aircraft flying at 40 000 ft (12.2 km) above sea level with $n_T = 0.3$, the ray paths just reach a focus at the ground ($h_g = 0$) when the aircraft has a Mach number of 1.3. At faster aircraft speeds, the rays do not focus before reaching ground level, whereas at slower speeds they do. The value of this critical Mach number varies with load factor, altitude and atmospheric conditions, as the data in figure 40 indicate.

Some pressure signatures are shown in figures 41 and 42 for a variety of accelerating flight conditions. In comparison with the nominal signatures of figure 10, these signatures with 0.15 and 0.30 g's acceleration have, in general, the same characteristic shapes.

Flight test comparison.- Measurements of the sonic boom signature of an F-104 in accelerating flight were made at Edwards AFB in 1964 (ref. 8). The aircraft accelerated from M = 0.9 to 1.5 at approximately 0.08 g's in level flight at an altitude of 37 200 ft (11.339 km). Results of the overpressures measured at the ground (altitude 2200 ft (670 km)) during these tests are shown in figure 43, together with calculated results obtained in the present study. The calculated results were obtained using the F-function for the F-104. An aircraft weight equal to the flight weight of 16 700 lbs (7580 kg) was used ($W/S = 96.5$ psf (470 kg/m^2)) along with the atmospheric temperature and wind profiles measured during the morning of the flight. The solid curves of figure 43 are the calculated results (using a reflection factor of 1.9) for the tailwind condition of the test, and also for a no-wind condition. Large overpressures (superbooms) are calculated for locations about 6 miles (10 km) from the reference station. These occur during the acceleration of the aircraft in the Mach number range 1.20 to 1.22. At lower supersonic speeds, the calculated ray-tube area becomes zero (rays focus) before the signal reaches the ground. The calculated ray paths for the ground focus condition apparently intersect the ground about 2 miles (3 km) in front of the actual raypaths, since a large overpressure was measured at a ground station

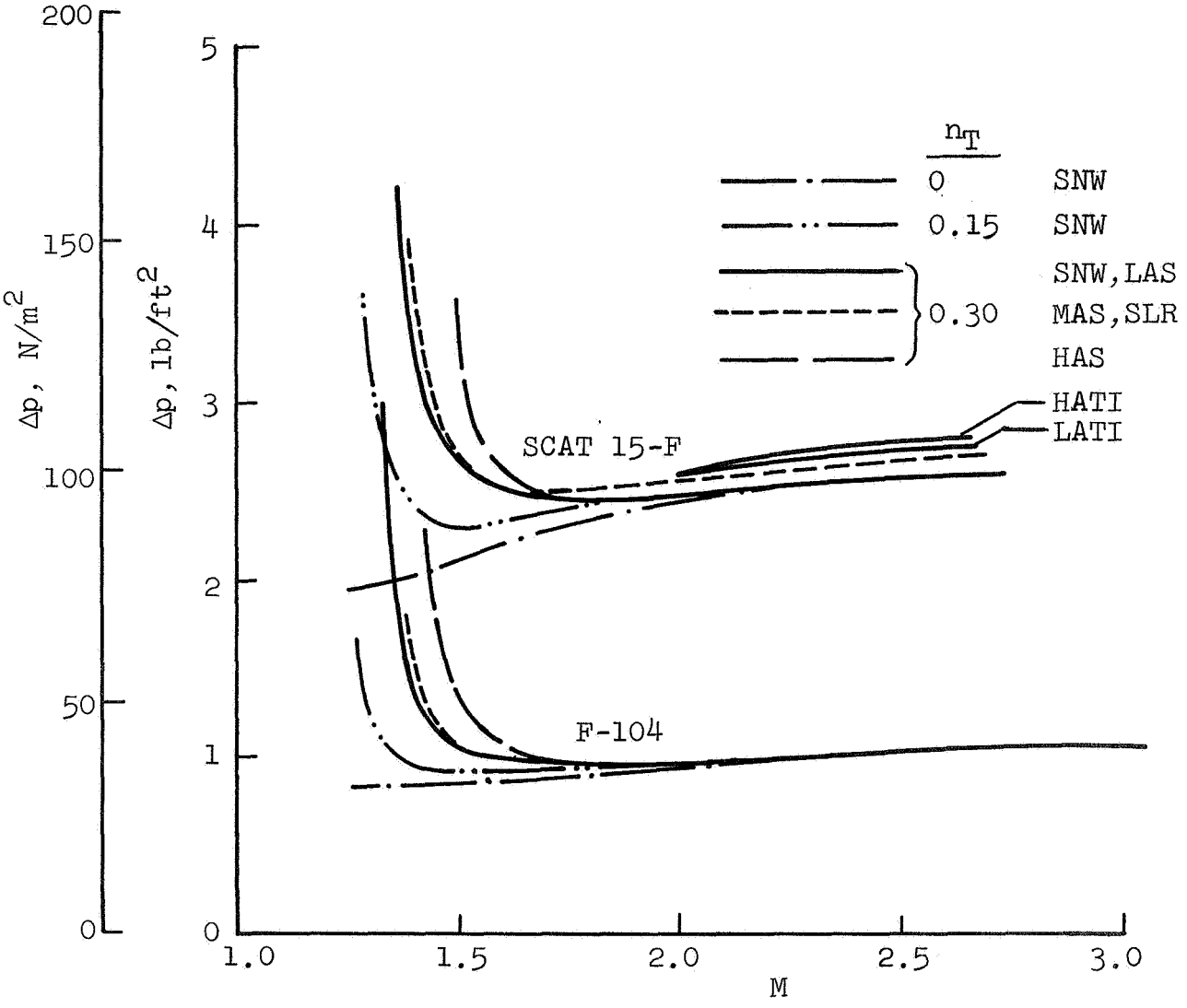

Figure 40. Acceleration effects on overpressure

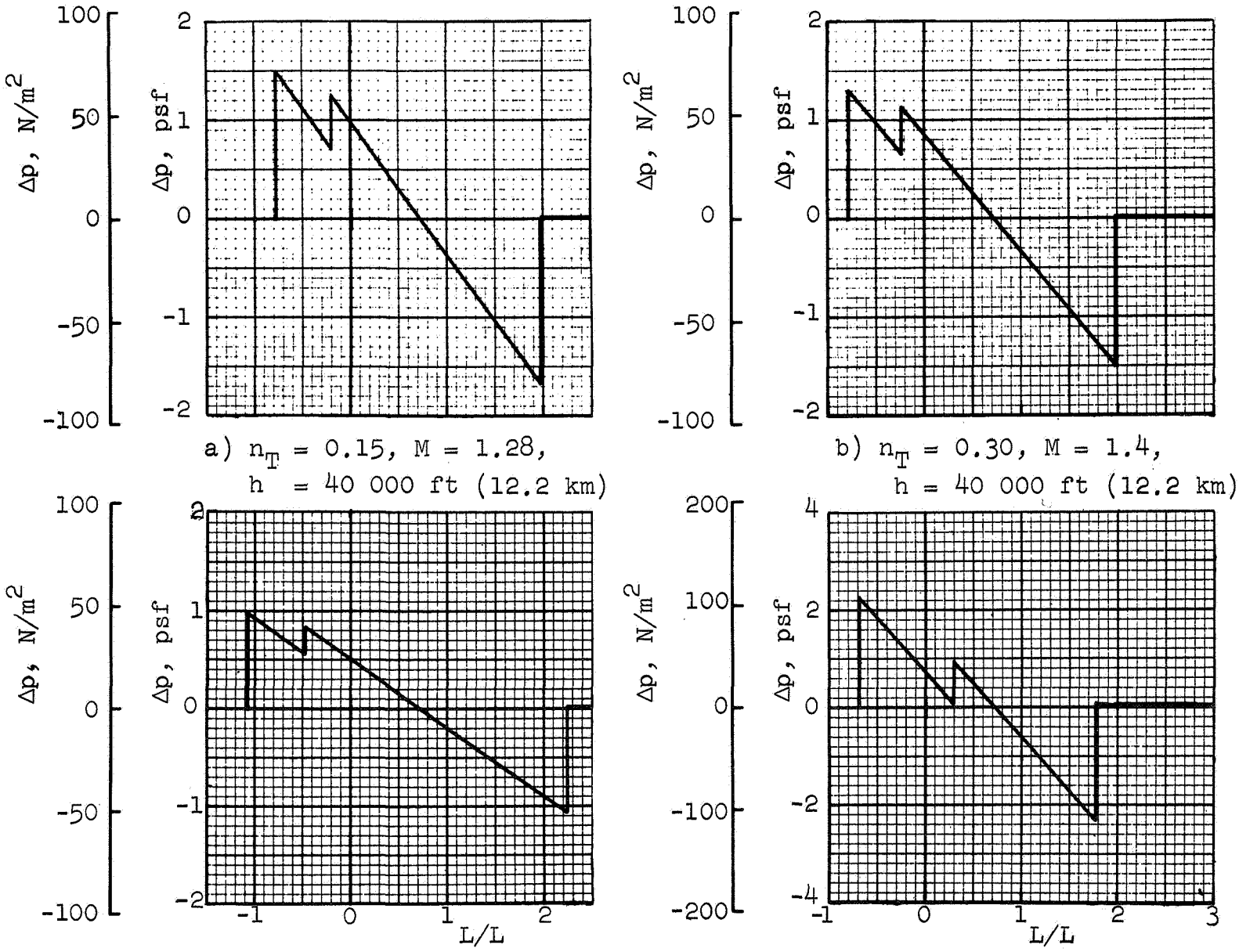

a) n_T = 0.15, M = 1.28,
h = 40 000 ft (12.2 km)

b) n_T = 0.30, M = 1.4,
h = 40 000 ft (12.2 km)

c) n_T = 0.30, M = 2.0,
h = 40 000 ft (12.2 km)

d) n_T = 0.30, M = 1.3,
h = 25 000 ft (7.6 km)

Figure 41. Signatures for accelerating aircraft; F-104, LAS

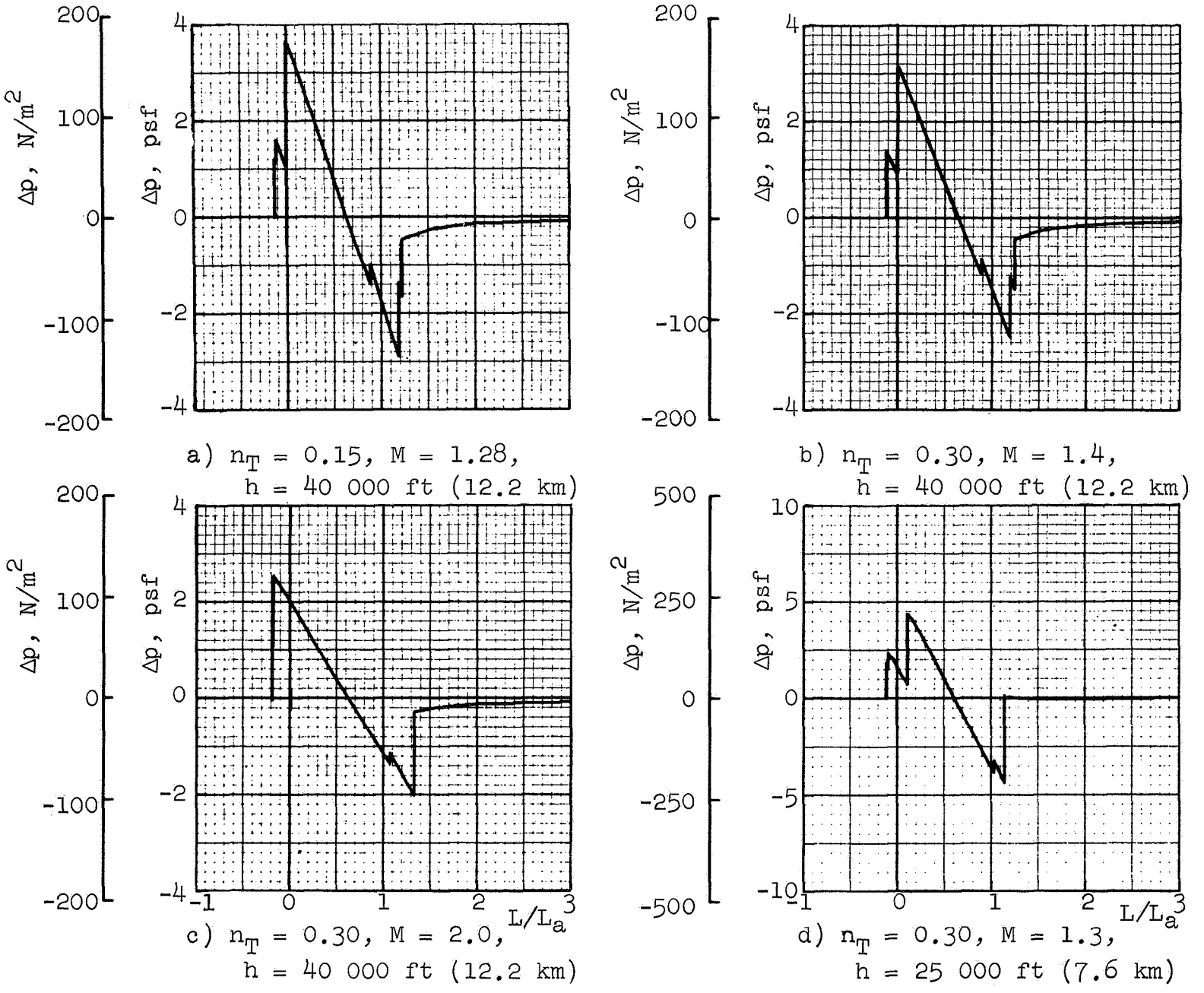

Figure 42. Signatures for accelerating aircraft; SCAT 15-F, LAS

Typical signatures

Measured at s = 8 miles | Measured at s = 9 miles | Calculated

Reference: Figure 12 of reference 8

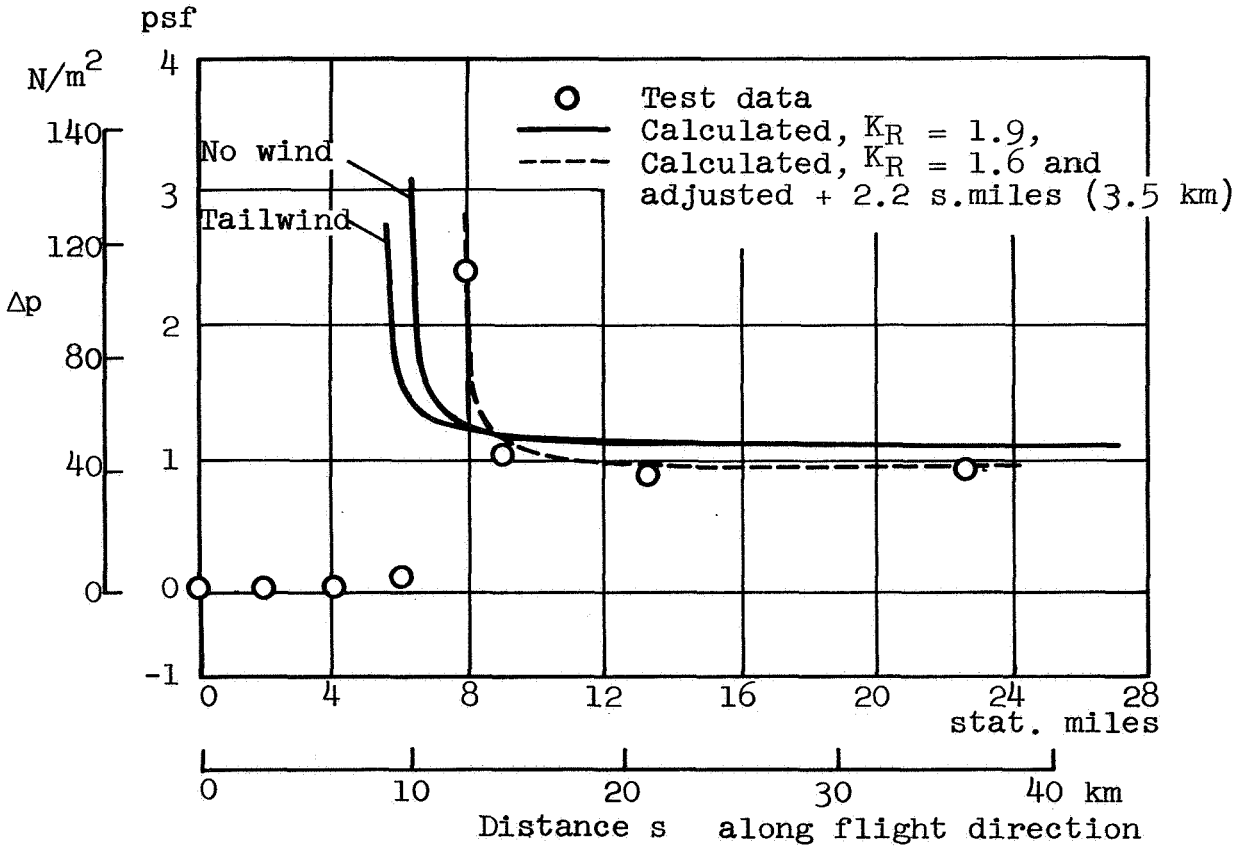

Figure 43. Overpressures for accelerated flight; F-104

8 miles (13 km) from the origin. For this condition the rays are nearly horizontal, glancing the ground, and therefore their location is very sensitive to atmospheric effects. A two mile dispersion between experiment and calculation is not felt to be excessive here.

The Mach number increases from 1.23 for the signature measured at 8 miles (13 km) from the reference station to 1.40 at 17.5 miles (28 km). The calculated overpressures for these locations are about 12% larger than the measured values. The dashed curve of figure 43 is the calculated data shifted to the right 2 miles (3 km) and adjusted vertically to match the $M = 1.40$ data (corresponding to reducing the reflection factor from 1.9 to 1.6). This curve fits the flight data well, indicating the validity in general of the calculated pressure variation along the ground.

In summary, for this comparison for accelerated flight, the calculated location of the superboom is 2 miles (3 km) short, whereas the predicted shape of the overpressure variation along the ground is excellent. Further comparisons between calculated and measured data are needed to develop bases for explaining and predicting deviations from calculated data.

Pullup Maneuver

Definitions and input data for the pullup maneuvers were presented in the preceding section entitled General Description and Program Inputs, figures 4 and 6. Characteristics of the pullup maneuver are that the load factor exceeds unity ($n_L > 1$), the flight path angle rate $\dot{\gamma}$ is positive, and neighboring ray paths along the flight path are divergent. The ray-tube area tends to increase faster than for level uniform flight, and therefore the sonic boom overpressure tends to be alleviated. The steepness of the flight path, measured by γ, also affects the overpressure, as an airplane in a dive, for example, has the axes of its Mach conoids tilted towards the ground giving shorter ray paths between the aircraft and ray-ground intersection.

Figure 44a shows overpressure ratio variations with flight path angle γ at two values of load factor and at two Mach numbers. The reference overpressures Δp_{ref} are the overpressures for uniform level flight at the Mach number considered (table III). At $M = 1.25$ for horizontal flight ($\gamma = 0$), the overpressures with pullup load factors of 1.5 and 3.0 are only about 30% of the reference values (no pullup, $n_L = 1$). At angles of -10 deg., the overpressures for these pullup load factors are increased to about 95% of the reference values. At Mach 2, the overpressures for $\gamma = 0$ are 27% larger than the reference values. Here the SCAT 15-F curves are slightly different than the F-104 curves because of details in their signature shapes.

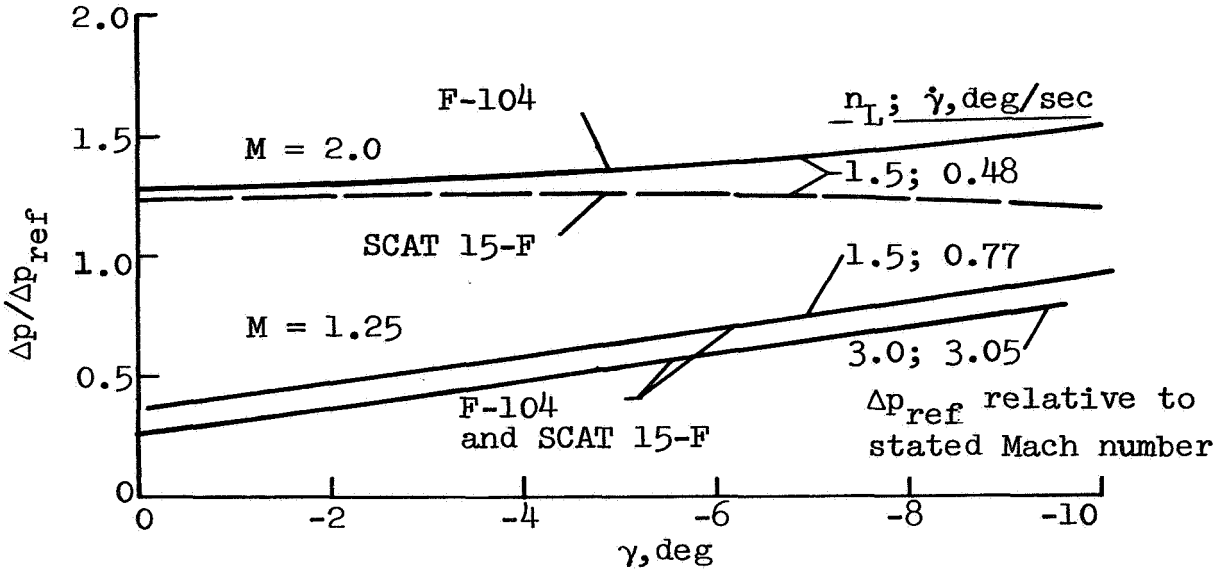

a) Variations with γ, SNW

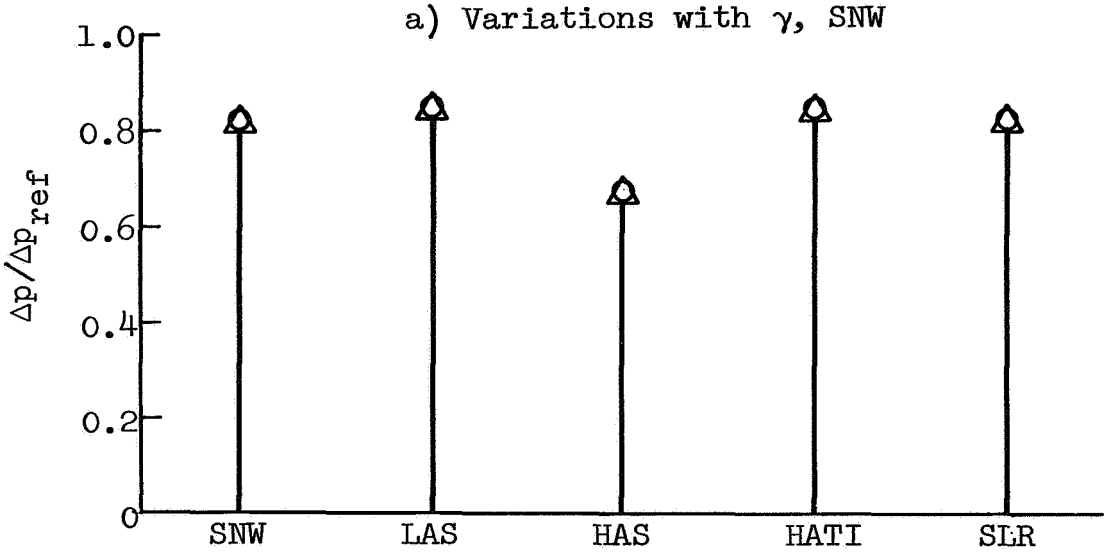

b) M = 1.25, γ = -4.9 deg, $\dot{\gamma}$ = 0.77 deg/sec

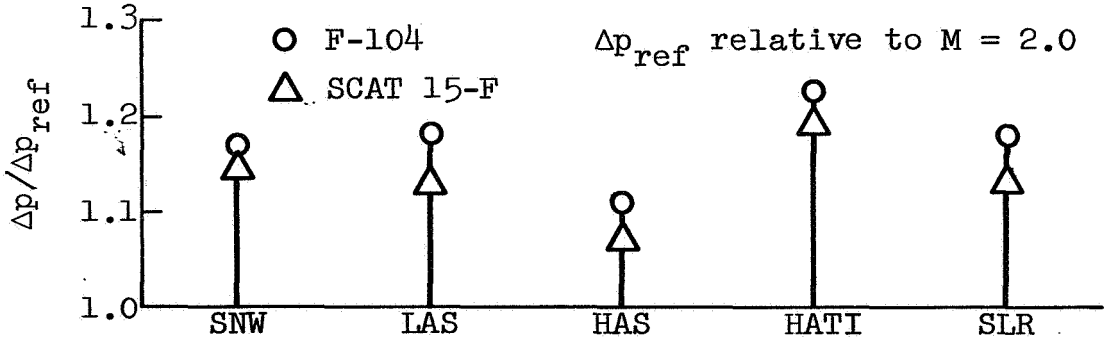

c) M = 2.0, γ = -4.2 deg, $\dot{\gamma}$ = 0.48 deg/sec

Figure 44. Overpressures for pullup maneuver

Figures 44b and 44c show effects of atmosphere on the pullup overpressures for dive angles near -4 deg., and for $M = 1.25$ and 2.0, respectively. Figure 45 shows similar data for a dive angle of -10 deg. Again, these data are obtained for the aircraft at 40 000 ft (12.2 km) altitude and for overpressures calculated at sea level. The headwind HAS here causes the pullup overpressures to decrease, whereas the inversion HATI causes them to increase slightly above nominal (SNW) values.

Signatures for a load factor of 1.5 are shown in figures 46 and 47. When these data are compared with the nominal signatures (fig. 10), it appears that the effect of the positive load factor on pressure signature at the ground is to move intermediate shocks to the left. This tendency is further shown in figure 48 for $n_L = 3$.

Pushover Maneuver

In a pushover maneuver (figs. 4 and 6), the load factor is less than unity ($n_L < 1$), the flight path angle rate $\dot{\gamma}$ is negative, and neighboring ray paths along the flight path are convergent. The rays tend to focus, leading to large sonic boom overpressures. As with other maneuvers, the flight path angle γ also has an effect on overpressures in a pushover maneuver.

Figure 49 presents some general results of overpressures obtained for the pushover maneuver at Mach 2.0, 40 000 ft (12.2 km) altitude, and a load factor $n_L = -0.5$. This is a rather large negative load factor, and at Mach 1.25 the ray-tube area focuses ($A = 0$) before the rays intersect the ground. Figure 49a shows variations with climb angle γ and azimuth angle ϕ for both aircraft in the standard atmosphere. At $\phi = 30$ deg , the rays focus before intersecting the ground. The reference Δp_{ref} is again taken from table III. For this large negative load factor ($n_L = -0.5$) the overpressure ratio is 50% larger when $\gamma = 10$ deg than when $\gamma = 0$, on the flight track ($\phi = 0$). The ratio is even larger off the flight track, as the rays then have a longer path length in which to progress towards focusing. The variation of overpressure with azimuth angle is shown in the previous figure 37. The larger values of the F-104 data in figure 49 are discussed later.

Figure 49b shows effects of the overpressure on the ground track for various atmospheres for a selected climb angle $\gamma = 4.3$ deg. The variations with atmosphere are small except for the headwind HAS. This headwind causes the rays to approach a focus near the ground and yields large overpressures compared to the results for other atmospheres. In figure 50 the overpressure variations with load factor are presented. These data highlight the sensitivity of the overpressure for negative load factors.

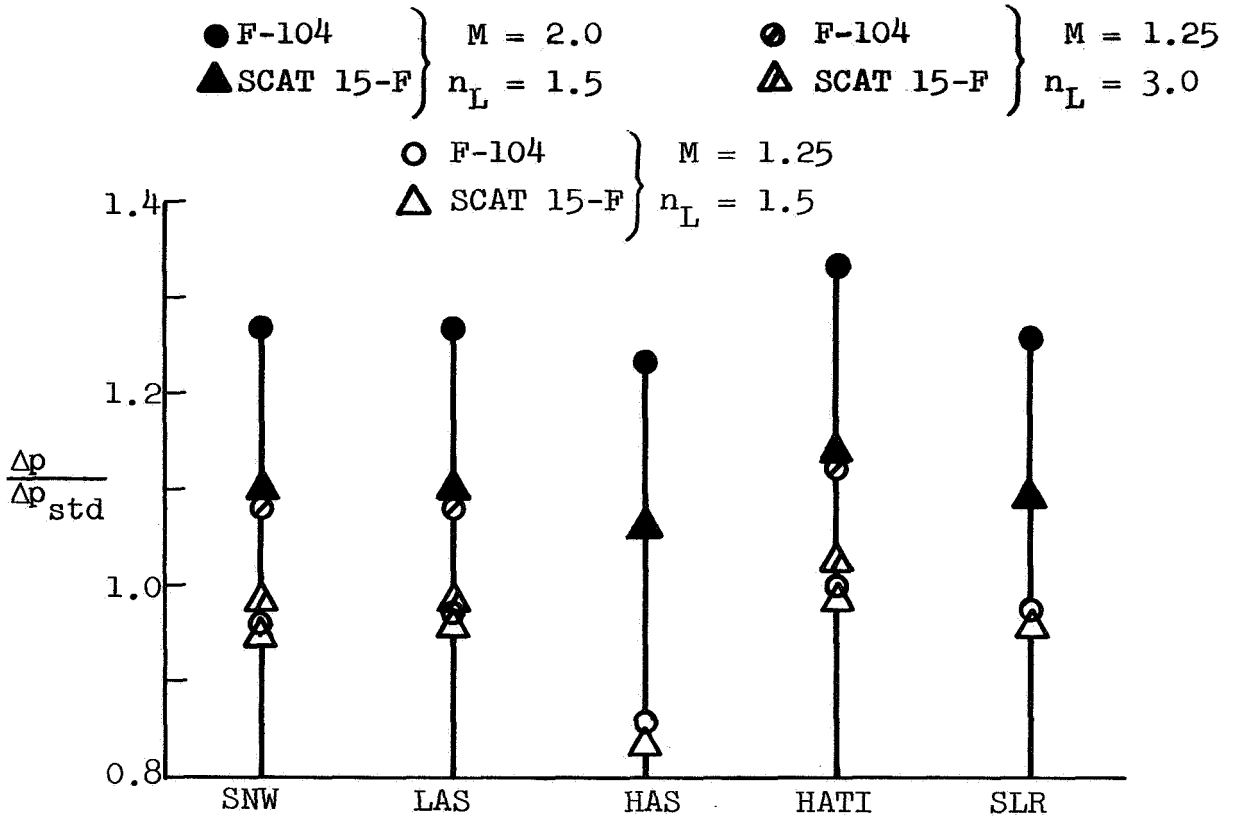

Figure 45. Overpressure ratios for dive-pullout maneuvers; $\phi = 0$, $\gamma = -10$ deg

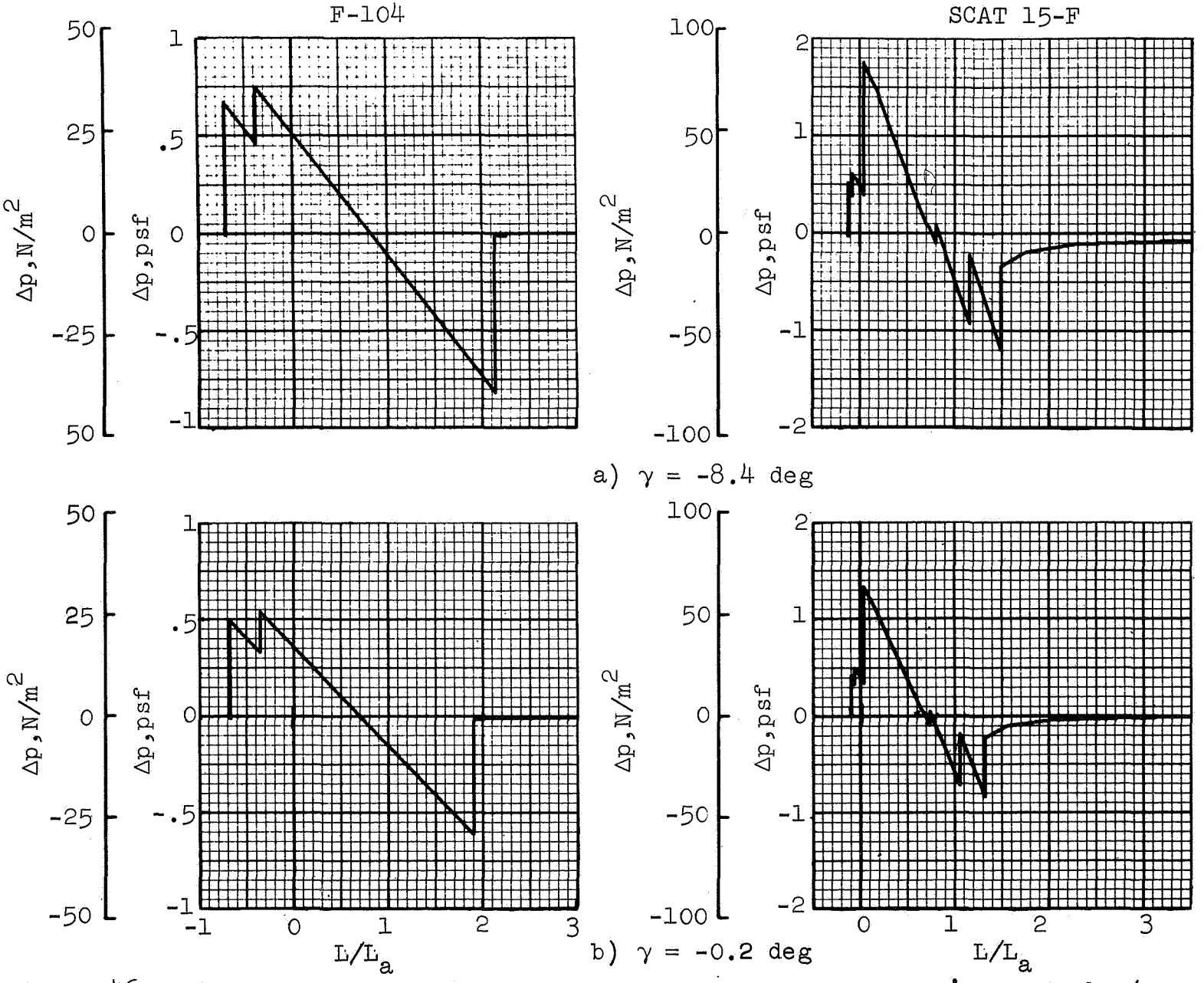

Figure 46. Signatures for pullup maneuver; M = 1.25, n_L = 1.5, $\dot{\gamma}$ = 0.77 deg/sec, SNW

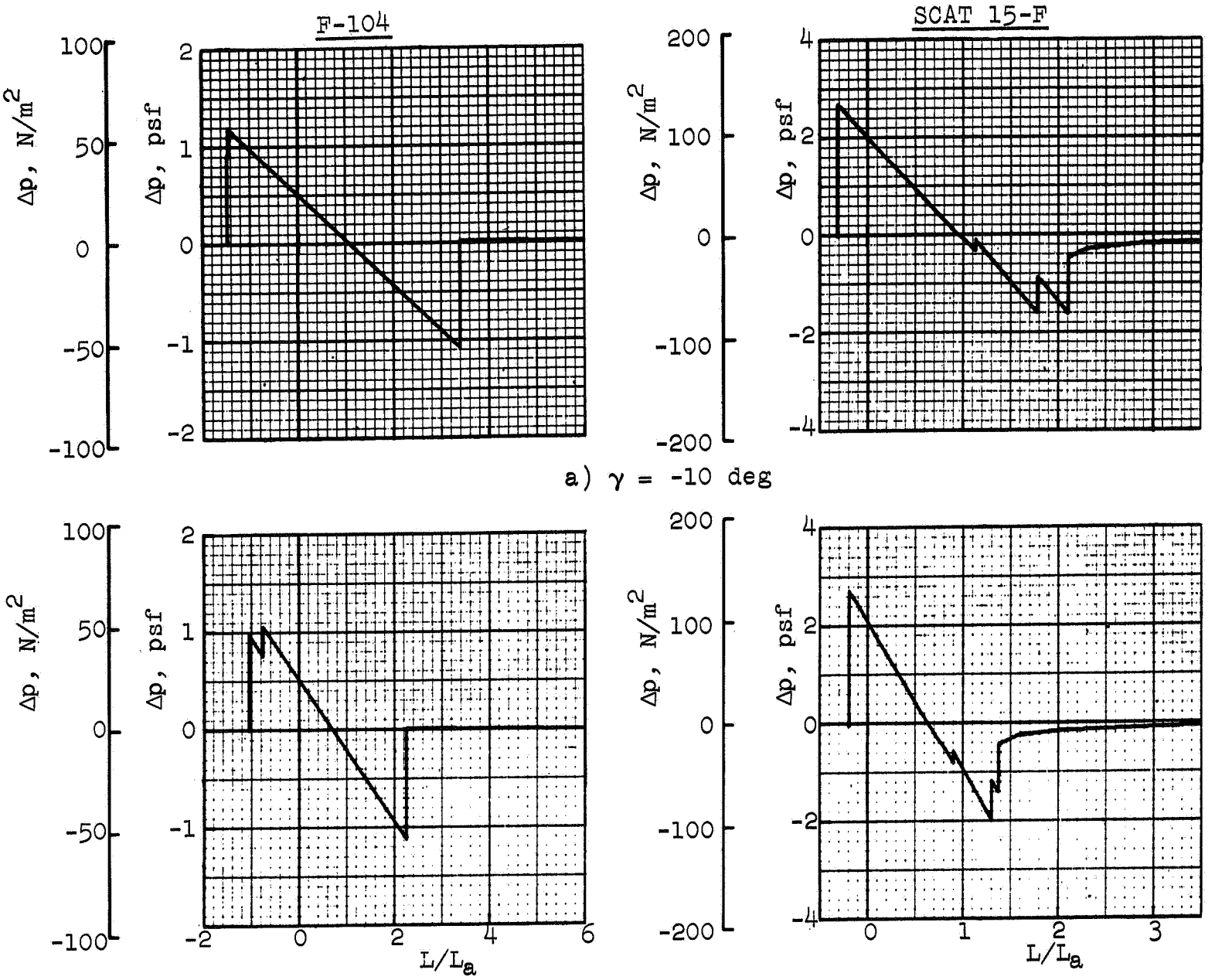

Figure 47. Signatures for pullup maneuver; M = 2.0, n_L = 1.5, $\dot{\gamma}$ = 0.48 deg/sec, SNW

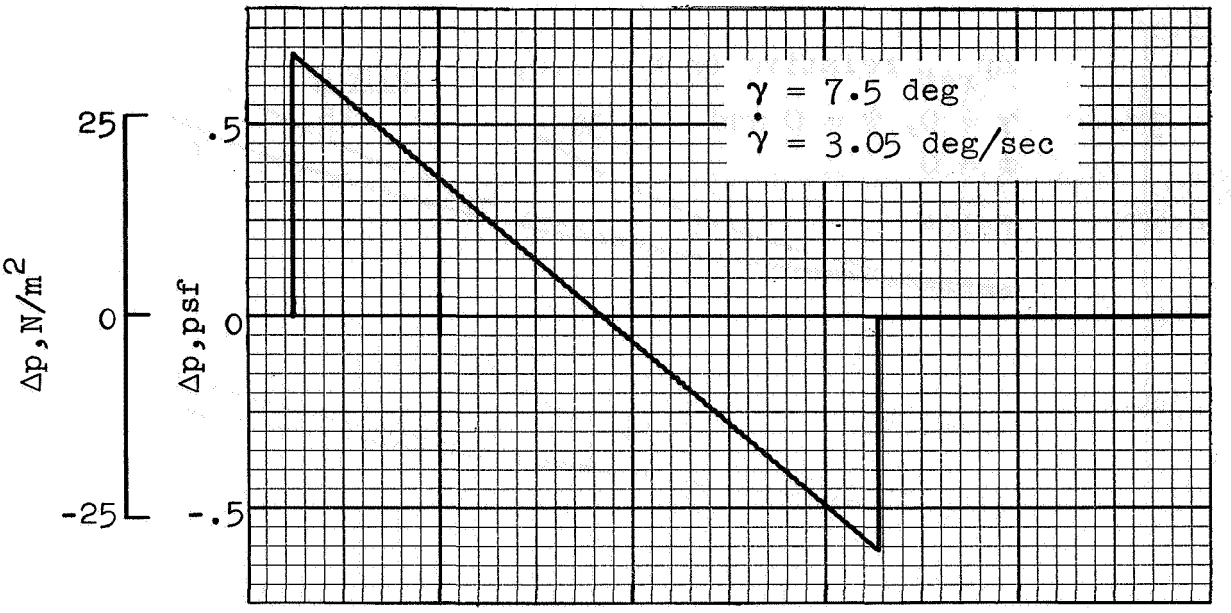

a) F-104

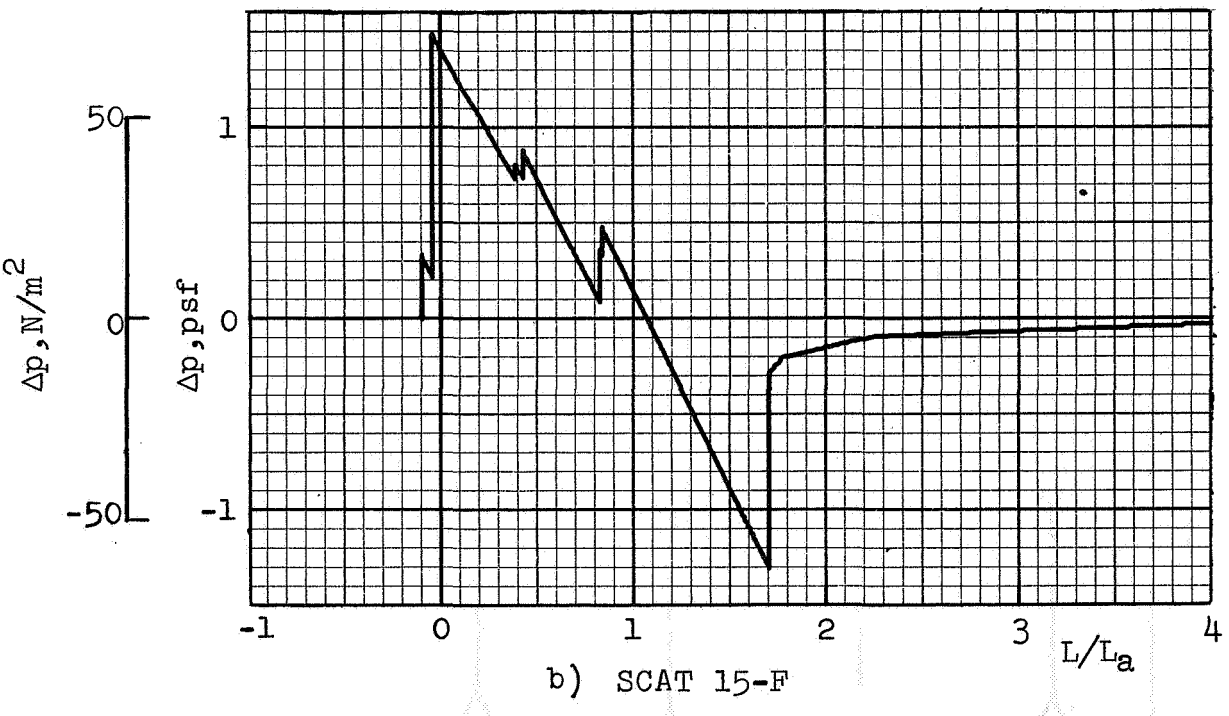

b) SCAT 15-F

Figure 48. Signatures for pullup maneuver; M = 1.25, n_L = 3, SNW

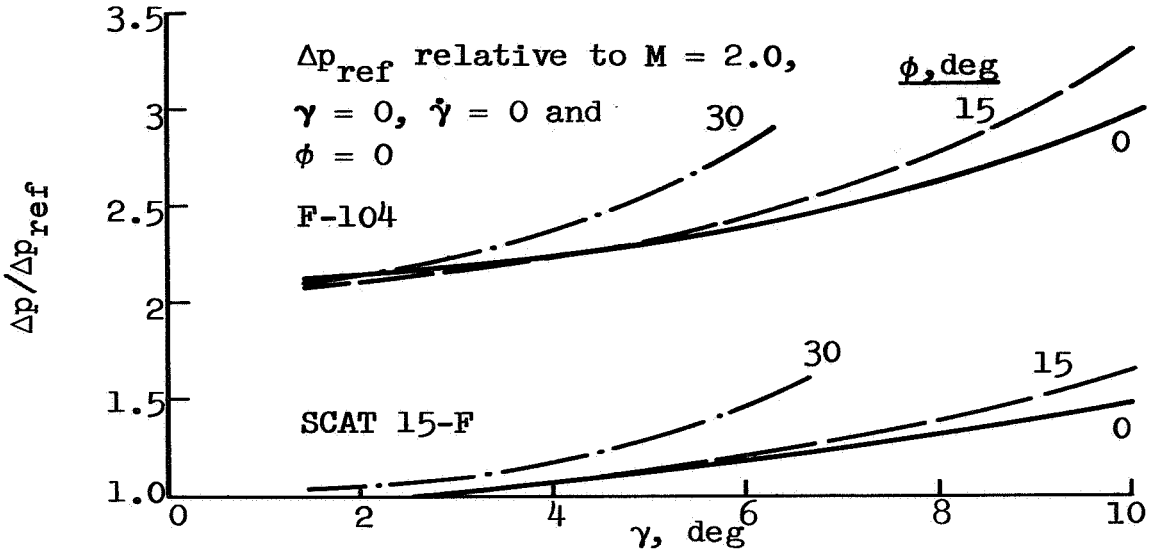

a) Variations with γ; $\dot{\gamma}$ = -1.4 deg/sec, SNW

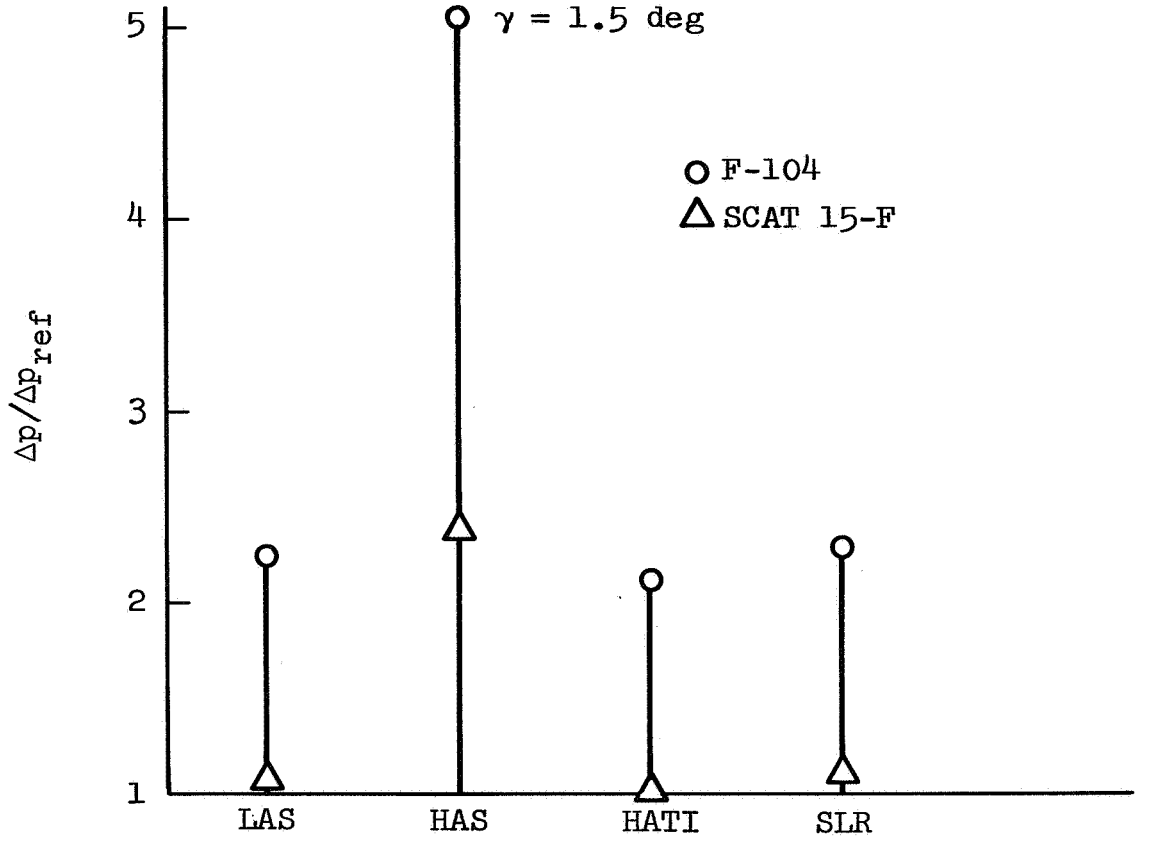

b) γ = 4.3 deg, $\dot{\gamma}$ = -1.4 deg/sec, ϕ = 0

Figure 49. Overpressures for pushover maneuver; M = 2, n_L = -0.5

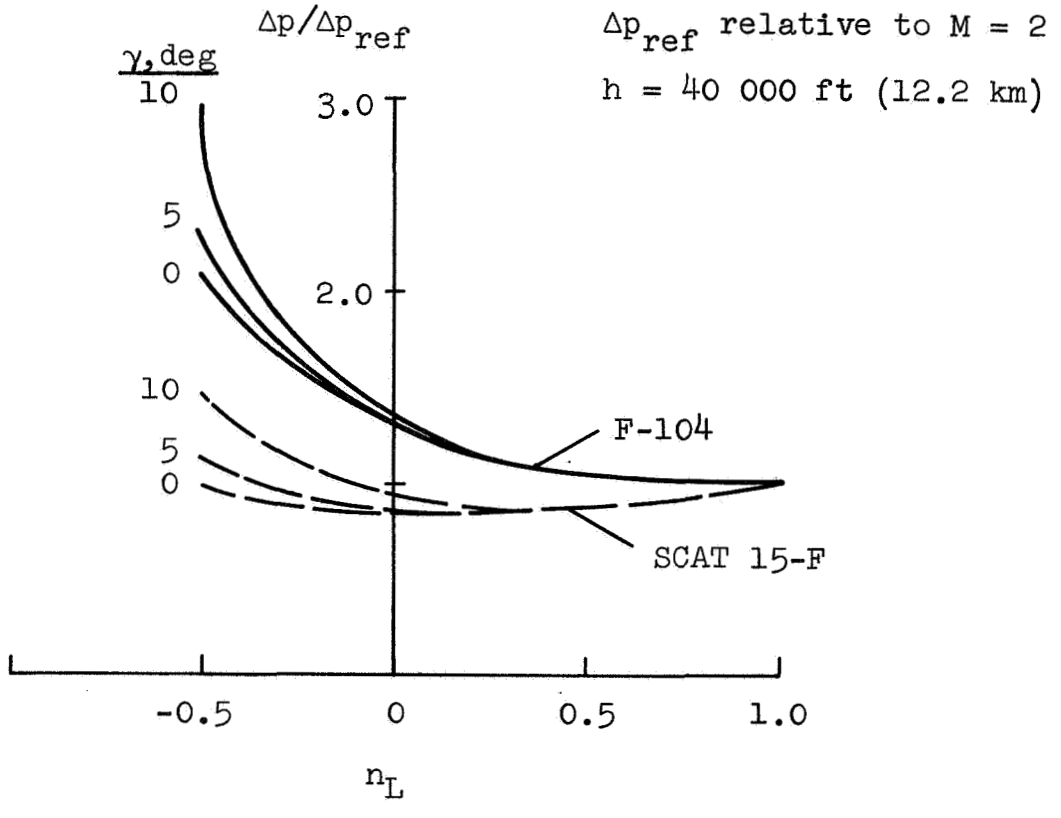

Figure 50. Overpressures for pushover maneuver, variation with load factor; M = 2

Further effects of atmosphere on the overpressure emanating from an aircraft in a pushover maneuver are given in figure 51 for a climb angle $\gamma = 10$ deg . Data for an additional aircraft altitude of 25 000 ft (7.6 km) are also shown here. The F-104 overpressure ratios are larger than the corresponding SCAT 15-F ratios because the negative load factor affects the signature shape near the leading shock in a different manner for each aircraft. This is dependent on their F-function variations with lift coefficient and signature aging. The overpressures ratios for $h = 25\ 000$ ft (7.6 km) compared to $h = 40\ 000$ ft (12.2 km) are substantially less in the HAS, as expected, because the aircraft is below the high-speed jet-stream. On the other hand, the inversion HATI has a larger overpressure ratio for the lower flight altitude.

The magnitudes of the overpressure ratios are substantially larger for the F-104 than for the SCAT 15-F, as shown in figures 49, 50 and 51. The reason for this is demonstrated in figure 52 which compares the signatures for each aircraft in the pushover ($\dot{\gamma} = -1.4$ deg/sec, $n_L = -0.5$) with their respective signatures in level flight ($\dot{\gamma} = 0$, $n_L = 1.0$). The level flight values of overpressure are used as the reference values in figures 49, 50 and 51. For the F-104, the leading shock is much stronger in the pushover than in level flight, whereas for the SCAT 15-F the leading shocks are nearly the same strength. For both aircraft, however, the shapes of the signatures are affected greatly by the pushover. This figure is an exhibit of the sensitive effect of $\dot{\gamma}$ terms in the equation for the ray-tube area (ref. 1, eq. (26)) and its influence on the age variable and phase distortion (ref. 1, eqs. (46) and (49)).

The marked effect of $\dot{\gamma}$ on the signatures is shown further in figures 53 to 56. Figures 53 and 54 show that the signatures are similar at climb angles of approximately 10 degrees and zero for the same value of $\dot{\gamma}$, but there are large changes in the signatures for $\dot{\gamma} = -1.4$ degrees/second compared to $\dot{\gamma} = 0$. The effects of changing $\dot{\gamma}$ are shown in figure 55 where increases from -1.4 degrees/second to zero cause intermediate shocks to progress from the vicinity of the trailing shock to the vicinity of the leading shock. These signature variations for further increases in $\dot{\gamma}$ are presented in figure 56 where data are shown at various values of $\dot{\gamma}$ corresponding to load factors between $n_L = 0.5$ and $n_L = 1$.

An important general conclusion is that the overpressure ratios (or amplification factors) are not always independent of aircraft type. A ratio obtained for a light-weight fighter in a pushover, for example, may not apply for a heavy-weight transport.

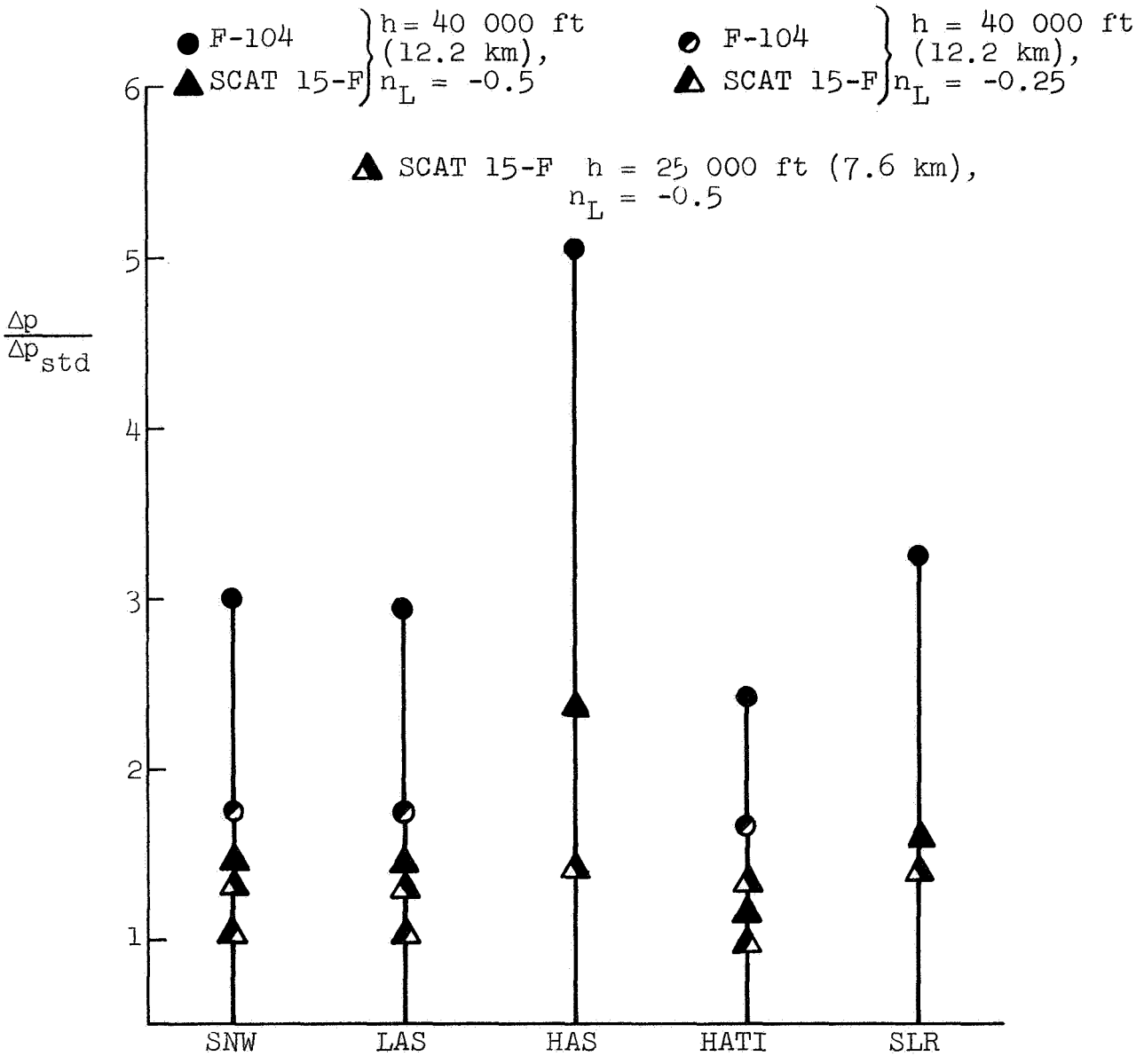

Figure 51. Overpressure ratios for climb-pushover maneuver; ϕ = 0, γ = 10 deg, M = 2.0

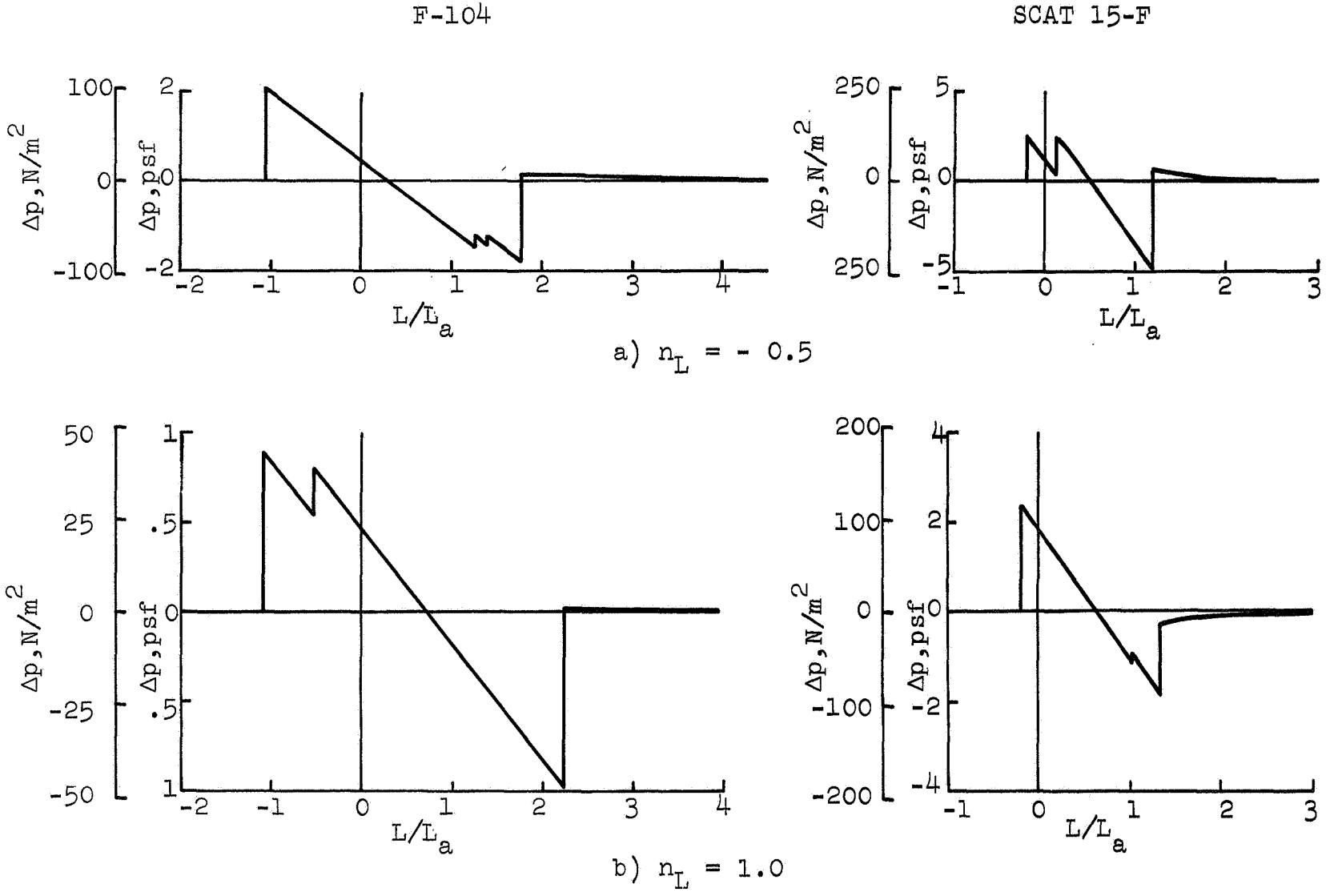

Figure 52. Signatures for pushover maneuver compared with level uniform flight at M = 2, SNW

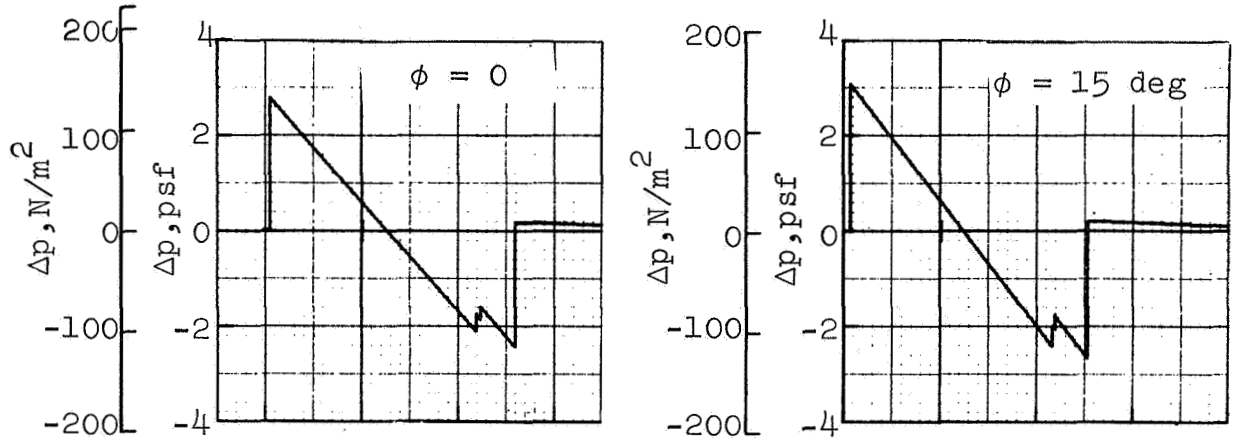

a) γ = 10 deg, $\dot{\gamma}$ = -1.42 deg/sec

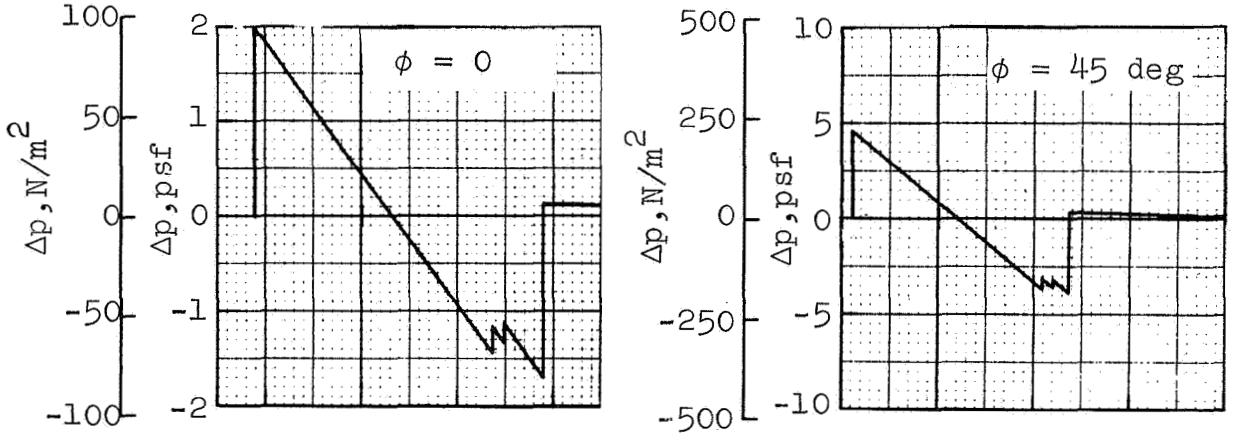

b) γ = 1.5 deg, $\dot{\gamma}$ = -1.42 deg/sec

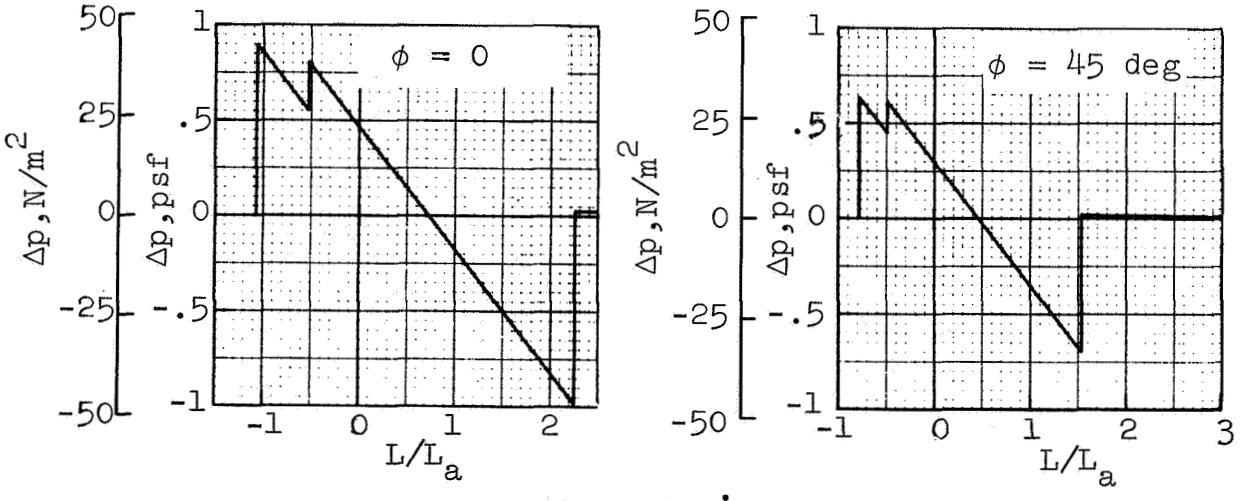

c) γ = 0, $\dot{\gamma}$ = 0

Figure 53. Signatures for pushover maneuver; M = 2.0, SNW, F-104

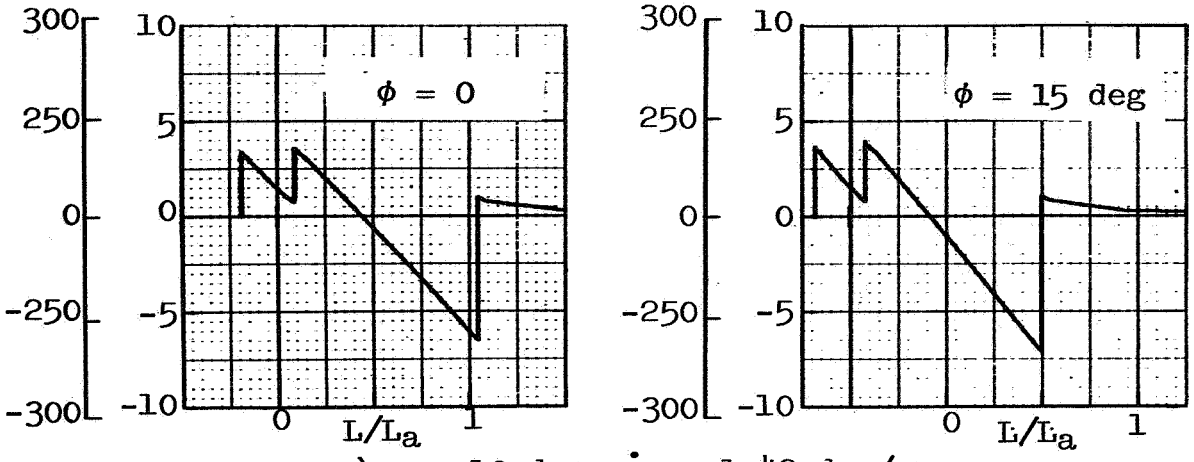

a) γ = 10 deg, $\dot{\gamma}$ = -1.42 deg/sec

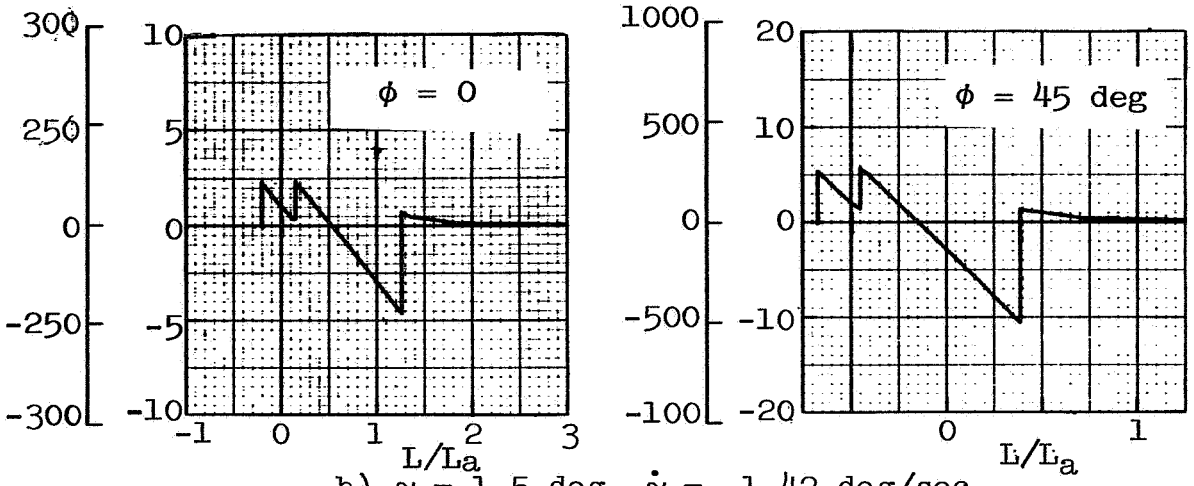

b) γ = 1.5 deg, $\dot{\gamma}$ = -1.42 deg/sec

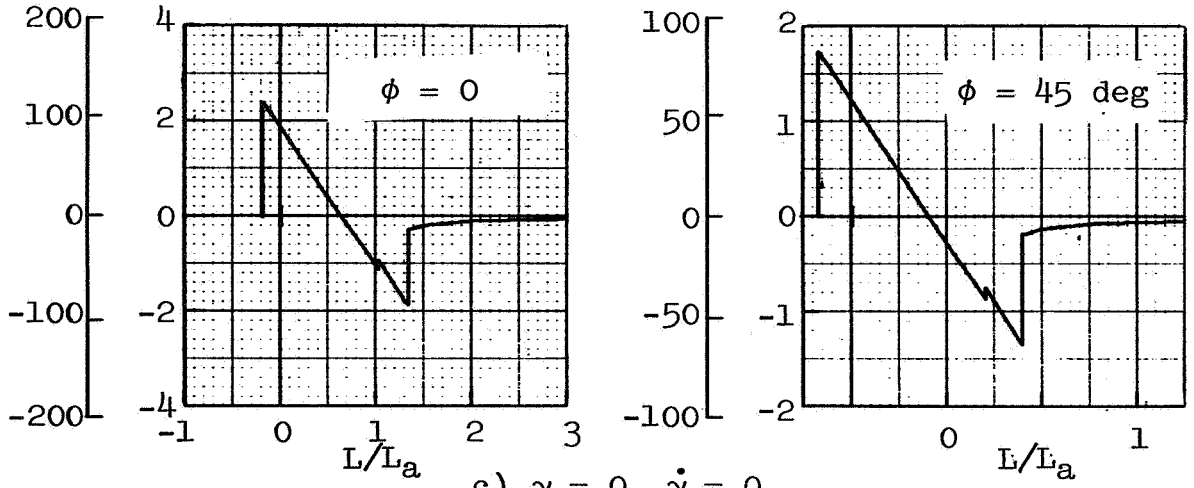

c) γ = 0, $\dot{\gamma}$ = 0

Figure 54. Signatures for pushover maneuver; M = 2.0, SNW, SCAT 15-F

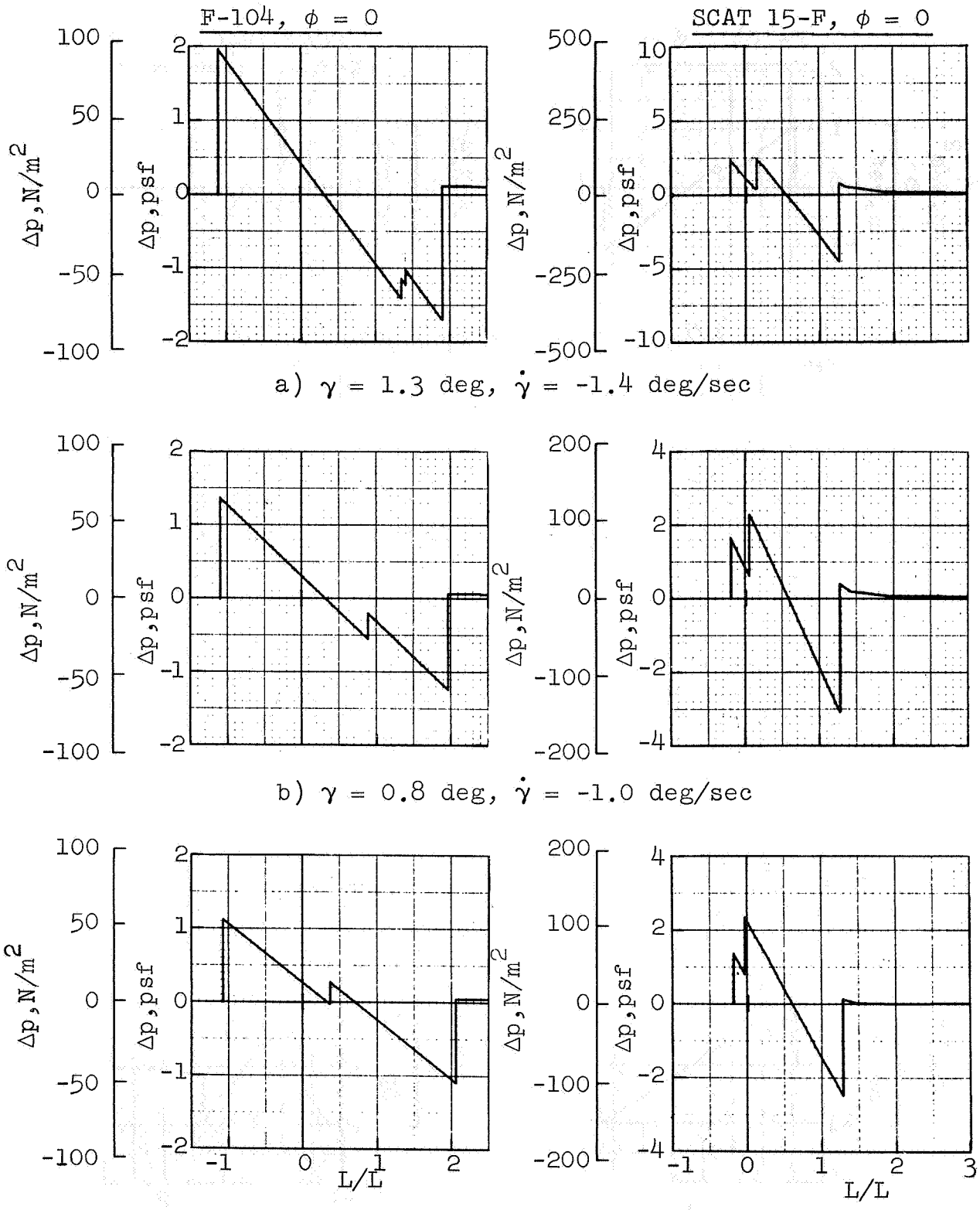

a) γ = 1.3 deg, $\dot{\gamma}$ = -1.4 deg/sec

b) γ = 0.8 deg, $\dot{\gamma}$ = -1.0 deg/sec

c) γ = 0.5 deg, $\dot{\gamma}$ = -0.6 deg/sec

Figure 55. Signatures for pushover maneuver, increasing $\dot{\gamma}$; M = 2

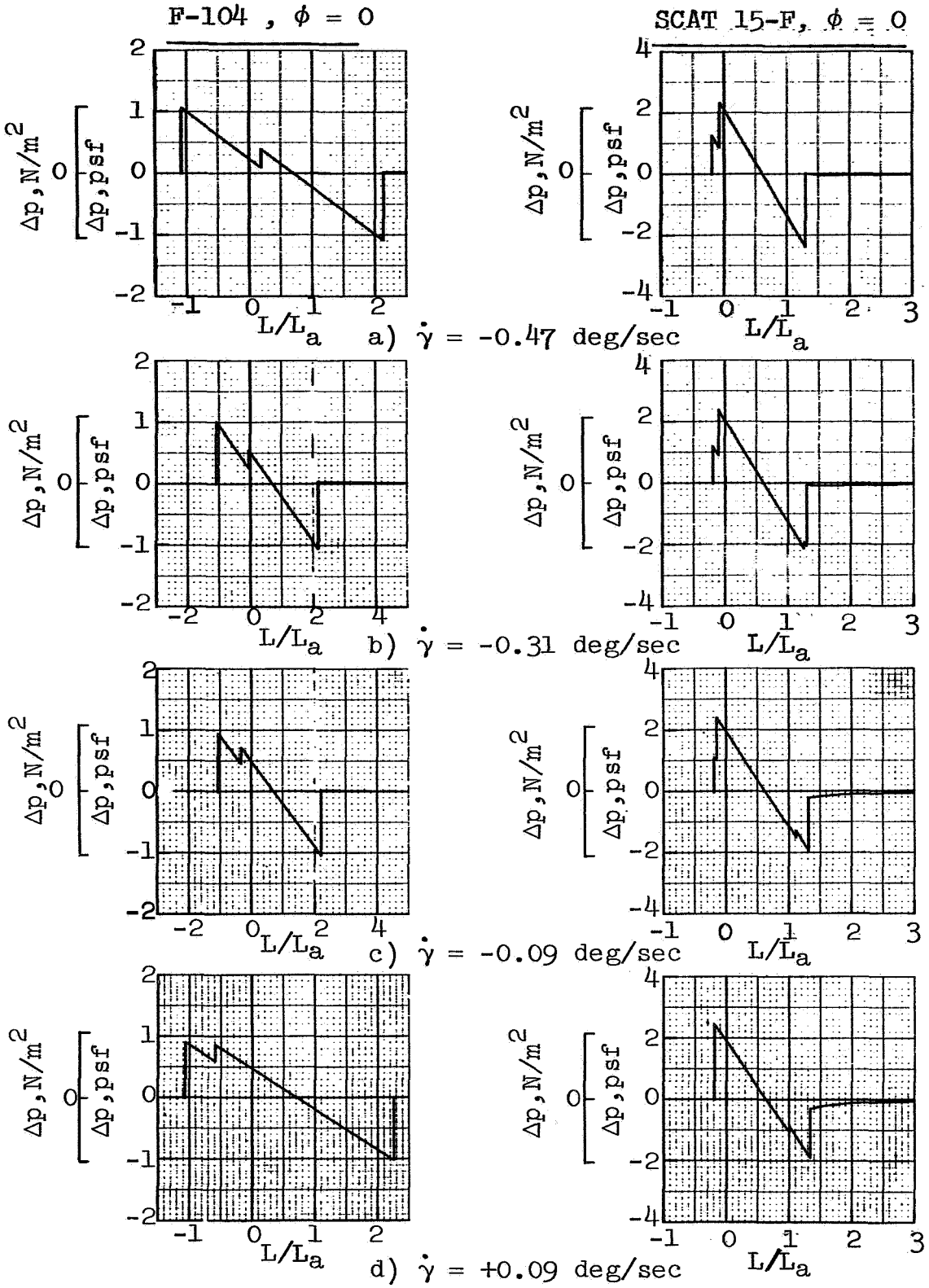

Figure 56. Signatures for pushover maneuver, increasing $\dot{\gamma}$; M = 2, γ = 0

Turn Maneuvers

Sonic boom propagation was calculated for constant altitude, circular turns at load factors n_L of 1.5 and 3.0 and Mach numbers of 1.5 and 2.0. (Figures 1, 4 and 5 again are referred to for nomenclature; in particular, ϕ_a is the bank angle and ψ is the heading (relative to north) of the aircraft.) The two load factors are achieved in equilibrium flight with aircraft bank angles ϕ_a of -48.19 and -70.53 degrees, respectively. The aircraft altitude is 40 000 ft (12.2 km). Overpressure ratios are summarized in figure 57 for the F-104 and SCAT 15-F aircraft for rays parameterized by $\psi = 90$ degrees and $\phi = 0$. For these values, the wind LAS is a headwind which increases the overpressures approximately 8% (above SNW) at $M = 1.25$, but has essentially no effect at Mach 2.0. The inversion HATI causes small changes in overpressure amounting to an increase of 2% for $M = 2.0$ and $n_L = 1.5$.

Variations of overpressures with changes in azimuth angle are presented in figure 58. Positive values of ϕ parameterize rays which leave the aircraft in a direction towards the inside of the turn circle; these are termed inner rays. Rays propagating outward (ϕ negative) are termed outer rays. For $M = 1.25$, the inner rays give large values of the overpressure ratios, rising from 1.2 at $\phi = 0$ to about 7 at $\phi = 10$ degrees. Farther in ($\phi > 10$ degrees), the inner rays focus before reaching the ground. Figure 59, to be discussed in detail later, shows the loci of the ray-ground intersections for $\phi = 0$ and 10 degrees. These form approximate boundaries of a "superboom ring" where large overpressures occur; ray focusing exists inside this ring. The radius of the superboom ring, for this maneuver only, is about twice the radius of aircraft turn circle (ground track). This superboom ring does not develop at Mach 2.0, as shown by the moderate overpressures in figure 58a, because the load factor $n_L = 1.5$ is not large enough to cause ray focusing even at large ϕ's. As mentioned earlier, the ray-path and focusing characteristics are independent of aircraft type and therefore these features apply here to both the F-104 and SCAT 15-F.

Figure 58b shows how the overpressure varies in an LAS east-wind situation. The aircraft heading of $\psi = 90$ degrees corresponds to a headwind, and as ψ reduces to zero the wind becomes a sidewind from starboard. For this maneuver and wind, all of the inner rays which were calculated at $\phi = 15$ degrees focused before reaching the ground. This figure therefore shows data only for negative ϕ's. The rays parameterized by $\phi = -30$ degrees become horizontal before reaching the ground for this LAS wind environment when $\psi > 0$.

A detailed summary of this turn maneuver ($M = 1.25$, $n_L = 1.5$) is given in figure 59. First, the aircraft locations are shown on

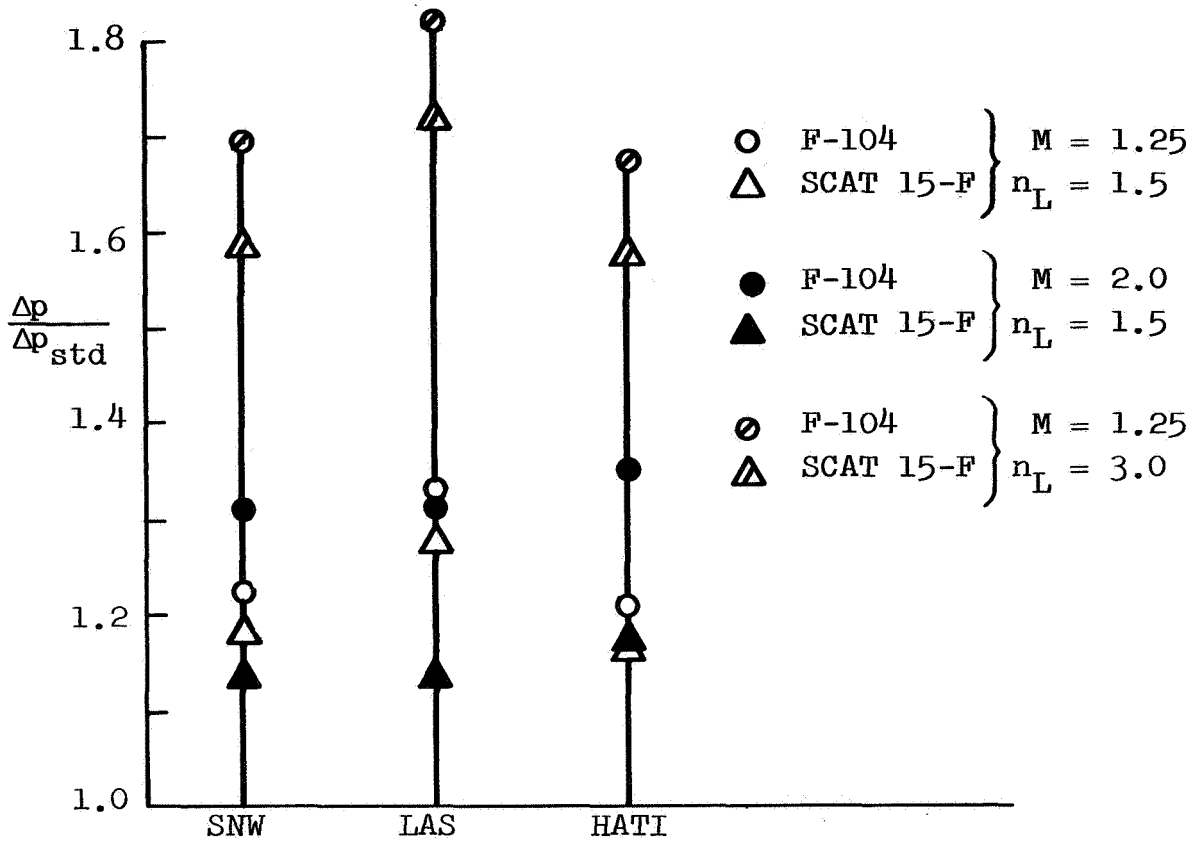

Figure 57. Overpressure ratios for turn maneuver; $\phi = 0$, $t_a = 0$

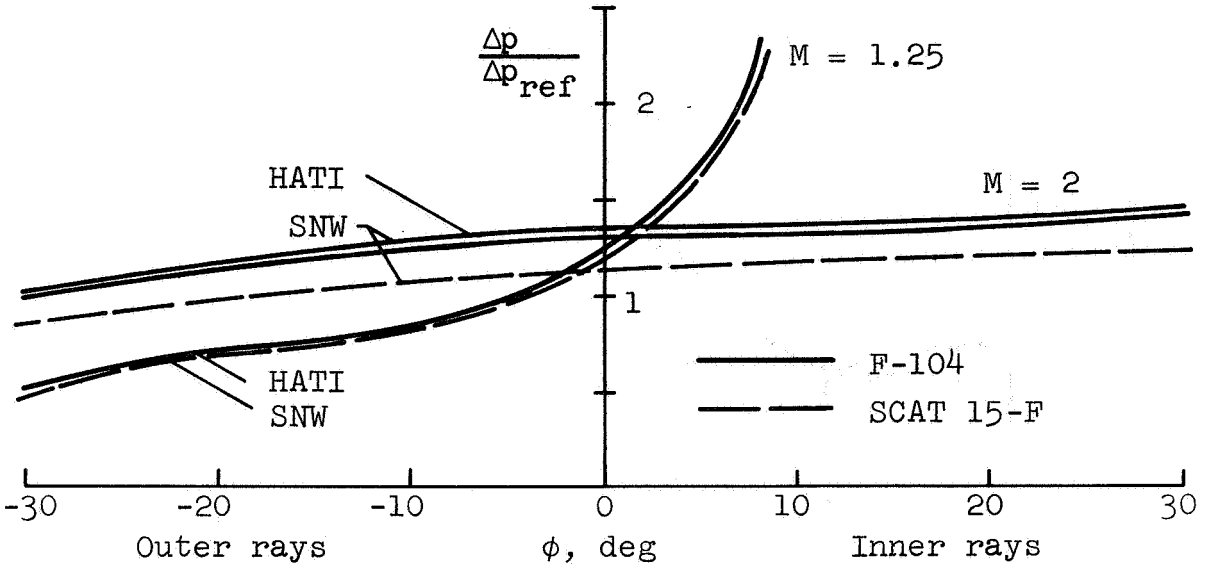

a) No wind

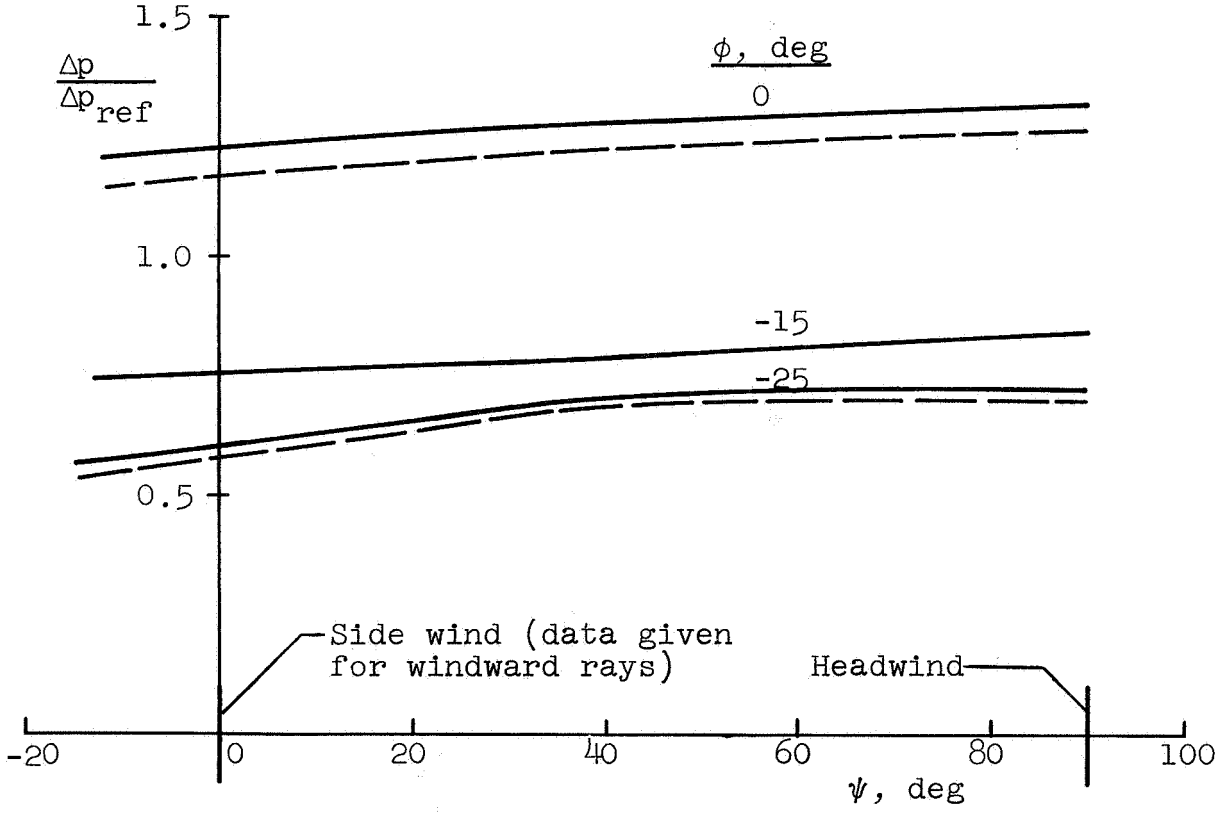

b) Wind LAS, M = 1.25

Figure 58. Overpressures for turn maneuvers at various azimuth angles

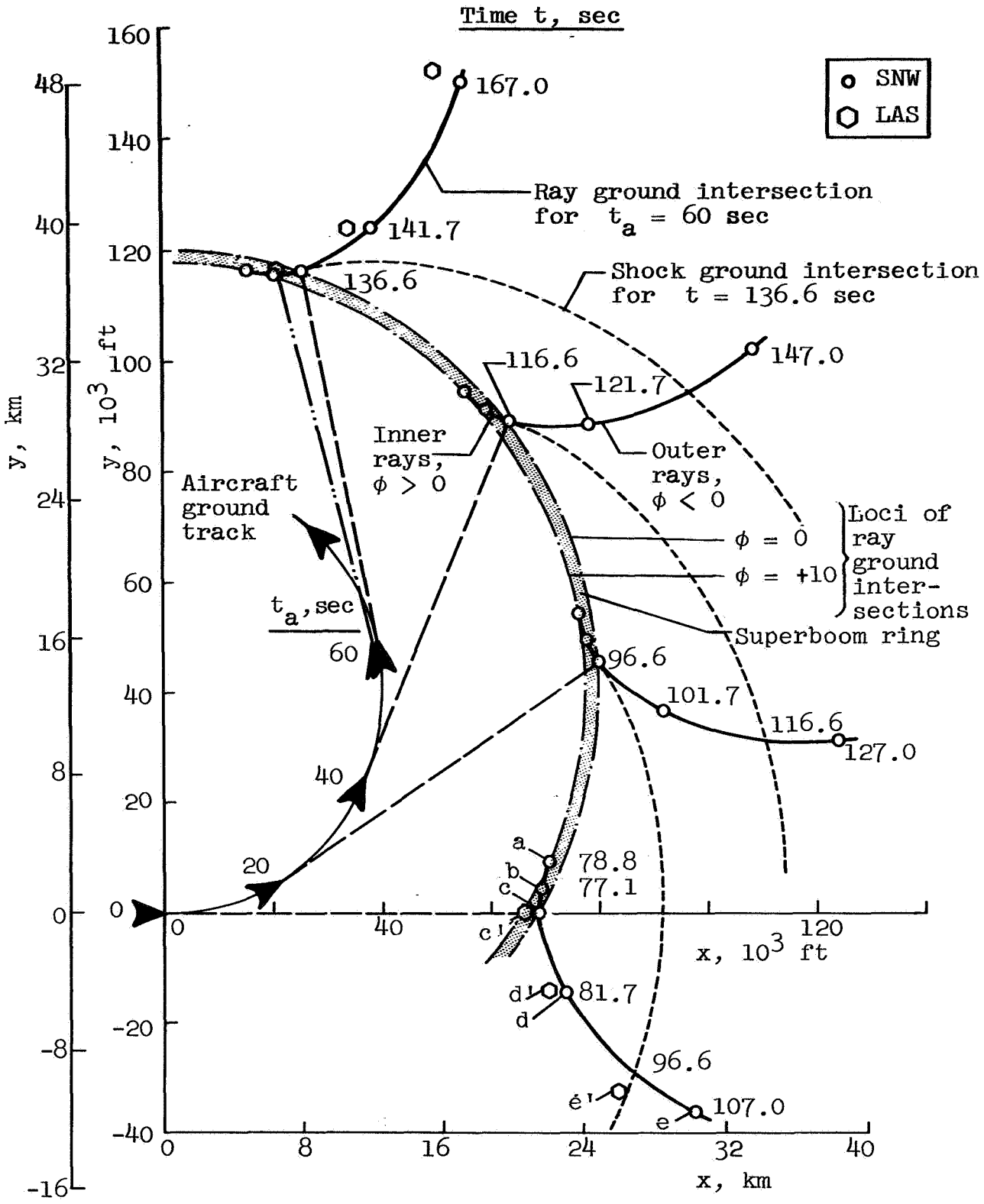

Figure 59. Overpressures and ground intersections for turn maneuver; n_L = 1.5, M = 1.25, SNW and LAS

its ground track for several maneuver times, t_a . The center of the turn circle and ray loci circles, for ϕ = constant, is at x = 0 , y = 41 000 ft (12.5 km). The ground intersections of rays are plotted for each t_a and intersection times for selected rays are given. Displacements of the ground track and ray-ground intersections caused by an east wind (LAS) are also indicated. Along the ray-ground intersection line for $t_a = 0$, the overpressures are as follows:

Location		Overpressure - psf (N/m^2) F-104	SCAT 15-F
	a	6.7 (320)	15.1 (722)
	b	1.4 (67)	3.1 (148)
SNW	c	1.0 (48)	2.3 (110)
	d	0.6 (29)	1.4 (67)
	e	0.4 (19)	0.9 (43)
	c'	1.1 (53)	2.4 (115)
LAS	d'	0.7 (34)	1.5 (72)
	e'	0.4 (19)	0.9 (43)

It is coincidental that at point c (SNW, $\phi = 0$), the overpressure for the F-104 is 1.0 (psf units). These overpressures (for SNW) apply at corresponding ray-ground intersections throughout the maneuver, as it is a steady turn.

For this plot, advantage was taken of the ground intersection interpolation subroutine in the digital program. This provided a set of values of overpressure, time, and ray location common to two ray-ground intersection curves for plotting the shock-ground intersections (dashed curves). These latter are the loci of the shock wave on the ground at given times. This shock location curve has a cusp at the ray-ground intersection where $\phi = 0$. One end of this curve terminates within the superboom ring when ray focusing occurs; the other end, shown here, is terminated at approximately the location where the rays are horizontal, beyond which no boom can occur.

Similar detail is given in figure 60 for M = 2.0 and $n_L = 1.5$. The turn radius here is almost identical to the radius of the ray locus $\phi = 0$. Also, as mentioned before, no superboom ring exists for this flight condition; the lateral extent of the boom is limited for both the inner and outer rays by their refraction beyond grazing (beyond ray horizontal). Overpressures for locations on the ray-ground intersection lines for this flight condition are as follows:

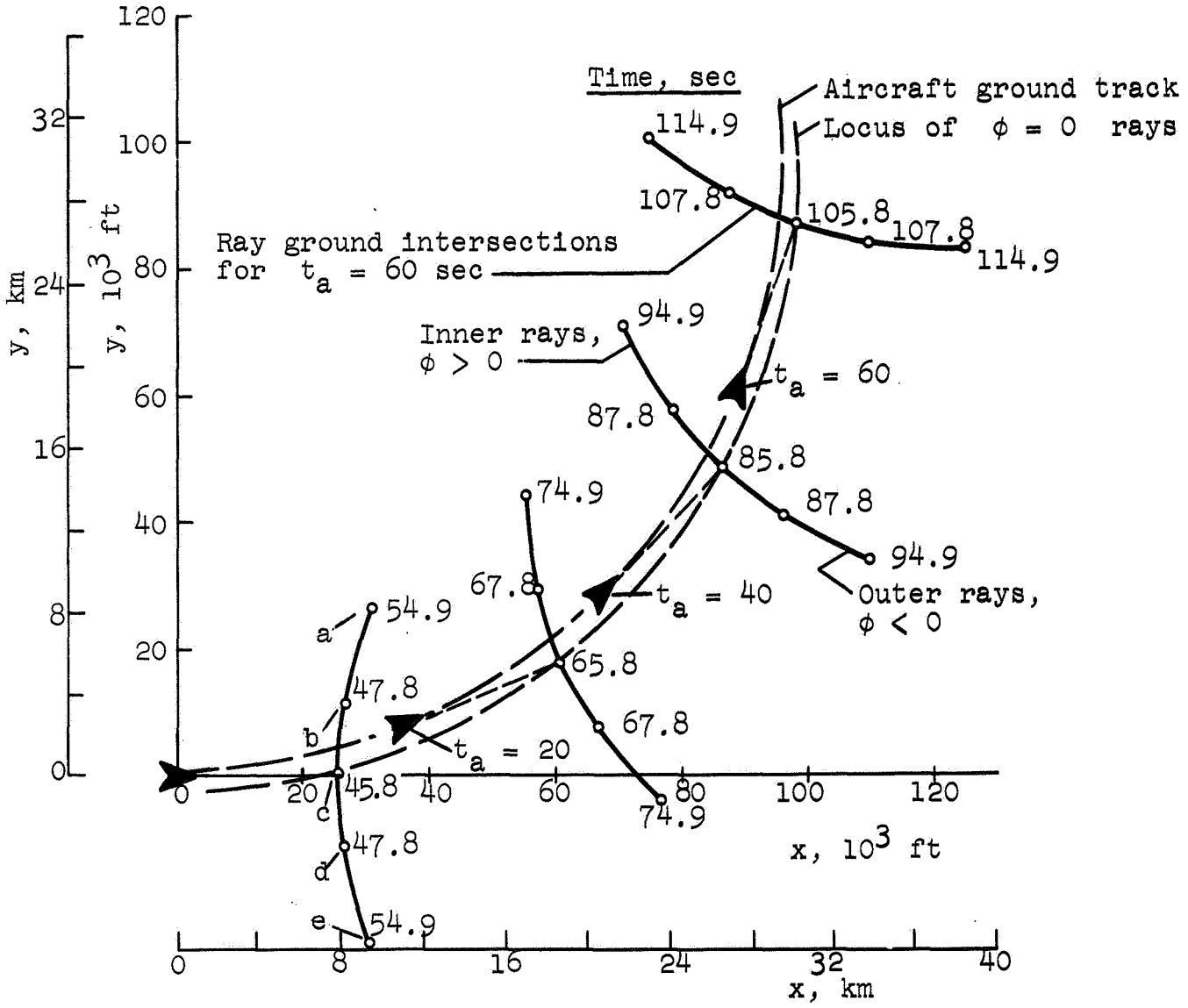

Figure 60. Overpressures and ground intersections for turn maneuver; $n_L = 1.5$, M = 2.0, SNW

Location	Overpressure - psf (N/m^2) F-104		SCAT 15-F	
a	1.3	(62)	3.0	(143)
b	1.3	(62)	2.9	(138)
c	1.2	(58)	2.8	(134)
d	1.1	(53)	2.5	(119)
e	0.9	(43)	2.1	(100)

These results illustrate important effects of flight conditions on ground overpressures in turn maneuvers. A superboom ring can exist for combinations of altitude, Mach number and load factor which cause ray focusing. If a given overpressure limit were to be prescribed, aircraft maneuver constraints on rate-of-turn (or bank angle) as functions of Mach number and altitude should be determined.

Porpoising Maneuver

Reference 11 reports a flight experiment designed to show effects of changing the vertical load factor n_L. The pilot cycled the elevon with a period of 1 sec. to obtain load factor increments of $\pm$ 0.5. This yields a porpoising maneuver wherein the aircraft undergoes small cyclic changes in flight path angle, altitude, angle-of-attack and attitude. For the aircraft flying at $M_\infty = 1.5$ at $h = 37\,200$ ft (11.2 km) above Edwards AFB (with $\Delta h \approx \pm$ 20 ft (6 m)), no important effects on overpressure were measured, surprisingly. Reference 12, for example, indicates that significant changes in overpressure may result from such a maneuver; as shown there for $M = 1.1$, $h = 15\,000$ ft (4.5 km) and $\Delta h \approx \pm$ 100 ft (30 m). The preceding results in this report for pullup and pushover also imply that strong effects may be expected.

The present study included calculations of a porpoising maneuver, similar to the flight test condition, sketched in figure 61. For these calculations the load factor was taken as constant over each half-cycle of the maneuver, and the flight path angle and rates were calculated for a flight path consisting of circular arcs.

Results from the porpoising maneuver calculations are shown in table VII for maneuver points selected to show effects of changing flight path angle γ and its rate $\dot{\gamma}$. Data are presented for both a uniform atmosphere (UNW) and the 1962 U.S.

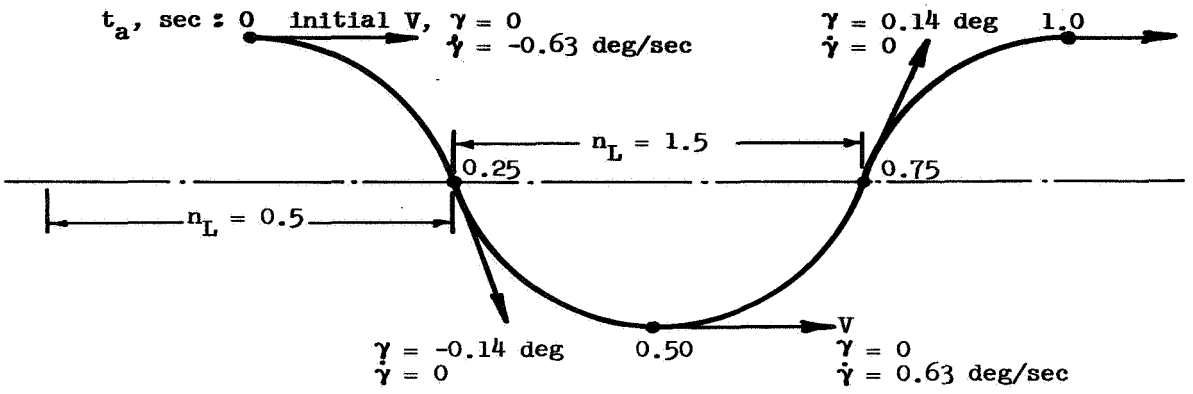

Figure 61. Porpoising maneuver

standard atmosphere (SNW) with an aircraft altitude of 40 000 ft (12.2 km). Further data, corresponding to the flight experiment, are shown for an aircraft altitude of 37 200 ft (11.2 km) over Edwards AFB. The uniform atmosphere data are shown multiplied by the atmospheric correction factor K_A (ref. 2) and by new factors K_A' and K_A'' required to adjust Δp (UNW) to Δp (SNW) at the first maneuver point.

These tabular data point out that the UNW results cannot be modified by a simple correction factor to get SNW results for maneuvering flight. These are again, as described previously in the section Pushover Maneuver, essential differences in the signatures which results from the variation of ray-tube area caused by the rate terms in the area equation, and from the aging of the signal.

Table VII shows that Δp at maneuver point 3.1 is larger than at 4.1 in the uniform atmosphere, but smaller in the standard atmosphere. Evidently the aging in the two atmospheres is significantly different. This is shown clearly in figure 62 where the signatures are shown for these maneuver points and atmospheres.

Also, variations in $\dot{\gamma}$ have a strong effect on the overpressure. Changing $\dot{\gamma}$ from -0.634 to + 0.634 deg/sec reduced Δp by 44%. On the other hand, changing γ from -0.1425 to + 0.1425 deg had essentially no effect. The F-function, it may be noted, changes with $\dot{\gamma}$ because it depends, in part, on the

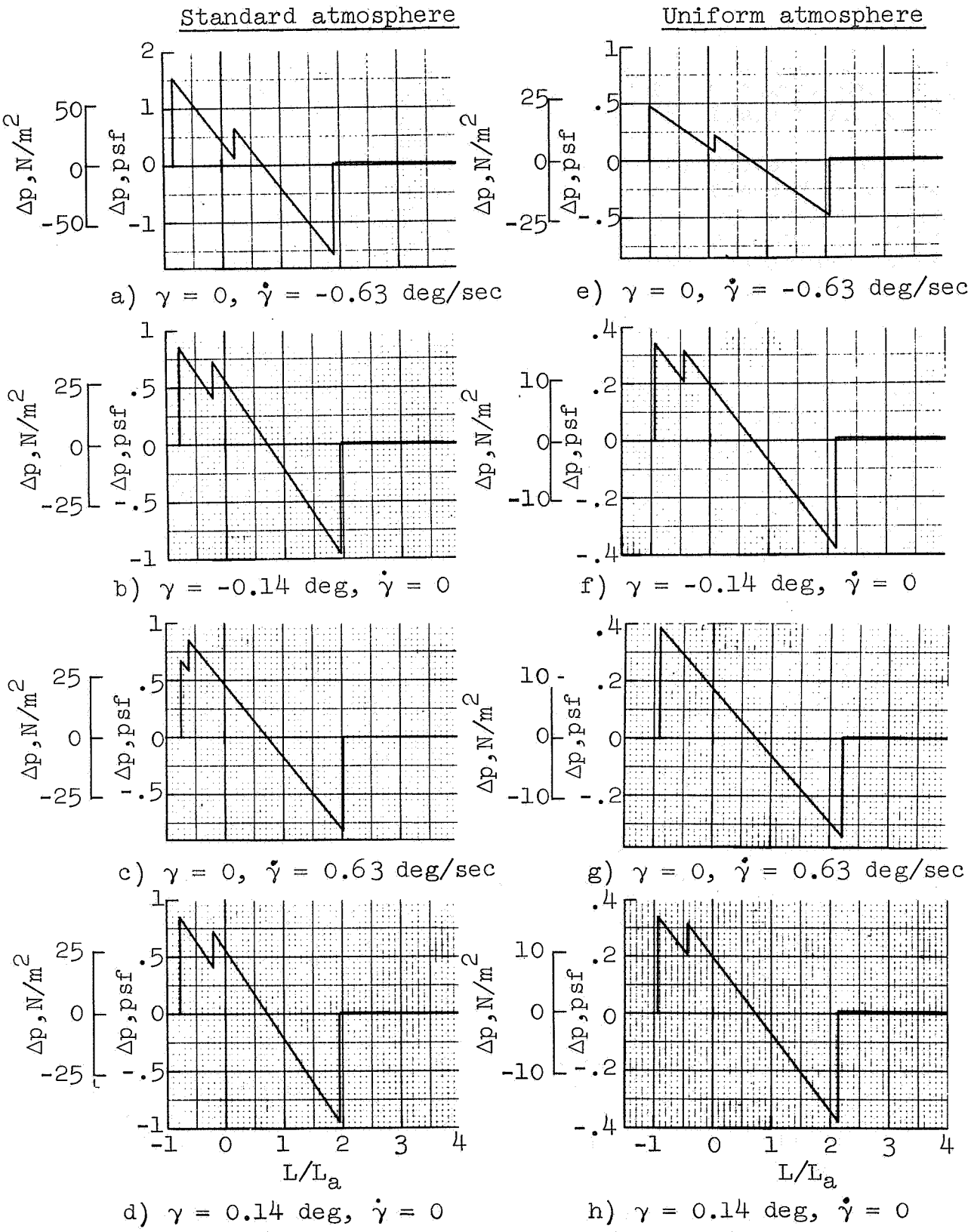

Figure 62. Signatures for porpoising flight at $n_L = \pm 0.5$

lift coefficient C_L which varies with load factor n_L. The pressure variation with $\dot{\gamma}$, however, is much larger than would be expected simply because of the variation of F with C_L.

These calculation results indicate strong effects of the flight path angle rate on overpressures at the ground. It would appear necessary to perform further flight experiments to generate such overpressures experimentally and to uncover atmospheric and flight condition effects and reasons for differences between measurements and computations.

CONCLUDING REMARKS

The analysis and computer program of reference 1 has provided a means for calculating sonic boom pressure signatures for arbitrary flight conditions and for atmospheric conditions with horizontal stratification. These techniques have been used to obtain results, presented herein, for a wide variety of aircraft maneuvers and atmospheres. The present results covered a broad scope of variation of parameters to point out significant effects and parameter sensitivities, and to provide a general source of data for sonic boom evaluations. Both a fighter-type aircraft (F-104) and an SST-type (SCAT 15-F) were used as a basis for these calculations. Complete F-functions were used as input for determining their overall pressure signatures as distorted by nonlinear propagation effects. These signatures included all of their shock waves.

Parametric data have been presented which show the sonic boom overpressure, the length of the signature, the ray-travel time and the ray-ground distance for various atmospheres, winds, aircraft Mach numbers and altitudes. Features of the digital program were demonstrated showing where ray-ground intersections and shock-ground intersections occur for turn maneuvers, along with other geometric and sonic boom characteristics.

Comparisons of overpressures with previous analytic results have been made. These are restricted basically to uniform flight inasmuch as previous analyses did not include capabilities for calculating overpressures for general aircraft maneuvers. They did, however, include variations of atmospheric temperature profile, wind speed and direction, and aircraft Mach number. The agreement with the results of reference 4 for those uniform flight conditions which were examined is remarkably good, although differences were shown for some conditions near ray focusing.

Several comparisons of overpressures with previous experimental results for accelerating and porpoising flight were also made. For the accelerating flight, good agreement with measured

overpressures was shown, except a displacement of about 2 miles in ground location remains unexplained. For the porpoising flight, significant effects of the flight path angle rate on the signature shape and overpressure were calculated, although not realized in the flight measurements.

A very important part of the present results has been the pressure signatures and their variations with both atmospheric and flight conditions. Among the various features illustrated by these results, the following are particularly noteworthy:

a) The variation of the signatures with aircraft altitude and propagation distance were shown. A large part of the aging of the signal occurs within the first few thousand feet of propagation distance. The pressure signature represented by the initial F-function distorts very rapidly and, for such complex F-functions as used here, multiple shock waves quickly appear. Some of these shocks merge as the wave front continues to travel through the atmosphere, but the signature at the ground need not be a fully developed N-wave. In general, aging in a standard atmosphere exhibits an asymptotic limit whereas in a uniform atmosphere aging increases indefinitely.

b) Overpressure ratios are not independent of aircraft type, so that detailed evaluation of sonic boom characteristics may require data to be generated for each specified aircraft. Also, realistic atmospheres (such as the 1962 U.S. standard) and complete signatures should be used for specific sonic boom analysis.

c) The lengths of the signatures calculated with realistic atmospheres, such as SNW, are shorter than the lengths calculated with uniform atmospheres (UNW).

d) Effects of wind-speed profile and wind direction were also analyzed. It was shown that highest overpressures occur with the headwind for ray paths, both on and off the flight track.

e) Large overpressures may result from longitudinal acceleration, pushover and turn maneuvers.

With these generalized results at hand, studies related to specific aircraft can be more adequately defined. These studies can, for example, result in useful performance characteristics related to sonic boom constraints, such as maneuver limitations as functions of speed, altitude and wind conditions. In addition, flight experiments can be defined to establish pressure measurements under superboom conditions, using the present computer program to determine ray paths and overpressure variations along the ground.

REFERENCES

1. Hayes, Wallace D.; Haefeli, Rudolph C.; and Kulsrud, H.E.: Sonic Boom Propagation in a Stratified Atmosphere, with Computer Program. NASA CR-1299, 1969.

2. Lansing, Donald L.: Application of Acoustic Theory to Prediction of Sonic Boom Ground Patterns from Maneuvering Aircraft. NASA TND-1860, 1964.

3. Friedman, Manfred P.: A Description of a Computer Program for the Study of Atmospheric Effects on Sonic Booms. NASA CR-157, 1965.

4. Kane, Edward J.; and Palmer, Thomas Y.: Meteorological Aspects of the Sonic Boom. FAA SRDS Report No. RD-64-160, Sept. 1964 (Available from DDC as AD-610463).

5. Whitham, George B.: The Flow Pattern of a Supersonic Projectile, Comm. Pure Appl. Math., vol. 5, 1952.

6. Carlson, Harry W.: Correlation of Sonic Boom Theory with Wind Tunnel and Flight Measurements. NASA TR R-213, 1964.

7. U.S. Standard Atmosphere, 1962. U.S. Government Printing Office, Washington, D.C., 1962.

8. Maglieri, Domenic J.; Hilton, David A.; and McLeod, Norman J.: Experiments on the Effects of Atmospheric Refraction and Airplane Accelerations on Sonic Boom Ground-Pressure Patterns. NASA TN D-3520, 1966.

9. Hubbard, Harvey H.; Maglieri, Domenic J.; Huckel, Vera; and Hilton, David A.: Ground Measurements of Sonic Boom Pressures for the Altitude Range of 10 000 to 75 000 Feet. NASA TR R-198, 1964.

10. Lansing, Donald L.; and Maglieri, Domenic J.: Comparisons of Measured and Calculated Sonic Boom Ground Patterns Due to Several Different Aircraft Maneuvers. NASA TN D-2730, 1965.

11. Garrick, I.E.; and Maglieri, Domenic J.: A Summary of Results on Sonic Boom Pressure-Signature Variations Associated with Atmospheric Conditions. NASA TN D-4588, 1968.

12. Randall, D.G.: Methods for Estimating Distributions and Intensities of Sonic Bangs. A.R.C. Technical Report R&M No. 3113, 1959.

TABLE I

Schedule of Solutions

Maneuver	Set no.	Run no.		Atmosphere			Initial Mach no.			Initial altitude	
				No wind	Wind variations	Temperature variations					
		F-104	SCAT 15-F	UNW SNW	LAS MAS HAS	LATI HATI SLR	1.25	1.3	2.0	40 000 ft (12.2 km)	25 000 ft (7.6 km)
Steady flight, $\phi = 0$ only	1	1 2 3 4 5 6	7 8 9 10 11 12	X X	 X X	 X X	X ↓ ↓ ↓ X	 X	 	X ↓ ↓ ↓	
Steady flight, vary altitude of signature. h_g = 30K; 20K; 10K ft (9.1; 6.1; 3.0 km) $\phi = 0$ only	2	13-15 16-18 19-21	22-24 25-27 28-30	X	 X	 X	X ↓ X	X		X ↓	
Steady flight, vary Mach no. M = 1.3, 1.5, 2.0, 3.0 $\phi = 0$	3	31-34 35-38 39-42 43-46 63-67	47-50 51-54 55-58 59-62	X X	 X	 X X X	Various ↓ ↓ ↓			X ↓ ↓	
Steady flight, vary aircraft altitude. h = 25 000; 50 000; 80 000 ft (7.6; 15.3; 24.5 km) $\phi = 0$	4	63-65 66-68 69-71 72-74 75-77	76A-77A-78 79-81 82-84 85-87 88-90	X X	 X 	 X	X ↓ ↓ ↓			Various ↓ ↓	
Steady flight, tailwind $\phi = 0$	5	91 92 93 94-96	97 98 99 100-102	 Repeat above group	X X	 	X ↓ ↓		 X	X ↓ ↓	
Steady flight, vary wind direction ϕ = 45, 90, 135° $\phi = 0$	6		103-105 103B		X X		X X			X X	
Steady flight, lateral range effects near cutoff	7	106 107 108 109 110-113	114 115 116 117 118-121	X X Repeat above group	 X 	 X 	X ↓ ↓ ↓		 X	X ↓ ↓ ↓	
Horizontal acceleration, n_T = 0.3 g's	8	122 123 124 125 126 127 128 136-142	129 130 131 132 133 134 135 143-149	X X Repeat above group	 X X X 	 X X 	X ↓ ↓ ↓ ↓ ↓ ↓		 X	X ↓ ↓ ↓ ↓ ↓ ↓	
Dive-pull up, n_L = 1.5 g's	9	150 151 152 153 154 160-164	155 156 157 158 159 165-169	X X Repeat above group	 X 	 X X 	X ↓ ↓ ↓ ↓		 X	X ↓ ↓ ↓ ↓	
Climb-pushover, n_L = -0.5 g's	10	170 171 172 173 174 180-184	175 176 177 178 179 185-189 190-194	X X Repeat above group	 X 	 X X 	X 		 X	X ↓ ↓ ↓ ↓	 X
90° turn, n_L = 1.5 g's	11	195 196 197 201-203	198 199 200 204-206	X X Repeat above group	 	 X 	X 		 X	X ↓ ↓	
Low altitude, horizontal acceleration, n_T = 0.3 g's	12	207 208 209	210 211 212	X X	 	 X	X ↓ ↓			 	X ↓ ↓
Horiz. acceleration, n_T = 0.15 g's	13	213 214 215	216 217 218	X X	 	 X	 		X ↓ ↓	X ↓ ↓	
Dive-pullout[1] Climb-pushover[2] 90° turn[1]	14	219-221 222-224 225-227	228-230 231-233 234-236	Repeat above group " " " " " "			X ↓ ↓			X ↓ ↓	
Flight test, acceleration	15	237-240					Mach 1.18 to 1.51			37200 ft. (11.4 km)	
Short period oscillation, n_L = 0.5 to 1.5 g's	16	241		X			Mach 1.5			35000 ft. (10.6 km)	

[1] n_L = 3.0 g's

[2] n_L = -0.25 g's

TABLE II .-SUMMARY OF SONIC BOOM RESULTS

Set number	Run number	Aircraft	Maneuver time	Azimuth angle, ϕ	Δp (Peak overpressure)		$\frac{\Delta p}{\Delta p_{std}}$	$\frac{\Delta p}{\Delta p_{ref}}$	L_1/L_A	Ray-ground intersection					Remarks
										t	x		y		
			secs	deg	lb/ft^2	N/m^2				secs	ft	km	ft	km	
1	1	F-104	0	0	0.31	14.8	0.38		2.91	68.9	0	0	53334	16.26	
	2				.82	39.3	1.00		2.72	76.6			68730	20.95	
	3				.88	42.1	1.07		2.72	76.5			66181	20.17	
	4				1.61	77.0	1.97		2.85	114.5			97774	29.80	M = 1.3
	5				.84	40.2	1.025		2.67	74.0			64406	19.63	
	6				.88	42.1	1.07		2.72	78.4			70851	21.60	
	7	SCAT 15-F			.78	37.3	.95		1.39	68.9			53334	16.26	
	8				1.95	93.4	1.00		1.33	76.6			68730	20.95	
	9				2.11	101.0	1.08		1.33	76.5			66181	20.17	
	10				3.85	184.2	1.97		1.33	114.5			97774	29.80	M = 1.3
	11				1.96	93.8	1.005		1.31	74.0			64406	19.63	
	12				2.11	101.0	1.08		1.33	78.4			70851	21.60	
2	13	F-104	0	0	1.15	55.1	1.42		2.12	17.3	0	0	13666	4.16	
	14				.85	40.7	1.04		2.59	35.5			29151	8.89	
	15				.81	38.8	.99		2.66	55.0			47159	14.37	
	16				1.21	57.9	1.48		2.13	15.5			7789.8	2.37	M = 1.3
	17				.91	43.6	1.11		2.60	33.1			19816	6.04	
	18				.92	44.0	1.12		2.69	57.1			41022	12.50	
	19				1.15	55.1	1.42		2.11	17.2			13297	4.05	
	20				.90	43.1	1.11		2.59	34.9			27799	8.47	
	21				.85	40.6	1.05		2.66	54.5			46024	14.03	
	22	SCAT 15-F			2.30	110.1	1.18		1.23	17.3			13668	4.17	
	23				1.94	92.8	.995		1.28	35.5			29153	8.89	
	24				1.88	90.0	.96		1.31	55.0			47160	14.37	
	25				2.45	117.3	1.25		1.23	15.5			7789.8	2.37	M = 1.3
	26				2.07	99.1	1.06		1.29	33.1			19816	6.04	
	27				2.18	104.3	1.11		1.33	57.1			41022	12.50	
	28				2.31	110.6	1.18		1.22	17.2			13297	4.05	
	29				1.99	95.2	1.02		1.27	34.9			27799	8.47	
	30				1.97	94.3	1.01		1.31	54.5			46024	14.03	
3	31	F-104	0	0	.32	15.3	.39		2.92	64.7	0	0	48155	14.68	
	32				.34	16.3	.42		3.08	55.4			35777	10.90	
	33				.38	18.2	.47		3.78	47.7			23094	7.04	
	34				.43	20.6	.53		5.47	43.8			14142	4.31	
	35				.82	39.3	1.00			69.0			59338	18.09	
	36				.86	41.2	1.05			55.3			41046	12.51	

TABLE II.-SUMMARY OF SONIC BOOM RESULTS - *continued*

Set number	Run number	Aircraft	Maneuver time	Azimuth angle, ϕ	Δp (Peak overpressure)		$\frac{\Delta p}{\Delta p_{std}}$	$\frac{\Delta p}{\Delta p_{ref}}$	L_1/L_A	Ray-ground intersection					Remarks
										t	x		y		
			secs	deg	lb/ft^2	N/m^2				secs	ft	km	ft	km	
3	37	F-104	0	0	0.94	45.0	1.15	1.0		45.8	0	0	25402	7.74	
	38				1.06	50.7	1.30			41.4			15293	4.66	
	39				1.85	88.6	2.26			111.7			97621	29.75	h_g = 219ft(66m)
	40				.84	40.2	1.04	.98		34.8			24599	7.50	
	41				.90	43.1	1.10	.96	3.31	46.5			20540	6.26	
	42				1.02	48.8	1.25	.96	4.74	41.5			10089	3.08	
	43				.86	41.2	1.05		2.71	69.8			60252	18.36	
	44				.87	41.6	1.06	1.01	2.76	55.5			41159	12.55	
	45				.94	45.0	1.15	1.00	3.31	45.9			25391	7.74	
	46				1.05	50.3	1.28	.99	4.76	41.5			15277	4.66	
	47	SCAT 15-F			.80	38.3	.41		1.40	64.7			48155	14.68	
	48				.90	43.1	.46		1.44	55.4			35777	10.90	
	49				1.03	49.3	.52		1.73	47.7			23094	7.04	
	50				1.12	53.6	.57			43.8			14142	4.31	F-function at M = 2.7
	50F				1.19	56.9	.61		2.80	43.8			14142		
	51				1.96	93.8	1.005			69.0			59338	18.09	
	52				2.10	100.5	1.08			55.3			41046	12.51	
	53				2.46	117.8	1.26			45.8			25402	7.74	
	54				2.74	131.2	1.41			41.4			15293	4.66	F-function at M = 2.7
	54F				2.92	139.8	1.50		2.41	41.4			15293	4.66	
	55				4.25	203.5	2.18		1.40	109.8			95539	29.12	h_g = 300ft(90m)
	56				2.06	98.6	1.06	.98		59.4			39098	11.92	
	57				2.36	112.9	1.21	.92		46.5			20540	6.26	
	58				2.65	126.9	1.36	.96	2.18	41.5			10089	3.08	
	58F				2.82	135.0	1.45	1.03	2.41	41.5			10089	3.08	F-function at M = 2.7
	59				2.05	98.2	1.05		1.34	69.8			60252	18.36	
	60				2.12	101.5	1.09	1.01	1.36	55.5			41159	12.55	
	61				2.45	117.3	1.21		1.52	45.9			25391	7.74	
	62				2.71	129.8	1.39	.99	2.19	41.5			15277	4.66	F-function at M = 2.7
	62F				2.89	138.4	1.48	1.05	2.42	41.5			15277	4.66	
	63	F-104			.76	36.4	.93	.91	2.75	88.1			82021	25.00	LATI,M=1.2
	64				1.08	51.7	1.32	1.02	4.74	41.5			15244	4.65	LATI,M=3.0
	65				.79	37.8	.97	.95	2.73	84.2			76508	23.32	HATI,M=1.2
	66				1.10	52.7	1.34	1.04	4.74	41.8			15075	4.59	HATI,M=3.0
	67				1.07	51.2	1.31	1.28	2.78	97.7			93682	28.55	SLR ,M=1.2

TABLE II.-SUMMARY OF SONIC BOOM RESULTS - continued

Set number	Run number	Aircraft	Maneuver time	Azimuth angle, ϕ	Δp (Peak overpressure)		$\frac{\Delta p}{\Delta p_{std}}$	$\frac{\Delta p}{\Delta p_{ref}}$	L_1/L_A	Ray-ground intersection					Remarks
										t	x		y		
			secs	deg	lb/ft^2	N/m^2				secs	ft	km	ft	km	
4	63	F-104	0	0	.88	42.1	1.07		2.52	41.0	0	0	33334	10.16	
	64				.22	10.5	.27		3.26	86.1			66667	20.32	
	65				.07	3.4	.09		6.42	136.4			106660	32.51	
	66				1.52	72.8	1.85		2.38	43.5			39076	11.91	
	67				.77	36.9	.94			93.9			82062	25.01	
	68				.54	25.9	.66		5.03	142.2			118190	36.02	
	69				1.58	75.7	1.93		2.38	43.3			37546	11.44	
	70				.83	39.7	1.01		2.83	93.7			78996	24.08	
	71				.58	27.8	.71			142.0			113670	34.65	
	72				1.54	73.7	1.88		2.49	56.1			50153	15.29	
	73				1.59	76.1	.82		3.03	123.9			102750	31.32	h_g=600ft(180m)
	74				.60	28.7	.73			135.9			93882	28.62	
	75				1.56	74.6	1.90		2.41	47.2			44161	13.46	
	76				.84	40.4	1.03		2.84	95.6			84184	25.66	
	77				.58	27.8	.71		5.03	143.6			119860	36.53	
	76A	SCAT 15-F			1.70	81.3	.87		1.28	41.0			33334	10.16	
	77A				.50	23.9	.26		1.69	86.1			66667	20.32	
	78				.19	9.1	.097		3.76	136.4			106660	32.51	
	79				2.82	135.0	1.45			43.5			39078	11.91	
	80				1.68	80.4	.86		1.54	93.9			82063	25.01	
	81				1.56	74.7	.80			142.2			118190	36.02	
	82				2.92	139.8	1.49			43.4			37547	11.44	
	83				1.82	87.1	.93		1.54	93.7			78998	24.08	
	84				1.66	79.5	.85			142.1			113670	34.65	
	85				2.97	142.2	1.52			56.2			50159	15.29	
	86				3.53	169.0	1.81		1.59	123.9			102750	31.32	h_g=600ft(180m)
	87				1.72	82.4	.88			135.9			93882	28.62	
	88				2.91	139.3	1.49		1.25	47.2			44161	13.46	
	89				1.83	87.6	.94		1.54	95.6			84184	25.66	
	90				1.68	80.4	.86		2.92	143.6			119860	36.53	
5	91	F-104	0	0	.77	36.9	.94		2.72	77.4	0	0	72067	21.97	
	92				.80	38.3	.98		2.71	74.5			69652	21.23	
	93				.80	38.3	.98		2.70	67.9			66960	20.41	
	94				.95	45.5	1.16	1.01	3.30	45.8			26856	8.19	
	95				.95	45.5	1.16	1.01	3.30	45.7			27461	8.37	
	96				.98	46.9	1.20	1.04	3.30	45.3			30505	9.30	
	97	SCAT 15-F			1.85	88.6	.95			77.4			72067	21.97	
	98				1.91	91.5	.98		1.33	74.5			69652	21.23	
	99				1.88	90.0	.97			67.9			66960	20.41	

TABLE II.-SUMMARY OF SONIC BOOM RESULTS - continued

Set number	Run number	Aircraft	Maneuver time	Azimuth angle, ϕ	Δp (Peak overpressure)		$\frac{\Delta p}{\Delta p_{std}}$	$\frac{\Delta p}{\Delta p_{ref}}$	L_1/L_A	Ray-ground intersection					Remarks
										t	x		y		
			secs	deg	lb/ft^2	N/m^2				secs	ft	km	ft	km	
5	100	SCAT 15-F	0	0	2.47	118.3	1.27		1.52	45.8	0	0	26856	8.19	
	101				2.48	118.7	1.27	1.01	1.52	45.7			27461	8.37	
	102				2.57	123.1	1.32			45.3			30505	9.30	
	103				.84	40.2	1.03	1.00	2.75	90.2			84770	25.84	HAS, M=1.2, η=0
	104				.765	36.6	.935	.91	2.72	74.8			76393	23.28	HAS, M=1.2
	105				1.09	52.2	1.33	1.03	4.73	41.3			20532	6.26	HAS, M=3.0
6	103	SCAT 15-F	0	0	1.99	95.3	1.02		1.33	79.0	-2600	- .79	68987	21.03	
	104				1.95	93.4	1.00		1.33	76.6	-3628.6	-1.11	68730	20.95	
	105				1.92	91.9	.985		1.33	75.0	-2552.9	- .78	69237	21.10	
	106	F-104			.82	39.3	1.00	.97	2.75	90.2	-11000	-3.35	84770	25.84	HAS, M=1.2, η=90
	107				1.06	50.8	1.29	1.00	4.75	41.4	-5583.3	-1.70	15292	4.66	HAS, M=3.0, η=90
7	106	F-104	0	0	.31	14.8	.38		2.91	68.9	0	0	53333	16.26	
				45	.24	11.5	.29		2.77	97.4	39999	12.19	75424	22.99	
				86.66	.04	1.9	.05		4.44	1182.0	685380	208.90	915400	279.01	
	107			0	.82	39.2	1.0		2.72	76.6	0	0	68729	20.95	
				20	.76	36.3	.93		2.66	86.4	19952	6.08	77784	23.71	
				33.44	.65	31.1	.79		2.70	129.7	49487	15.08	119740	36.50	
	108														NO RAY-GROUND INTERSECTION
	109			0	.88	42.0	1.07		2.72	78.4	0	0	70850	21.60	
				20.	.85	40.6	1.04		2.67	91.2	21394	6.52	83403	25.42	
				25.78	.88	42.0	1.07		2.71	112.7	34405	10.49	105470	32.15	
	110			0	.38	18.2	.46		3.77	47.7	0	0	23093	7.04	
				20	.36	17.2	.44		3.29	50.8	14558	4.44	24576	7.49	
				80	.12	5.7	.14		2.86	274.8	226840	69.14	132990	40.54	
	111			0	.94	44.9	1.15		3.31	45.8	0	0	25401	7.74	
				20	.89	42.5	1.09		2.89	49.4	16259	4.96	27447	8.37	
				54.69	.45	21.5	.55		2.32	130.0	106010	32.31	75006	22.86	
	112														NO RAY-GROUND INTERSECTION

TABLE II.-SUMMARY OF SONIC BOOM RESULTS - continued

Set number	Run number	Aircraft	Maneuver time	Azimuth angle, ϕ	Δp (Peak overpressure)		$\frac{\Delta p}{\Delta p_{std}}$	$\frac{\Delta p}{\Delta p_{ref}}$	L_1/L_A	Ray-ground intersection					Remarks
										t	x		y		
			secs	deg	lb/ft^2	N/m^2				secs	ft	km	ft	km	
7	113	F-104	0	0	.94	44.9	1.15		3.31	45.9	0	0	25391	7.74	
				20	.89	42.5	1.09		2.90	49.5	16266	4.96	27459	8.37	
				51.41	.52	24.8	.63		2.33	112.8	89381	27.24	66025	20.12	
	114	SCAT 15-F		0	.78	37.3	.40		1.39	68.9	0	0	53333	16.26	
				45	.62	29.7	.32		1.29	97.4	39999	12.19	75424	22.99	
				86.66	.10	4.8	.05		2.09	1182.0	685380	208.90	915400	279.01	
	115			0	1.95	93.4	1.00		1.33	76.6	0	0	68729	20.95	
				20	1.85	88.6	.95		1.30	86.4	19952	6.08	77784	23.71	
				33.44	1.63	78.1	.84		1.28	129.7	49487	15.08	119740	36.50	
	116														NO RAY-GROUND INTERSECTION
	117			0	2.11	101.0	1.09		1.33	78.4	0	0	70850	21.60	
				20	2.07	30.6	1.06		1.31	91.2	21394	6.52	83403	25.42	
				25.78	2.19	104.9	1.12		1.31	112.7	34405	10.49	105470	32.15	
	118			0	1.03	49.3	.53		1.73	47.7	0	0	23093	7.04	
				45	.80	38.2	.41		1.19	67.5	39999	12.19	32659	9.95	
				87.54	.10	4.8	.05		1.89	1111.0	930610	283.64	537780	163.92	
	119			0	2.46	117.8	1.26		1.52	45.8	0	0	25401	7.74	
				20	2.35	112.5	1.21		1.32	49.4	16259	4.96	27447	8.37	
				54.69	1.23	58.9	.63		1.07	130.0	106010	32.31	75006	22.86	
	120														NO RAY-GROUND INTERSECTION
	121			0	2.46	117.8	1.26		1.52	45.9	0	0	25391	7.74	
				20	2.36	113.0	1.21		1.32	49.5	16266	4.96	27459	8.37	
				51.41	1.41	67.5	.72		1.09	112.8	89381	27.24	66025	20.12	
8	122	F-104	0	0	2.42	115.9			2.83	64.8	0	0	53995	16.46	
			2		1.70	81.4			2.79	65.1			54372	16.57	
			6		1.31	62.7			2.77	66.3			55907	17.04	
	123		10		1.33	63.7			2.77	70.2	0	0	58787	17.92	
			30		1.01	48.4			2.87	82.1			75728	23.08	
			50		.98	46.9			3.08	98.1			101670	30.99	

TABLE II.-SUMMARY OF SONIC BOOM RESULTS - continued

Set number	Run number	Aircraft	Maneuver time	Azimuth angle, ϕ	Δp (Peak overpressure)		$\frac{\Delta p}{\Delta p_{std}}$	$\frac{\Delta p}{\Delta p_{ref}}$	L_1/L_A	Ray-ground intersection					Remarks
										t	x		y		
			secs	deg	lb/ft^2	N/m^2				secs	ft	km	ft	km	
8	124	F-104	10	0	1.42	67.9			2.78	71.2	0	0	58717	17.90	
			30		1.01	48.4			2.87	82.4			74540	22.72	
			50		.97	46.4			3.07	98.3			99789	30.42	
	125		20		1.31	62.7			2.84	79.4			62454	19.04	
			30		1.05	50.3			2.89	84.6			69270	21.11	
			50		.96	46.0			3.09	99.3			90843	27.69	
	126		10		1.28	61.3			2.77	70.2			60659	18.49	
			30		1.01	48.4			2.87	82.1			78097	23.80	
			50		.99	47.4			3.08	98.2			104560	31.87	
	127		10		1.25	59.9			2.76	69.8			59423	18.11	
			30		1.03	49.3			2.87	82.1			77429	23.60	
			50		1.01	48.4			3.08	98.3			104100	31.73	
	128		10		1.38	66.1			2.77	70.6			61349	18.70	
			30		1.01	48.4			2.87	82.2			78350	23.88	
			50		.98	46.9			3.08	98.2			104700	31.91	
	129	SCAT 15-F	0		6.03	288.7			1.38	64.8			53995	16.46	
			2		4.22	202.1			1.37	65.1			54372	16.57	
			6		3.23	154.7			1.37	66.3			55907	17.04	
	130		10		3.28	157.0			1.37						
			30		2.52	120.7			1.38						
			50		2.50	119.7			1.44						
	131		10		3.51	168.1			1.37						
			30		2.52	120.7			1.38						
			50		2.49	119.2			1.44						
	132		20		3.28	157.0			1.38						
			30		2.63	125.9			1.39						
			50		2.45	117.3			1.44						
	133		10		3.16	151.3			1.37						
			30		2.53	121.1			1.38						
			50		2.53	121.1			1.44						
	134		10		3.09	147.9			1.37						
			30		2.57	123.1			1.38						
			50		2.58	123.5			1.44						

TABLE II.-SUMMARY OF SONIC BOOM RESULTS - continued

Set number	Run number	Aircraft	Maneuver time	Azimuth angle, ϕ	Δp (Peak overpressure)		$\frac{\Delta p}{\Delta p_{std}}$	$\frac{\Delta p}{\Delta p_{ref}}$	L_1/L_A	Ray-ground intersection					Remarks
										t	x		y		
			secs	deg	lb/ft^2	N/m^2				secs	ft	km	ft	km	
8	135	SCAT 15-F	10	0	3.41	163.3			1.37		0	0			
			30		2.54	121.6			1.38						
			50		2.50	119.7			1.44						
	136	F-104	0		.98	46.9			3.32	45.8			25401	7.74	
			4		.99	47.4			3.37	49.4			32524	9.91	
			6		.99	47.4			3.40	51.3			36160	11.02	
	137		0		.98	46.9			3.32	45.8			23953	7.30	
			4		.98	46.9			3.37	49.4			30969	9.44	
			6		.98	46.9			3.40	51.2			34551	10.38	
	138		0		.98	46.9			3.32	45.9			23356	7.12	
			20		1.01	48.4			3.86	63.2			59410	18.11	
			30		1.05	49.3			4.16	72.4			81187	24.75	
	139		0												NO DATA
			20		.98	46.9			3.86	63.5			14849	4.53	
			30		1.00	47.9			4.15	72.7			12933	3.94	
	140		0		1.00	47.9			3.32	45.8			25298	7.71	
			20		1.03	49.3			3.86	63.3			62484	19.04	
			30		1.05	50.3			4.15	72.5			84826	25.85	
	141		0		1.02	48.8			3.33	46.1			24947	7.60	
			20		1.05	50.3			3.87	63.6			62242	18.97	
			30		1.07	51.2			4.16	72.8			84614	25.79	
	142		0		.98	46.9			3.33	45.9			25391	7.74	
			20		1.01	48.4			3.87	63.3			62538	19.06	
			30		1.03	49.3			4.17	72.5			84870	25.87	
	143	SCAT 15-F	0		2.58	123.5			1.52						
			4		2.60	124.5			1.54						
			6		2.61	125.0			1.55						
	144		0		2.57	123.1			1.52						
			4		2.59	124.0			1.54						
			6		2.60	124.5			1.55						
	145		0		2.56	122.6			1.52						
			20		2.65	126.9			1.76						
			30		2.69	128.8			1.89						

TABLE II.-SUMMARY OF SONIC BOOM RESULTS - continued

Set number	Run number	Aircraft	Maneuver time	Azimuth angle, ϕ	Δp (Peak overpressure)		$\frac{\Delta p}{\Delta p_{std}}$	$\frac{\Delta p}{\Delta p_{ref}}$	L_1/L_A	Ray-ground intersection					Remarks
										t	x		y		
			secs	deg	lb/ft^2	N/m^2				secs	ft	km	ft	km	
8	146	SCAT 15-F	0	0	2.49	119.2			1.52		0	0			
			20		2.57	123.1			1.76						
			30		2.61	125.0			1.89						
	147		0		2.61	125.0			1.52						
			20		2.71	129.8			1.76						
			30		2.75	131.7			1.89						
	148		0		2.67	127.8			1.52						
			20		2.77	132.6			1.76						
			30		2.80	134.1			1.90						
	149		0		2.57	123.1			1.52						
			20		2.65	126.9			1.76						
			30		2.68	128.3			1.90						
9	150	F-104	0		.79	37.8	.96		3.07	56.9			43318	13.20	γ = -10 deg
			6		.67	32.1	.82		2.82	69.3			60068	18.31	γ = 4.9 deg
			12		.56	26.8	.685		2.66	85.7			80598	24.57	γ = -0.24 deg
	151		0		.80	38.3	.975		3.07	56.9			41465	12.64	
			6		.69	33.0	.84		2.82	69.2			57783	17.61	
			12		.60	28.7	.73		2.66	85.6			77774	23.76	
	152		0		.70	33.5	.855		3.08	62.0			42358	12.91	
			4		.55	26.3	.67		2.91	76.4			59317	18.08	
			6		.47	22.5	.57		2.85	87.5			71716	21.86	
	153		0		.82	39.3	1.00		3.07	56.7			42028	12.81	
			6		.70	33.5	.855		2.82	68.4			57864	17.64	
			12		.58	27.8	.71		2.66	83.2			76439	23.30	
	154		0		.80	38.3	.975		3.07	57.1			43474	13.25	
			6		.68	32.6	.83		2.83	69.8			60606	18.47	
			12		.56	26.8	.685		2.66	87.4			82559	25.16	
	155	SCAT 15-F	0		1.85	88.6	.95		1.66						
			6		1.60	76.6	.82		1.52						
			12		1.33	63.7	.68		1.42						

TABLE II.-SUMMARY OF SONIC BOOM RESULTS - continued

Set number	Run number	Aircraft	Maneuver time	Azimuth angle, ϕ	Δp (Peak overpressure)		$\frac{\Delta p}{\Delta p_{std}}$	$\frac{\Delta p}{\Delta p_{ref}}$	L_1/L_A	Ray-ground intersection					Remarks
										t	x		y		
			secs	deg	lb/ft^2	N/m^2				secs	ft	km	ft	km	
9	156	SCAT 15-F	0	0	1.87	89.5	.96		1.66		0	0			
			6		1.64	78.5	.84		1.52						
			12		1.43	68.5	.735		1.42						
	157		0		1.63	78.0	.835		1.67						
			4		1.30	62.2	.67		1.57						
			6		1.10	52.7	.565		1.53						
	158		0		1.92	91.9	.985		1.66						
			6		1.67	80.0	.855		1.52						
			12		1.41	67.5	.725		1.42						
	159		0		1.86	89.1	.955		1.67						
			6		1.63	78.0	.835		1.52						
			12		1.36	65.1	.70		1.43						
	160	F-104	0		1.19	57.0		1.27	4.88	41.5			15752	4.80	M=2, γ=10 deg
			12		1.10	52.7		1.17	3.76	52.4			42793	13.04	γ= -4.16 deg
			20		1.07	51.2		1.14	3.32	61.5			61644	18.79	γ= -0.28 deg
	161		0		1.19	57.0		1.27	4.88	41.5			14451	4.40	
			12		1.11	53.1		1.18	4.06	52.4			41156	12.54	
			20		1.06	50.8		1.13	3.32	61.5			59725	18.20	
	162		0		1.16	55.5		1.235	4.89	41.7			10554	3.22	
			12		1.04	49.8		1.11	3.76	52.9			36241	11.05	
			20		.97	46.4		1.03	3.29	62.7			54248	16.53	
	163		0		1.25				4.90	41.9			15526	4.73	
			12		1.15				3.78	52.8			42453	12.94	
			20		1.10				3.32	61.8			61199	18.65	
	164		0		1.18				4.89	41.6			15736	4.80	
			12		1.11				3.78	52.5			42777	13.04	
			20		1.06				3.33	61.6			61633	18.79	
	165	SCAT 15-F	0		2.71				2.43						
			12		2.81				1.80						
			20		2.76				1.57						
	166		0		2.70				2.43						
			12		2.79				1.79						
			20		2.75				1.57						

TABLE II.-SUMMARY OF SONIC BOOM RESULTS - continued

Set number	Run number	Aircraft	Maneuver time	Azimuth angle, ϕ	Δp (Peak over-pressure)		$\frac{\Delta p}{\Delta p_{std}}$	$\frac{\Delta p}{\Delta p_{ref}}$	L_1/L_A	Ray-ground intersection					Remarks
										t	x		y		
			secs	deg	lb/ft^2	N/m^2				secs	ft	km	ft	km	
9	167	SCAT 15-F	0	0	2.61	125.0		1.06	2.43						
			12		2.63	125.9		1.07	1.79						
			20		2.52	120.7		1.02	1.55						
	168		0		2.82	135.0		1.14	2.43						
			12		2.92	139.8		1.19	1.80						
			20		2.87	137.4		1.17	1.57						
	169		0		2.69	128.8		1.09	2.44						
			12		2.78	133.1		1.13	1.80						
			20		2.74	131.2		1.11	1.57						
10	170	F-104	6	0	.80	38.3			2.72	83.4	0	0	76581	23.34	Level Flight
			6	-10	.79	37.8			2.70	85.6	9291.3	2.83	78575	23.95	$\gamma = \dot{\gamma} = 0$
			6	-30	.68	32.6			2.65	113.9	36776.0	11.21	105300	32.10	
	175	SCAT 15-F	6	0	1.94	92.9			1.34						
			6	-10	1.91	91.5			1.33						
			6	-30	1.69	80.9			1.29						
	180	F-104	0	0	2.81	134.5		2.99							
				15	3.10	148.4		3.30							
				30											
			4	0	2.12	101.5		2.26							
				15	2.13	102.0		2.26							
				30	2.30	110.1		2.44							
			6	0	1.99	95.3		2.12	3.02	54.0			39284	11.97	
				15	1.97	94.3		2.10							
				30	1.98	94.8		2.11							
			6	-15	1.97	94.3		2.10	2.81	56.2	12439.0	3.79	40479	12.34	$\gamma = 0$ for
			6	-30	1.98	94.8		2.105	2.44	63.8	27757.0	8.46	44823	13.66	$t > 6.514$
			6	-45	4.58	219.3		4.88	2.25	84.8	53904.0	16.43	56930	17.35	
			8	0	.90	43.1		.96	3.33	55.2			41500	12.65	
			8	-15	.87	41.7		.925	3.07	57.2	12200.0	3.72	42635	13.00	
			8	-30	.79	37.8		.84	2.62	64.5	27117.0	8.27	46731	14.24	
			8	-45	.64	30.6		.68	2.32	84.0	51904.0	15.82	57799	17.62	
	181		0	0	2.75	131.7		2.93	2.55	53.3			36434	11.10	$\gamma = 10$ deg
			4		2.10	100.5		2.24	2.83	53.7			37024	11.28	$\gamma = 4.3$ deg
			8		.90	43.1		.96	3.33	55.2			39770	12.12	$\gamma = \dot{\gamma} = 0$

TABLE III.-SUMMARY OF SONIC BOOM RESULTS - continued

Set number	Run number	Aircraft	Maneuver time	Azimuth angle, ϕ	Δp (Peak overpressure)		$\frac{\Delta p}{\Delta p_{std}}$	$\frac{\Delta p}{\Delta p_{ref}}$	L_1/L_A	Ray-ground intersection					Remarks
										t	x		y		
			secs	deg	lb/ft^2	N/m^2				secs	ft	km	ft	km	
10	182	F-104	6	0	4.74	227.0		5.05	3.07	54.8	0	0	33002	10.06	γ = 1.47 deg
			8		.86	41.2		0.905	3.34	55.8			34766	10.60	
	183		0	0	2.27	108.7		2.42	2.54	53.4			37180	11.33	
			4		1.99	95.3		2.12	2.83	53.9			38105	11.61	
			8		.93	44.5		0.99	3.34	55.5			41045	12.51	
	184		0	0	3.07	147.0		3.27	2.56	53.5			38225	11.65	
			4		2.16	103.4		2.30	2.82	53.8			38731	11.81	
			8		.90	43.1		0.96	3.34	55.3			41489	12.65	
	185	SCAT 15-F	0	0	3.59	243.7		1.46							γ = 10 deg
				15	3.98	190.6		1.62							
				30											
			4	0	2.63	126.0		1.07							γ = 4.32 deg
				15	2.65	126.9		1.08							
				30	2.90	138.9		1.18							
			6	0	2.44	116.9		0.99							γ = 1.47 deg
				15	2.43	116.3		0.99							
				30	2.47	118.3		1.01	1.47						
			6	-15	2.43	116.3		0.99	1.36						
			6	-30	2.47	118.3		1.005	1.17						
			6	-45	5.94	284.4		2.32	1.06						
			8	0	2.41	115.4		1.02	1.53						
			8	-15	2.34	112.0		0.95	1.40						
			8	-30	2.13	102.0		0.87	1.20						
			8	-45	1.74	83.3		0.71	1.07						
	186		0	0	3.51	168.1		1.43	1.23						
			4		2.60	124.5		1.06	1.37						
			8		2.40	114.9		1.02	1.53						
	187		6		5.86	280.6		2.38	1.49						
			8		2.32	111.1		0.945	1.53						
	188		0	0	2.90	138.9		1.18	1.23						
			4		2.46	117.8		1.00	1.37						
			8		2.49	119.2		1.01	1.53						
	189		0	0	3.92	187.7		1.59	1.23						
			4		2.67	127.8		1.09	1.37						
			8		2.40	114.9		0.975	1.53						

TABLE II.-SUMMARY OF SONIC BOOM RESULTS - continued

Set number	Run number	Aircraft	Maneuver time	Azimuth angle, ϕ	Δp (Peak overpressure)		$\frac{\Delta p}{\Delta p_{std}}$	$\frac{\Delta p}{\Delta p_{ref}}$	L_1/L_A	Ray-ground intersection					Remarks
										t	x		y		
			secs	deg	lb/ft^2	N/m^2				secs	ft	km	ft	km	
10	190B	SCAT 15-F	0	0	3.22	154.2		1.31	1.15	31.8	0	0	22911	6.98	
				-10	3.18	152.3		1.29	1.12	32.5	5471.6	1.68	23304	7.10	
				-20	3.07	147.0		1.25	1.07	34.6	11493	3.50	24589	7.49	
				-30	2.88	137.9		1.17	1.00	38.9	18897	5.76	27173	8.28	
			4	0	3.23	154.7		1.31	1.29	34.4			27243	8.30	
			8		3.25	155.6		1.31	1.43	37.0			32381	9.87	
	191		0	0	3.21	153.7		1.30	1.15	31.8			21851	6.66	
			4		3.22	154.2		1.31	1.29	34.4			26129	7.96	
			8		3.70	177.2		1.50	1.43	37.0			31200	9.51	
	192		0	0	3.59	171.9		1.46	1.15	33.3			22537	6.87	
			4		3.53	169.0		1.43	1.29	35.3			25469	7.76	
			8		3.58	171.4		1.45	1.41	37.5			29535	9.00	
	193		0	0	3.25	155.6		1.31	1.15	31.9			22146	6.75	
			4		3.28	157.0		1.33	1.30	34.6			26719	8.14	
			8		3.86	184.8		1.57	1.43	37.3			31980	9.75	
	194		0	0	3.39	162.3		1.38	1.15	32.4			24191	7.37	
			4		1.29	61.8		.525	1.29	34.7			27971	8.53	
			8		3.66	175.2		1.49	1.42	37.2			32693	9.96	
11	195A	F-104	0	10	6.75	323.2	8.22		2.99	78.8	70714	21.55	9209.4	2.81	
				5	1.37	65.6	1.67		2.83	77.2	69211	21.09	4524	1.38	
					1.00	47.9	1.22		2.77	76.6	68729	20.95			
	195		0	-15	.62	29.7	.76		2.65	81.7	73429	22.38	-14253	-4.34	
			0	-30	.39	18.7	.475		2.53	107.0	97356	29.67	-36508	-11.13	
			40	0	1.00	47.9	1.22		2.77	116.6	63446	19.34	89288	27.21	
			60	0	1.00	47.9	1.22		2.77	136.6	25394	7.74	116480	35.50	
	196		0	0	1.08	51.6	1.32		2.77	76.5	66180	20.17	0	0	
			0	-25	.59	28.2	.72		2.57	94.9	83082	25.32	-27242	-8.30	
			20	0	1.06	50.6	1.29		2.77	96.5	76626	23.36	45346	13.82	
			40	0	1.02	48.7	1.25		2.77	116.5	59811	18.23	89166	27.18	
			60	0	.99	42.4	1.21		2.77	136.7	21159	6.45	116590	35.54	

TABLE II.-SUMMARY OF SONIC BOOM RESULTS - continued

Set number	Run number	Aircraft	Maneuver time	Azimuth angle, ϕ	Δp (Peak overpressure)		$\frac{\Delta p}{\Delta p_{std}}$	$\frac{\Delta p}{\Delta p_{ref}}$	L_1/L_A	Ray-ground intersection					Remarks
										t	x		y		
			secs	deg	lb/ft^2	N/m^2				secs	ft	km	ft	km	
11	197	F-104	0	0	.99	47.4	1.21		2.75	74.0	64404	19.63	0	0	
			0	-15	.65	31.1	.79		2.64	78.0	67954	20.71	13190	4.02	
			0	-30	.45	21.5	.55		2.52	94.1	82194	25.05	30822	9.39	
			40	0	.99	47.4	1.21		2.75	114.0	61831	18.85	85276	25.99	
			60	0	.99	47.4	1.21		2.75	134.0	26302	8.02	112250	34.21	
	198A	SCAT 15-F	0	10	15.14	724.9	7.75		1.55						
				5	3.13	149.9	1.60		1.51						
				0	2.30	110.1	1.18		1.49						
	198		0	-15	1.44	68.9	.74		1.44						
			0	-30	.90	43.1	.46		1.38						
			40	0	2.30	110.1	1.18		1.49						
			60	0	2.30	110.1	1.18		1.49						
	199		0	0	2.47	118.7	1.27		1.49						
			0	-25	1.36	65.1	.70		1.40						
			20	0	2.43	116.2	1.25		1.49						
			40	0	2.34	112.0	1.20		1.49						
	200		0	0	2.26	108.2	1.16		1.49						
			0	-15	1.51	72.3	.775		1.44						
			0	-30	1.04	49.8	.535		1.37						
			40	0	2.26	108.2	1.16		1.49						
			60	0	2.26	108.2	1.16		1.49						
	201	F-104	0	0	1.23	58.9		1.31	3.46	45.8	25401	7.74	0	0	
			40	0	1.23	58.9		1.31	3.45	85.8	86581	26.39	48320	14.73	
			40	-15	1.11	53.1		1.18	3.16	87.8	78697	23.99	57283	17.46	
			40	-30	.94	45.0		1.00	2.67	94.9	70863	21.60	70188	21.39	
			40	15	1.29	61.8		1.33	3.21	87.8	95991	29.26	40975	12.49	
			40	30	1.32	63.2		1.41	2.79	94.9	109330	33.32	33912	10.33	
			60	0	1.23	58.9		1.31	3.45	105.8	98010	29.87	86447	26.35	
	202		0	0	1.23	58.9		1.31	3.46	45.8	23953	7.30			
			30	0	1.23	58.9		1.31	3.46	75.8	72998	22.25	31762	9.68	
			30	-15	1.12	53.6		1.19	3.17	77.8	80651	24.58	22670	6.91	
			30	-30	.95	45.5		1.01	2.68	84.9	92030	28.05	13067	3.98	
			30	15	1.28	61.9		1.38	3.22	77.7	67034	20.43	42131	12.84	
			30	30	1.31	63.3		1.42	2.79	84.8	61754	18.82	56349	17.18	
			60.	0	1.22	58.8		1.30	3.45	105.8	94781	28.89	86439	26.35	

TABLE II-SUMMARY OF SONIC BOOM RESULTS- continued

Set number	Run number	Aircraft	Maneuver time	Azimuth angle, ϕ	Δp (Peak overpressure)		$\frac{\Delta p}{\Delta p_{std}}$	$\frac{\Delta p}{\Delta p_{ref}}$	L_1/L_A	Ray-ground intersection					Remarks
										t	x		y		
			secs	deg	lb/ft^2	N/m^2				secs	ft	km	ft	km	
11	203	F-104	0	0	1.27	60.8		1.35	3.46	46.1	24947	7.60	0	0	
			0	-15	1.16	55.5		1.24	3.17	48.0	25990	7.92	11651	3.55	
			0	-30	.98	46.9		1.04	2.68	54.8	29695	9.05	25716	7.84	
			0	15	1.33	63.7		1.42	3.23	43.6	25990	7.92	-11651	-3.55	
			0	30	1.35	64.6		1.44	2.79	54.8	29695	9.05	-25716	-7.84	
			40	0	1.27	60.8		1.35	3.46	86.1	86269	26.29	47990	14.63	
	204	SCAT 15-F	0	0	2.79	133.6		1.13	1.71						
			40	0	2.79	133.6		1.13	1.71						
			40	-15	2.53	121.1		1.03	1.57						
			40	-30	2.14	102.5		.87	1.32						
			40	15	2.94	140.8		1.20	1.59						
			40	30	2.99	143.2		1.22	1.37						
			60	0	2.79	133.6		1.13	1.71						
	205		0	0	2.78	133.1		1.18	1.71						
			30	0	2.78	133.1		1.18	1.71						
			30	-15	2.53	121.1		1.03	1.56						
			30	-30	2.14	102.5		.87	1.32						
			30	15	2.92	139.8		1.19	1.59						
			30	30	3.01	144.1		1.22	1.37						
			60	0	2.78	133.1		1.18	1.71						
	206		0	0	2.88	137.9		1.17	1.72						
			0	-15	2.62	125.4		1.16	1.57						
			0	-30	2.23	106.8		.91	1.32						
			0	15	3.02	144.6		1.23	1.59						
			0	30	3.07	147.0		1.25	1.37						
			40	0	2.88	137.9		1.17	1.72						
12	207	F-104	0	0	2.23	106.8			2.47	39.9	0	0	34466	10.51	
			0	-15	2.22	106.3			2.44	41.8	7766.4	2.37	36124	11.01	
			0	-30	2.28	109.2			2.40	48.9	17582	5.36	42333	12.90	
			60	0	1.86	89.5			2.89	88.1	0	0	114130	34.79	
			60	-15	1.81	86.7			2.69	89.3	7222.6	2.20	114180	34.80	
			60	-30	1.65	79.0			2.33	93.3	15897	4.84	117220	35.73	

TABLE II.-SUMMARY OF SONIC BOOM RESULTS - continued

Set number	Run number	Aircraft	Maneuver time	Azimuth angle, ϕ	Δp (Peak overpressure)		$\frac{\Delta p}{\Delta p_{std}}$	$\frac{\Delta p}{\Delta p_{ref}}$	L_1/L_A	Ray-ground intersection					Remarks
										t	x		y		
			secs	deg	lb/ft^2	N/m^2				secs	ft	km	ft	km	
12	208	F-104	0	0	2.27	108.7			2.47	39.8	0	0	33079	10.08	
			0	-15	2.27	108.7			2.44	41.7	7736.4	2.36	34664	10.57	
			0	-30	2.42	115.7			2.40	48.8	17510	5.34	40623	12.38	
			60	0	1.85	88.6			2.90	88.1	0	0	111410	33.96	
			60	-15	1.80	86.2			2.69	89.2	7211.6	2.20	112050	34.15	
			60	-30	1.65	79.0			2.33	93.3	15865	4.83	114320	34.84	
	209		0	0	2.14	102.5			2.45	39.3	0	0	32625	9.94	
			0	-15	2.11	101.0			2.42	40.9	7309.2	2.23	33997	10.36	
			0	-30	2.06	98.6			2.36	46.8	16144	4.92	38872	11.85	
			60	0	1.92	91.9			2.90	88.4	0	0	113620	34.63	
			60	-15	1.87	89.5			2.70	89.5	7019.2	2.14	114240	34.82	
			60	-30	1.71	81.9			2.33	93.3	15312	4.67	116410	35.48	
	210		0	0	4.28	205.4			1.26						
			0	-15	4.31	206.3			1.24						
			0	-30	4.56	218.3			1.20						
			60		3.89	186.3			1.38						
			60	-15	3.79	181.5			1.28						
			60	-30	3.51	168.1			1.10						
	211		0	0	4.35	208.3			1.26						
			0	-15	4.41	211.2			1.24						
			0	-30	4.83	231.3			1.20						
			60	0	3.87	285.3			1.38						
			60	-15	3.79	181.5			1.28						
			60	-30	3.52	168.5			1.10						
	212		0	0	4.07	194.9			1.26						
			0	-15	4.06	194.4			1.23						
			0	-30	4.07	194.9			1.19						
			60	0	4.03	193.0			1.39						
			60	-15	3.94	188.7			1.29						
			60	-30	3.66	175.2			1.10						
13	213		1	0	1.44	68.9			2.76	72.5	0	0	62404	19.02	
			1	-15	1.53	73.3			2.74	76.8	13739	4.19	66273	20.20	
			13	0	.97	46.5			3.44	57.9	0	0	43625	13.30	
			13	-15	.94	45.0			3.14	59.9	11841	3.61	44655	13.61	
			13	-30	.86	41.2			2.63	66.8	26302	8.02	48365	14.74	

TABLE II.-SUMMARY OF SONIC BOOM RESULTS - continued

Set number	Run number	Aircraft	Maneuver time	Azimuth angle, ϕ	Δp (Peak overpressure)		$\frac{\Delta p}{\Delta p_{std}}$	$\frac{\Delta p}{\Delta p_{ref}}$	L_1/L_A	Ray-ground intersection					Remarks
										t	x		y		
			secs	deg	lb/ft^2	N/m^2				secs	ft	km	ft	km	
13	214	F-104	1	0	1.50	71.8			2.76	72.3	0	0	60012	18.29	
			1	-15	1.64	78.5			2.74	76.6	13701	4.18	63749	19.43	
			13	0	.97	46.4			3.44	57.9	0	0	41847	12.75	
			13	-15	.94	45.0			3.14	59.9	11830	3.61	42814	13.05	
			13	-30	.85	40.7			2.62	66.8	26269	8.01	46295	14.11	
	215		1	0	1.24	59.4			2.75	70.7	0	0	59130	18.02	
			1	-15	1.25	59.9			2.71	74.3	12900	3.93	62225	18.97	
			1	-30	1.37	65.6			2.68	88.3	29754	9.07	74292	22.64	
			13	0	1.01	48.4			3.45	58.3	0	0	43218	13.17	
			13	-15	.98	46.9			3.14	60.1	11618	3.54	44188	13.47	
			13	-30	.89	42.6			2.63	66.8	25618	7.81	47624	14.52	
	216		1	0	3.51	168.1			1.36						
			1	-15	3.76	180.0			1.34						
			13	0	2.57	123.1			1.57						
			13	-15	2.50	119.7			1.43						
			13	-30	2.28	109.2			1.20						
	217		1	0	3.68	176.2			1.36						
			1	-15	4.04	193.4			1.34						
			13	0	2.56	122.6			1.57						
			13	-15	2.49	119.2			1.43						
			13	-30	2.28	109.2			1.20						
	218		1	0	3.02	44.6			1.35						
			1	-15	3.06	146.5			1.33						
			1	-30	3.44	164.7			1.29						
			13	0	2.66	127.4			1.57						
			13	-15	2.59	124.0			1.43						
			13	-30	2.36	113.0			1.20						
14	219	F-104	0	0	.89	42.6	1.08		3.95	47.7	0	0	28941	8.82	γ = -20 deg
			0	-15	.87	41.6	1.06		3.79	49.1	8466.3	2.58	30178	9.20	
			0	-30	.83	39.7	1.01		3.45	53.8	17936	5.47	34319	10.46	
			4	0	.69	33.0	.84		3.04	62.6	0	0	51531	15.71	γ = -7.54 deg
			8	0	.50	23.9	.61		2.79	82.4	0	0	76550	23.33	γ = 0

TABLE II.-SUMMARY OF SONIC BOOM RESULTS - continued

Set number	Run number	Aircraft	Maneuver time	Azimuth angle, ϕ	Δp (Peak overpressure)		$\frac{\Delta p}{\Delta p_{std}}$	$\frac{\Delta p}{\Delta p_{ref}}$	L_1/L_A	Ray-ground intersection					Remarks
										t	x		y		
			secs	deg	lb/ft^2	N/m^2				secs	ft	km	ft	km	
14	220	F-104	0	0	.89	42.6	1.08		3.96	47.7	0	0	27426	8.36	
			0	-15	.87	50.8	1.06		3.79	49.1	8456.4	2.58	28615	8.72	
			0	-30	.83	39.7	1.01		3.45	53.7	17909	5.46	32596	9.94	
			4	0	.70	33.5	.855		3.04	62.5	0	0	49482	15.08	
			8	0	.54	25.9	.66		2.79	82.3	0	0	73827	22.50	
	221		0	0	.92	44.5	1.12		3.96	47.9	0	0	28373	8.65	
			0	-15	.91	43.6	1.10		3.79	49.3	8288.6	2.53	29544	9.01	
			0	-30	.87	41.7	1.06		3.45	53.7	17470	5.32	33428	10.19	
			4	0	.73	35.0	.89		3.05	62.1	0	0	49886	15.21	
			8	0	.54	25.9	.66		2.78	79.8	0	0	72226	22.01	
	222		0	0	1.64	78.5		1.75	2.54	53.4	0	0	38155	11.63	γ = 10 deg
			0	-5	1.64	78.5		1.75	2.52	53.7	4505.5	1.37	38335	11.68	
			0	-10	1.64	78.5		1.75	2.49	54.6	9131.3	2.78	38891	11.85	
			0	-15	1.63	78.0		1.74	2.44	56.2	14013	4.27	39866	12.15	
			0	-20	1.63	78.0		1.74	2.38	58.6	19324	5.89	41344	12.60	
			6	0	1.51	72.3		1.61	2.92	55.2	0	0	41064	12.52	γ = 2.91 deg
	223		0	0	1.64	78.5		1.75	2.53	53.3	0	0	36434	11.11	
			0	-10	1.63	78.0		1.74	2.49	54.5	9116	2.78	37129	11.32	
			0	-20	1.64	78.5		1.75	2.38	58.5	19286	5.88	39444	12.02	
			6	0	1.49	71.3		1.59	2.92	55.1	0	0	39326	11.99	
			6	-10	1.49	71.3		1.59	2.83	56.1	8325.7	2.54	39842	12.14	
			6	-20	1.45	69.4		1.55	2.62	59.2	17432	5.31	41522	12.66	
	224		0	0	1.56	74.7		1.66	2.53	53.4	0	0	37180	11.53	
			0	-5	1.56	74.7		1.66	2.52	53.6	4389	1.34	37343	11.38	
			0	-10	1.55	74.2		1.65	2.49	54.5	8885.4	2.71	37844	11.53	
			0	-15	1.54	73.7		1.64	2.43	56.0	13609	4.15	38716	11.80	
			0	-20	1.52	72.8		1.62	2.37	58.2	18707	5.70	40025	12.20	
			6	0	1.50	71.8		1.60	2.92	55.4	0	0	40505	12.35	
	225		0	0	1.38	66.1	1.69		3.40	76.6	68729	20.95	0	0	
			0	3	2.46	118.0	3.00		3.57	76.8	68901	21.00	2704	.82	
			0	-3	1.08	51.8	1.32		3.30	76.8	68901	21.00	-2704	-.82	
			0	-20	.57	27.3	.70		2.99	86.4	77784	23.71	-19952	-6.08	
	225A		0	-33.44	.31	14.8	.378		2.87	129.7	119740	36.50	-49488	-15.08	

TABLE II.-SUMMARY OF SONIC BOOM RESULTS - continued

Set number	Run number	Aircraft	Maneuver time	Azimuth angle, ϕ	Δp (Peak overpressure)		$\frac{\Delta p}{\Delta p_{std}}$	$\frac{\Delta p}{\Delta p_{ref}}$	L_1/L_A	Ray-ground intersection					Remarks
										t	x		y		
			secs	deg	lb/ft^2	N/m^2				secs	ft	km	ft	km	
14	226	F-104	0	0	1.49	71.4	1.82		3.40	76.5	66180	20.17	0	0	
			0	-20	.66	31.6	.80		2.99	86.4	75202	22.92	-19970	-6.09	
	227		0	0	1.36	65.1	1.67		3.37		64404	19.63	0	0	
			0	-20	.63	30.2	.77		2.97		71048	21.66	-18224	-5.55	
			0	-40	.31	14.8	.378		2.77		110990	33.83	-53507	-16.31	
			0	-43.44	.23	11.0	.28		2.77		144630	44.08	-74583	-22.73	
	228	SCAT 15-F	0	0	1.91	91.5	.98		2.36						
			0	15	1.88	90.0	.965		2.26						
			0	30	1.80	86.2	.925		2.03						
			4	0	1.48	70.9	.76		1.81						
			8	0	0	0	0		1.63						
	229		0	0	1.91	91.5	.98		2.36						
			0	15	1.88	90.0	.965		2.26						
			0	30	1.81	86.7	.93		2.03						
			4	0	1.51	72.3	.775		1.81						
			8	0	1.19	57.0	.61		1.63						
	230		0	0	2.00	95.8	1.025		2.37						
			0	15	1.97	94.3	1.01		2.26						
			0	30	1.89	90.5	.97		2.03						
			4	0	1.57	75.2	.805		1.81						
			8	0	1.19	57.0	.61		1.63						
	231		0	0	2.51	120.2		1.02	1.21						
			0	5	2.51	120.2		1.02	1.21						
			0	10	2.51	120.2		1.02	1.19						
			0	15	2.51	120.2		1.02	1.16						
			0	20	2.53	121.1		1.03	1.13						
			6		2.25	107.7		0.915	1.41						
	232		0	0	2.50	119.7		1.015	1.21						
			0	10	2.51	120.2		1.02	1.19						
			0	20	2.54	121.6		1.03	1.13						
			6	0	2.24	107.3		0.91	1.41						
			6	10	2.22	106.3		0.90	1.36						
			6	20	2.19	104.9		0.89	1.25						
	233		0	0	2.39	114.4		0.975	1.21						
			0	5	2.39	114.4		0.975	1.20						
			0	10	2.38	114.0		0.975	1.19						

TABLE II.-SUMMARY OF SONIC BOOM RESULTS - concluded

Set number	Run number	Aircraft	Maneuver time	Azimuth angle, ϕ	Δp (Peak overpressure)		$\frac{\Delta p}{\Delta p_{std}}$	$\frac{\Delta p}{\Delta p_{ref}}$	L_1/L_A	Ray-ground intersection					Remarks
										t	x		y		
			secs	deg	lb/ft^2	N/m^2				secs	ft	km	ft	km	
14	233	F-104	0	15	2.36			0.96	1.16						
			0	20	2.34			0.94	1.13						
			6	0	2.24			0.94	1.41						
	234		0	0	3.09	148.0	1.59		1.91						
			0	3	5.54	264.2	2.84		1.99						
			0	-3	2.42	115.9	1.24		1.86						
			0	-20	1.27	60.8	.65		1.70						
	235		0	0	3.34	160.0	1.71		1.91						
			0	-20	1.46	70.0	.75		1.70						
	236		0	0	3.05	146.3	1.57		1.89						
			0	-20	1.39	66.6	.715		1.69						
			0	-40	.68	32.6	.35		1.58						
			0	-43.44	.50	23.9	.256		1.58						
15	237E		50		2.27	108.7			2.81	127.3			79993	24.38	
			55		1.64	78.5			2.78	128.5			81380	24.80	
			60		1.44	68.9			2.76	130.4			83744	25.53	
	237F		80		1.20	57.5			2.72	142.0			80256	24.46	
			100		1.14	54.6			2.71	156.7			99074	30.20	
			120		1.12	53.6			2.71	172.9			120750	36.80	
16	241A		0	0	1.50	71.8			2.66	48.4	0	0	35920	10.95	
			0	30	1.39	66.6			2.43	59.3	-24702	-7.53	44189	13.47	
			.5	0	.84	40.2			2.71	48.9	0	0	36645	11.17	
			.5	30	.74	35.4			2.45	59.8	-24702	-7.53	44914	13.69	
			1.0	0	1.50	71.8			2.66	49.4	0	0	37372	11.39	
			1.0	30	1.39	66.6			2.43	60.3	-24702	-7.53	45641	13.91	

TABLE III

Overpressures in Standard, No Wind Atmosphere

Mach No.	F-104		SCAT 15-F	
	lb/ft^2	N/m^2	lb/ft^2	N/m^2
1.20	0.84	40.1	-	-
1.25	0.82	39.2	1.95	93.1
1.3	0.82	39.2	1.96	93.6
1.5	0.86	41.1	2.10	100.3
2.0	0.94	44.9	2.46	117.4
3.0	1.06	50.6	2.74	130.9
3.0	-	-	2.92[1)]	142.8

[1)] F-function for M = 2.7

TABLE IV

Temperature Effects on Overpressure Ratio

Atmosphere Designation	Mach No.	$\Delta p/(\Delta p$ SNW)		
		Calculated		From ref. 2 - fig. 8
		F-104	SCAT 15-F	
SLR (A-3)	1.20	1.28	----	1.26
	1.25	1.09	1.08	1.09
	1.3	1.06	1.05	1.04
	1.5	1.01	1.01	1.01
	2.0	1.00	1.00	1.00
	3.0	0.99	0.99	0.99
	3.0		1.05[1)]	
LATI (B-4)	1.20	0.91	----	0.90
	1.25	0.975	0.95	0.96
	3.0	1.02	----	1.01
HATI (D-3)	1.20	0.95	----	0.915
	1.25	1.02	1.00	0.95
	3.0	1.04	----	1.03

1) F-function for M = 2.7

TABLE V

Wind Effects on Overpressure Ratio

Wind Designation	Mach No.	$\Delta p/(\Delta p_{std})$ (no wind)		
		Calculated		From ref. 2 - fig. 12
		F-104	SCAT 15-F	
Headwind, LAS	1.25	1.06	1.08	-----
MAS	1.25	1.02	1.03	-----
HAS	1.25	Beyond cutoff and A = 0		-----
	1.3	2.27	2.36	1.16
	1.5	0.98	0.98	1.015
	2.0	0.96	0.96	0.985
	3.0	0.96	0.96	0.98
Tailwind, LAS	1.25	0.94	0.95	0.95
	2.0	1.01	1.01	1.00
MAS	1.25	0.98	0.98	0.97
	2.0	1.01	1.01	1.00
HAS	1.20	0.91	----	-----
	1.25	0.98	0.97	-----
	2.0	1.04	1.04	1.025
	3.0	1.03	----	1.035
Sidewind, HAS	1.20	0.97		0.95
	1.5	1.00		1.00
	3.0	1.00		1.025

TABLE VI

Wind Direction Effects on Overpressure

ϕ (deg)	$\eta = 0$	45°	90°	135°	180°
0	2.01	1.99	1.95	1.92	1.91
10		1.97	1.93	1.90	
20		1.90	1.86	1.82	
30		1.76	1.73	1.67	
-10		1.96	1.92	1.89	
-20		1.86	1.83	1.81	
-27.8		1.70			
-30			1.64	1.66	
0		1.9902			
2		1.9904			
4		1.9886			
6		1.9847			
8		1.9789			
-2		1.9880			
-4		1.9837			
-6		1.9773			
-8		1.9687			

Note: Values in the table are overpressures (psf) for given ϕ and η .

TABLE VII

Effects of $\dot{\gamma}$ and Atmosphere on Overpressure

			Uniform Atmosphere				1962 U.S.Standard Atmosphere	
			h = 40 000 ft (12.2 km) h_g = 0				h=37 200 ft (11.3 km) h_g= 2 200 ft (670 m)	40 000 ft (12.2 km) 0
Maneuver point	γ, deg	$\dot{\gamma}$, deg/sec	Δp psf(N/m^2)	$K_A \Delta p$ psf(N/m^2)	$K_A' \Delta p$ psf(N/m^2)	$K_A'' \Delta p$ psf(N/m^2)	Δp psf(N/m^2)	Δp psf(N/m^2)
1.1	0	-0.634	0.478 (22.8)	1.24 (59.4)	1.503 (71.9)	1.545 (73.9)	1.503 (71.9)	1.545 (73.9)
2.1	-0.1425	0	0.343 (16.4)	0.89 (42.5)	1.078 (51.5)	1.110 (53.0)	0.959 (45.8)	0.859 (41.0)
3.1	0	+0.634	0.386 (18.4)	1.00 (47.9)	1.212 (58.0)	1.248 (59.6)	0.838 (40.0)	0.851 (40.6)
4.1	+0.1425	0	0.341 (16.3)	0.86 (41.0)	1.07 (51.1)	1.103 (52.7)	0.954 (45.5)	0.854 (40.7)